République Algérienne Démocratique et Populaire
Ministre de l'Enseignement Supérieur et de la Recherche Scientifique
Université de Saida - Dr. Moulay Tahar
Faculté des Technologies

Thèse
Présentée pour obtenir le diplôme de

Doctorat 3^{me} cycle

Spécialité: Commande Électrique
Filière: Électrotechnique

Par
HAMLAT AISSA

Thème :

Contribution au développement d'une stratégie de contrôle d'un système hybride composé de deux sources pile à combustible et super-condensateur dédié à la traction électrique

Thèse soutenue le 26 06 2024 devant le jury composé de:

No.	Nom et Prénom	Grade	Établissement	Qualité
1	Hartani Kadda	Prof	Université de Saida Dr. Moulay Tahar	Président
2	Sekour M'hamed	Prof	Université de Saida Dr. Moulay Tahar	Rapporteur
3	Mankour Mohamed	Prof	Université de Saida Dr. Moulay Tahar	Co-rapporteur
4	Azzedine Hamid	Prof	Centre Universitaire Nour Bachir ElBayadh	Examinateur
5	Allali Ahmed	Prof	Université des Sciences et de la Technologie USTO	Examinateur
6	Mostefai Mohamed	Prof	Université de Saida Dr. Moulay Tahar	Examinateur


بسم الله الرحمن الرحيم

ABSTRACT

This thesis is part of the results of cutting-edge research conducted by the Electrotechnical Engineering Laboratory on efficient energy management in electric and hybrid vehicles. The thesis mainly focuses on an innovative energy management and monitoring system for hybrid energy storage systems, which includes fuel cells and ultracapacitors. Firstly, improved energy storage devices were carefully designed and simulated to match the characteristics of fuel cells. Furthermore, the behavior of hybrid electric systems has been significantly enhanced, primarily by utilizing advanced fuzzy logic control (FLC) as the fundamental controller, ensuring efficient meeting of load demands. This developed approach is based on the overall vehicle speed and the state of charge of the supercapacitor (SOC). Furthermore, a robust nonlinear control strategy is designed by integrating backstepping and super-twist sliding mode control techniques. This strategy ensures smooth operation and continuous coordination of the hybrid electric system. It specifically addresses the output of converter, setpoint generation, and power supervision, ensuring exceptional performance. The study concluded with a comprehensive numerical simulation conducted with two proposed scenarios: The first one testing and comparing a backstepping super sliding mode controller (BS STSMC) with fuzzy logic with a typical proportional-integral (PI) controller with a rule-based deterministic energy management system. The simulation used an extra-urban driving cycle (EUDC) and New European Driving Cycle (NEDC) tests scenario for fuel cell electric vehicles (FCEVs). Secondly, an energy management through energy sharing test scenario was used with the proposed back-stepping sliding super sliding mode controller (BS STSMC). The analysis results convincingly demonstrated that the proposed control strategy effectively reduces the hydrogen consumption by the fuel cell while maintaining a consistently high state of charge in the supercapacitor.

Keywords: *Fuel cell* , *Supercapacitor*, *energy management*, *hybrid electric vehicle*. *Fuzzy Logic* , *Control (FLC)* , *State of Charge (SOC)*, *Hybrid Power Systems (HPS)*

RESUMÉ

Cette thèse fait partie des résultats d'une les résultats d'une recherche de pointe menée par le Laboratoire de génie électrotechnique (LGE) sur la gestion efficace de l'énergie dans les véhicules électriques et hybrides. La thèse se concentre principalement sur un système innovant de gestion et de contrôle de l'énergie pour les systèmes de stockage d'énergie hybrides, qui comprennent des piles à combustible et des supercondensateurs. Tout d'abord, des dispositifs de stockage d'énergie améliorés ont été soigneusement conçus et simulés pour correspondre aux caractéristiques des piles à combustible. En outre, le comportement des systèmes électriques hybrides a été considérablement amélioré, principalement par l'utilisation d'un contrôle logique flou avancé (FLC) comme contrôleur fondamental, garantissant une réponse efficace aux exigences de la charge. Cette approche est basée sur la vitesse globale du véhicule et l'état de charge du supercondensateur (SOC). En outre, une stratégie de contrôle non linéaire robuste est conçue en intégrant des techniques de contrôle par mode coulissant de type backstepping et super-twist. Cette stratégie garantit le bon fonctionnement et la coordination continue du système électrique hybride. Elle traite spécifiquement la sortie du convertisseur, la génération du point de consigne et la supervision de la puissance, ce qui garantit des performances exceptionnelles. L'étude s'est terminée par une simulation numérique complète réalisée avec deux scénarios proposés : Le premier testait et comparait un contrôleur backstepping super-twisting (BS STSMC) intégrant un algorithme flou par rapport à un contrôleur proportionnel-intégral (PI) typique avec un système de gestion de l'énergie déterministe basé sur des règles. La simulation a utilisé un cycle de conduite extra-urbain (EUDC) et un nouveau cycle de conduite européen (NEDC) pour les véhicules électriques à pile à combustible (FCEV). Deuxièmement, un scénario d'essai de gestion de l'énergie par partage de l'énergie a été utilisé avec le backstepping super-twisting sliding mode controller (BS STSMC) proposé. Les résultats de l'analyse ont démontré de manière convaincante que la stratégie de contrôle proposée réduit efficacement la consommation d'hydrogène par la pile à combustible tout en maintenant un état de charge constamment élevé dans le supercondensateur.

Mot clé: *Pile à combustible* , *Supercondensateur*, *Gestion energie*, *véhicule électriuqe hybride*. *Logique floue*, *L'état de charge (EDC)*, *Systemes de puissance Hybrid*

ملخص

تعد هذه الأطروحة جزءاً من نتائج الأبحاث المتطورة التي يقودها مختبر الهندسة الكهروتقنية حول الإدارة الفعالة للطاقة في المركبات الكهربائية والهجينة. حيث ترتكز الأطروحة بشكل أساسي على نظام مبتكر لإدارة ومراقبة الطاقة لأنظمة تخزين الطاقة الهجينة، والتي تشمل خلايا الوقود والمكثفات الفائقة. أولاً، تم تصميم أجهزة تخزين الطاقة المحسّنة ومحاكاتها بعناية لتتناسب مع خصائص خلايا الوقود. وعلاوة على ذلك، تم تحسين سلوك الأنظمة الكهربائية الهجينة بشكل كبير، وذلك في المقام الأول من خلال استخدام التحكم المنطقي الضبابي المتقدم كوحدة تحكم أساسية، مما يضمن تلبية متطلبات الحمولة بأداء فعال. يعتمد هذا النهج المطور على السرعة الإجمالية للمركبة وحالة شحن المكثف الفائق . بالإضافة إلى ذلك، تم تصميم استراتيجية تحكم قوية غير خطية من خلال دمج تقنيات التحكم في الوضع المنزلق الفائق الالتواء. تضمن هذه الاستراتيجية التشغيل السلس والتنسيق المستمر للنظام الكهربائي الهجين. وتتناول على وجه التحديد مخرج المحول، وتوليد نقطة التوازن، والإشراف على الطاقة، مما يضمن أداءً استثنائياً. اختتمت الدراسة بمحاكاة عددية شاملة أجريت مع سيناريوهين مقترحين: الأول يختبر ويقارن وحدة تحكم في الوضع المنزلق الفائق ذات التقويم الخلفي مع المنطق الضبابي مع وحدة تحكم تناسبية تكاملية نموذجية مع نظام إدارة الطاقة الحتمي القائم على القواعد. استخدمت المحاكاة سيناريو اختبارات دورة القيادة خارج المناطق الحضرية ودورة القيادة الأوروبية الجديدة للمركبات الكهربائية التي تعمل بخلايا الوقود . ثانياً، تم استخدام سيناريو اختبار إدارة الطاقة من خلال سيناريو اختبار مشاركة الطاقة مع وحدة التحكم في الوضع المنزلق الفائق الانزلاقية المنزلقة المقترحة.

تُظهر نتائج التحليل بشكل مقنع أن استراتيجية التحكم المقترحة تقلل بشكل فعال من استهلاك الهيدروجين من قبل خلية الوقود مع الحفاظ على حالة شحن عالية باستمرار في المكثف الفائق.

كلمات مفتاحية :

خلية الوقود ، المكثف الفائق، إدارة الطاقة ، االمركبة الكهربائية الهجينة ،المنطق الضبابي، حالة مستوى الشحن ، نظام الطاقة الهجين

ACKNOWLEDGEMENTS

The greatest thanks go above all to Allah who alone has guided us on the right path throughout our lives and given us the courage, the will and the strength to undertake this research work.

It is with great pleasure and a deep sense of gratitude that I would like to express my sincere thanks to my thesis supervisor **Prof. M'hamed sekour** , Professor at the University of Dr. Tahar Molay, and my thesis co-supervisor **Prof. Mohamed Mankour** Professor at the University of Dr. Tahar Molay. Without their continuous motivation and encouragement, this research could not have been successfully completed.

My sincere thanks to **Prof. Mohamed Mostefai**, Professor at the University of Tahar Molay Saida, for agreeing to examine this work and to be a member of the jury.

My sincere thanks and gratitude to **Prof. Ahmed Allali** , Professor at the University of Science and Technology of Oran Mohamed-Boudiaf USTOMB, for agreeing to judge this work .

Many thanks to Prof. **Prof. Hamid Azzedine**, Professor at the University centre Nour Bachir el-Bayadh , for agreeing to examine this work and to be a member of the jury.

All respect, appreciation, and thanks to **Prof. Hartani Kadda**, Professor at the University of Tahar Molay Saida,for their trust and acceptance as the chairman of the jury for my thesis.

I am very grateful to **Prof. Tarik Chikouche**, head of the Doctoral Formation Team, as well as **Prof. Larbi Boumediene** Director of Electrotechnical Engineering Laboratory .

Finally, I would like to express my gratitude to my friends and colleagues at the Electrotechnical Engineering Laboratory . I sincerely thank them for the unforgettable moments we have shared. I also extend my heartfelt thanks to my parents, sisters and my brother , as well as my wife . They have provided encouragement, inspiration, and support throughout my years of research. Lastly, I am grateful to all the faculty members and staff at the Faculty of Technology.

AISSA HAMLAT

To my parents,

To my brother and sisters

To my wife,

To my daughters, Bakhta and Hafsa, and my sister Duaa,

.

Contents

LIST OF ACRONYMS AND ABBREVIATIONS

P_{fc}	Fuel cell Power
P_{laod}	Power Load
P_{sc}	Super-capacitor Power
$\eta_{DC/AC}$	The efficiency ofthe DC/AC converter
$\eta_{DC/DC}$	The efficiency of the DC/DC converter
η_{motor}	The efficiency of the motor
A-HESS	active hybrid energy storage systems
BS STSMC	backstepping super-twist sliding mode control
BS-DTC	Back-stepping Direct Torque control
DP	Dynamic Programming
EDLC	Electrochemical Double Layer Capacitors
EEC	Equivalent Energy Consumption
EMS	Energy Management Systems
F1PD-PI	Fuzzy 1+Proportional+Derivative-Proportional+Integral
FC	Fuel Cell
FCEV	Fuel Cell Electric Vehicles
FESS	Flywheel Energy Storage System
FLC	Fuzzy Logic Control
FLE	Fuzzy Logic Estimator
GOEMS	global Optimal Energy Management Systems
HBSS	Hybrid Battery-Supercapacitor Storage
HES	High Energy Source
HESS	Hybrid Energy Storage Systems
HPS	High Power Source

IBC	interleaved boost converter
MPC	Model Predictive Control
OEMS	optimization-based energy management strategy
P-HESS	passive hybrid energy storage systems
PEMFC	Proton Exchange Membrane Fuel Cell
PFC	power follower control
PH	Predictive Horizon
PMC	Power Management Control
PMP	Pontryagin's Minimum Principle
RBM	The rule-based methods
RL	Reinforcement learning
SC	speracapacitors
SFCS	series fuzzy control strategy
SMES	superconducting magnetic energy storage
SMS	State Machine Strategy
STSMC	super-twisted sliding mode algorithm
SVM	Space Vector Modulation
TCS	The thermostat control strategy

LIST OF FIGURES

LIST OF TABLES

GENERAL INTRODUCTION

Context:

Energy is a necessary currency for success. Humans have relied on a number of energy sources to meet their demands throughout our civilised history, including fossil fuels and solar power generation [19]. However, energy production and use also have negative environmental consequences, including global climate change, acid rain, air pollution, smog, radioactive waste, and habitat destruction [20].

As global electricity consumption continues to increase and fossil fuel power plants remain significant contributors to greenhouse gas emissions, it is crucial to transition to alternative energy sources that generate little or no greenhouse gases. Doing so can help mitigate the environmental impact of energy production and use and ensure the long-term sustainability of human civilization [21].

Transport is one of the principal contributors to global emissions, after electricity and heat generation, followed closely by manufacturing, construction and agriculture [22].In many countries, cities are experiencing rapid growth, which has resulted in an increased usage of cars and other private vehicles. This fast-paced urban expansion and the subsequent rise in driving activity are significant contributing factors to air pollution [23, 24].New powertrains, which are based on electric motors and batteries, have led to significant reductions in both fuel consumption and emissions. However, batteries have encountered several challenges, such as limited range, slow recharging, and a heavy weight. In order to tackle these issues, the use of hydrogen fuel cells in urban transportation has emerged as a potential solution. Fuel cells have the ability to provide clean energy for automobiles, effectively addressing the aforementioned drawbacks [25, 26].

Hydrogen gas is a renewable fuel source that can be produced through various methods. There are two main methods of producing hydrogen: grey and blue hydrogen, which rely on non-renewable sources of energy and produce greenhouse gas emissions, and green hydrogen, which is produced using renewable energy sources and does not produce harmful emissions [27]. The proton exchange membrane fuel cell (PEMFC) technology is a crucial component of fuel cell electric vehicle (FCEVs). FCEVs powered by PEMFCs offer exceptional efficiency, low emissions, and a low environmental impact.

This is because PEMFCs convert the chemical energy of hydrogen gas into electrical energy through an electrochemical reaction with oxygen, producing only water vapor as a by-product [28]. As a result,

FCEVs are considered a cleaner and more sustainable alternative to traditional gasoline-powered vehicles [29].

The increasing popularity of PEMFCs in energy conversion and storage systems highlights the potential of this technology in addressing the world's energy challenges [30].Clean energy technologies have enabled the development of low-carbon hydrogen production methods.

To improve overall performance and address the issue of slow fuel cell dynamics, it is recommended to combine it with a high specific energy storage solution such as supercapacitors. This is because supercapacitors have fast dynamics and can complement the fuel cell's shortcomings [31].

Formulating a Research Problem:

Effective energy management is crucial for electric vehicles that coexist with fuel cells and supercapacitor (SC) energy storage systems. This is necessary to ensure an efficient distribution of power that takes into account the strengths and weaknesses of each energy storage system.

The main issue being investigated is how to keep the unwanted effects of reduced fuel cell performance at a minimum while the fuel cell is operating. It is essential to minimise the impact of load variations on the fuel cell while reducing fuel consumption. Secondly, it is important to maintain a power balance between the energy storage units and the demand, and to improve transient performance for better responsiveness. Then, for stable operation, reduce steady-state errors as well as keeping the SOC of the supercapacitor in a suitable range.

Motivation:

The slow start-up and warm-up times of fuel cells, as well as their ability to handle high dynamic power, are also limited. As a result of these shortcomings, it is not suitable as the only source of energy for vehicles. To address these issues, it is common practice to integrate energy storage systems (ESS) with fuel cells in the design of fuel cell hybrid electric vehicles (FCHEVs). This integration aims to solve the drawbacks of fuel cells by improving their performance through the capabilities of energy storage systems.Moreover, this type of configuration complicates the FCHEV powertrain and poses a challenge to the design of the energy management strategy.

Finding an effective energy management approach is required to maximize the performance of each power source and achieve particular targets such as reducing hydrogen consumption, increasing the average lifespan of power sources, and promising continuous energy storage.

The non-linear behaviour of power sources, converters and loads adds complexity to the hybrid electric system. While the power management system plays an important role in the generation of traction energy, it does not always succeed in solving the problems related to the power flow. Therefore, the development of a robust control strategy becomes the second task in the design of the power management system for fuel cell vehicles.

Overview of the contributions:

This thesis aims to develop an efficient electrical energy management strategy for an electric traction application. The focus is on the challenges of integrating different energy sources, managing energy flows between components and reducing energy consumption. A systems approach is used to develop models and enhancement strategies to overcome these challenges.

This thesis aims to contribute to the implementation of energy management strategies based on fuzzy logic. It is based on LGE laboratory work on the control of electrical energy in electric vehicles. By taking into account the power demand and the state of charge of the supercapacitor, the appropriate performance domain for each energy source can be determined. However, relying only on Fuzzy Logic does not always allow the power demanded by the load and the storage units to be distributed efficiently, especially under real driving conditions. Robust control of the converters linked to each source is crucial to ensure that safety limits, such as the state of charge, are respected during driving. The thesis focuses on the development of strategies to improve energy management by adjusting the scaling factor on the basis of specific indicators related to the energy storage units, in particular the state of charge and the vehicle speed.

The research will concentrate on two major topics. The first is concerned with the investigation and modeling of the behavior of the different dual-source system components, as well as the size of the powertrain and electrical energy sources. The second section tries to investigate and create energy management systems that take into consideration the dynamics of electrical energy sources and their operational condition.

The motivation and main contributions of this thesis are introduced in this chapter. The remaining sections of the thesis are structured as follows:

Structure of the thesis

In **Chapter 1** , State of the Art on Hybrid Electric Vehicles and Energy Management, we provide a detailed introduction to fuel cell electric vehicles (FCVs) and their complex characteristics. The chapter discusses the fundamental architecture of FCVs, examines the integration of hydrogen fuel cells with various energy sources such as electrical energy, and explores different design approaches for hybrid hydrogen vehicles. Additionally, it analyzes potential synergies between hydrogen and other energy sources, as well as the integration of various electrical energy sources.

In **Chapter 2**, a synthetic description of PEM fuel cell systems is provided, offering a valuable overview of the fundamental concepts and principles of this technology. The chapter also discusses supercapacitors, expanding the scope of applications and exploring potential advances and integration opportunities in this field. These insights contribute to the sharing of existing knowledge and highlight the significance of renewable energy technologies.

In **Chapter 3**, titled "Exploring the Essentials of the Design Process," we delve into the entire process of designing a fuel cell hybrid electric vehicle (FCHEV) that meets road traffic requirements. We then examine the mathematical models employed to choose our energy sources. Additionally, we provide clear diagrams depicting the theoretical and functional layout and investigate different energy conversion configurations.

Chapter 4 presents the research carried out in this thesis on energy management methodologies, focusing on the design of base layer and secondary layer controls that aim to steer the flow of energy from sources to load. The main objective of this chapter is to outline the control objectives that aim to optimize energy distribution within a storage device. To this end, two scenarios have been proposed, the first using fuzzy logic control (FLC) and the second applying frequency distribution, which have been presented and evaluated at a high level in the field of energy management. Next, the use of a backstepping sliding mode approach is explored as a low-layer control. In addition, the integration of an additional technique, Super-Twisting, is examined to assess its ability to improve the robustness of backstepping in Boost converter calculations. This comprehensive approach not only improves overall system efficiency, but also contributes to the advancement of energy management techniques.

We finish our contribution with a **conclusion** , and a peek into the future of our work.

List of Publications and Conferences

The main body of this thesis is based on the following papers:

• A. hamlat, M. h. sekour, M. mankour, M. yahiaoui, M. khalfaoui, and B. brahmi. Advanced Power Management and Control Using Fuzzy Backstepping Super-Twisting Controls Designed for Fuel Cell Supercapacitors Hybrid Power Systems for Traction Applications, *Journal of Control, Automation and Electrical Systems,*,2023/06/09 2023.

• A. Hamlat, M. Sekour, M. Mankour, and M. Khalfaoui. An Improved Energy Management System for Fuel Cell/Ultra-capacitor Electric Vehicle Based Fuzzy Logic Control,*" Artificial Intelligence and Heuristics for Smart Energy Efficiency in Smart Cities: Case Study: Tipasa, Algeria. Springer International Publishing, 2022*.

Chapter 1

State of the art on: Hybrid Electric Vehicles and Energy Management

The objective of the initial chapter is to provide an introduction to the diverse clean energy sources employed in an electric propulsion system, including the fuel cell and supercapacitor.First we will introduce environmental and economic challenges related to electric vehicles and hybrid electric vehicles.

Contents

1.1 Introduction

This chapter provides a comprehensive and detailed overview of fuel cell electric vehicles (FCVs) and analyzes their complex characteristics. The chapter begins with an explanation of the architectural foundations that define fuel cell electric vehicles. Subsequently, we consider the integration of hydrogen fuel cells with different energy sources, with a special focus on the combination of electrical energy sources. In addition, the chapter examines different design schemes for hybrid hydrogen vehicles and explores the area covered by other potential synergies between hydrogen and simple energy sources. Finally, we deal with the smooth integration of many electrical energy sources. We also provide an overview of the scientific literature on energy management strategies and examine the various proposed control mechanisms, including both classical methods and those based on non-linear models.

1.2 Fuel Cell Electric Vehicles Architecture

A fuel cell, a hydrogen storage unit, a battery, a unidirectional DC-DC converter for the fuel cell side, a bidirectional DC-DC converter for an auxiliary unit , a motor drive converter, and an electric motor comprise the energy transfer chain for FCEVs. Figure 1.1 illustrates the power-train configuration of a Fuel Cell Electric Vehicle (FCEV). During the operation of an FCEV, the Fuel Cell (FC) stack serves as the energy source for the DC-bus and maintains the required voltage level . The DC-DC converter unidirectional , directly connected to the FC, plays a crucial role in maintaining a constant DC-bus voltage and transferring the generated energy to the motor drive converter. The DC-AC converter, also known as an inverter, is responsible for supervising the motor speed and torque to ensure safe operation. Lastly, the electric motors, under the supervision of the drive controller, convert the electrical energy into mechanical energy.

1.3 Hydrogen Fuel Cell Electric Vehicles

Regarding the field of transportation, the use of hydrogen-electric vehicles has grown significantly to almost 35,000 FCEV all over the world, with close to 600 hydrogen refueling points getting ready by the last quarter of 2020 [1].Figure 1.2 is a pie chart illustrating the pattern of FCEV use in industrial nations up to the end of 2020. It shows that the South Korean government is the first country in the world to use FCEVs, as well as China, the USA, Japan and Europe.

FCEVs are the fruit of years of research and the development of many generations of electric and hybrid vehicles. Despite the technological similarities, the energy sources used are different.The energy

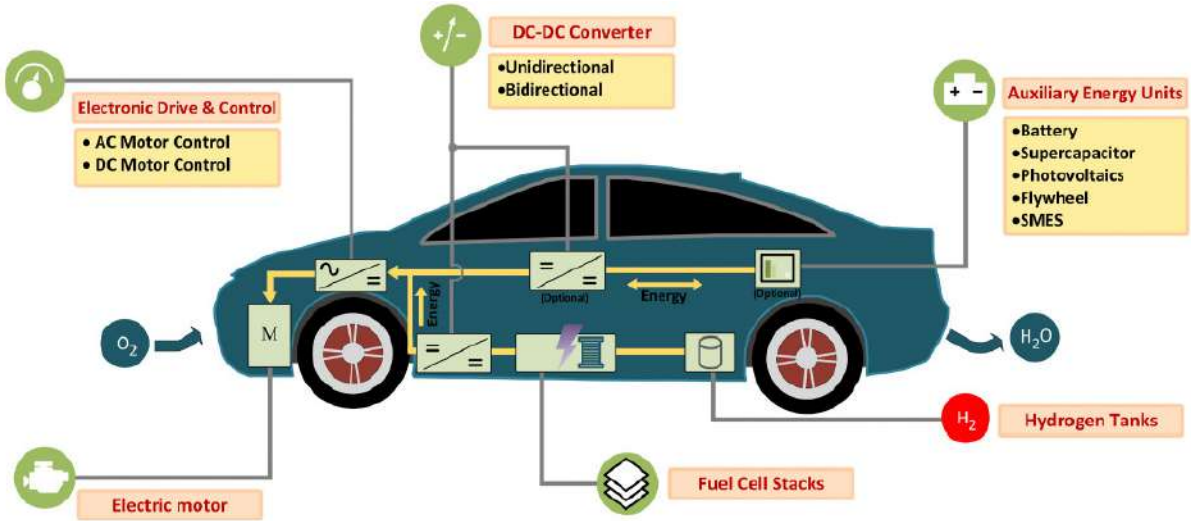

Figure 1.1: Main diagram of an FCEV power conversion structure, including auxiliary power supplies

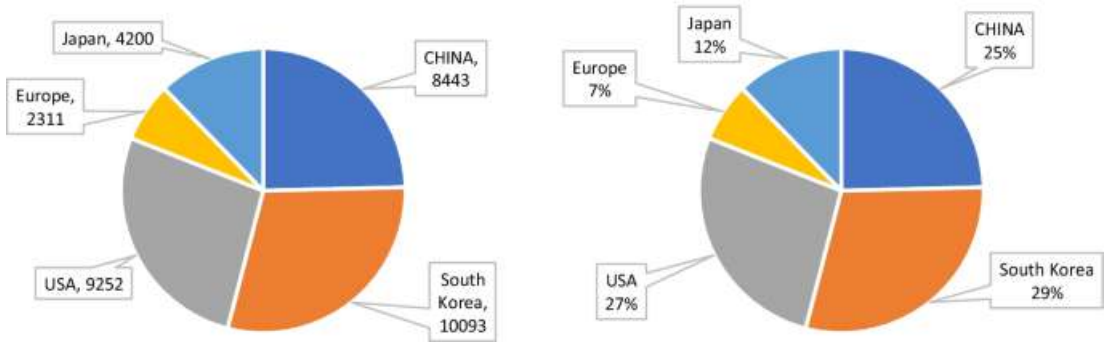

Figure 1.2: the pattern of FCEV use in industrial nations up to the end of 2020 [1]

from a fuel cell can be used immediately to power the vehicle's traction motor, or stored in a battery or supercapacitor. Regenerative braking is only possible if a storage system (batteries or capacitors) is installed. In the presence of such a storage system, the vehicle is described as a FCHEV (Fuel Cell Hybrid Electric Vehicle) [32]. From a technical standpoint, both electric vehicles (EVs) and fuel cell vehicles (FCVs) fall under the category of electric vehicles. EVs utilize electricity stored in a battery as their power source, whereas FCVs use a fuel cell that produces electricity from hydrogen [33]. While FCVs have the advantage of offering refuelling times comparable to those of petrol internal combustion engines, they face challenges such as limited infrastructure, high fuel costs and technical complexities related to storing hydrogen on board in a non-high pressure form. In addition, hydrogen production requires processes such as reforming, gasification or electrolysis [34].

1.3.1 Fuel Cell and Energy Sources Combination

Figure 1.3 depicts the categorization of Fuel Cell Electric Vehicles(FCEV) based on the utilized energy units. In FCEVs, the primary energy generation unit is the Fuel Cell (FC), accompanied by auxiliary power supply components. In hybrid configurations involving FCs , various energy generation and storage units are incorporated to complement the FC stacks. These additional energy sources include batteries, speracapacitors(SC), superconducting magnetic energy storage (SMES), photovoltaic panels, and flywheels. They serve as supplementary energy providers in FCEVs.

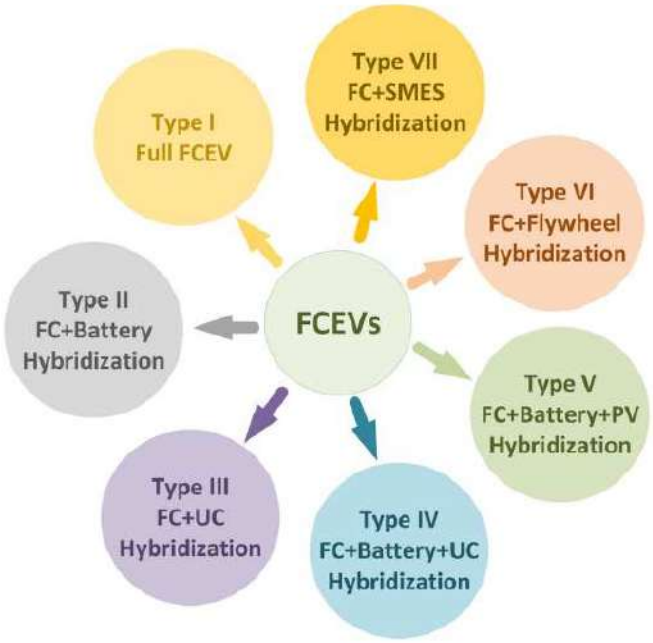

Figure 1.3: Types of energy sources combination systems implemented in FCEVs

Fuel cell powered vehicles can be classified into two main types: fully FC vehicles and hybrid FC vehicles. Various combination architectures can be found in the literature to accommodate these classifications. The categorization of FC-powered vehicles is as follows:

- Fully FC vehicles
- FC + Battery Hybridization
- FC + SC Hybridization
- FC + Battery + SC Hybridization
- FC + Battery + PV
- FC + Flywheel Hybridization

- FC + SMESSMES Hybridization

1.3.2 Fully Fuel Cell Vehicles

This type of vehicle uses a FC stack as a source of energy [35].The schematic 1.4 illustration shows the general configuration of a fully functional FCEV. It is based exclusively on the FC stack as the primary energy source, without any auxiliary energy sources. It has a simple structure consisting of a fuel tank, FC cell, DC-DC power converter, inverter and electric motor. These vehicles have a number of advantageous features, including long range, fast charging time, high efficiency, cold start capability, silent operation due to the absence of moving parts, uninterrupted power supply and low emissions. Complete FCEVs find suitable applications in a variety of fields, including low-speed vehicles such as forklift trucks, buses, trams and marine vehicles.In the modern day, fuel cells have also found their way into high-speed vehicles. To create high-speed vehicles, many adaptations can be made to the fundamental structure of the power-train. Major automakers such as Honda, Toyota and Hyundai are actively engaged in the development of high-performance fuel cells. Various energy management strategies are being implemented, focusing on aspects such as fuel efficiency, reducing energy losses and improving overall vehicle efficiency [36, 37].

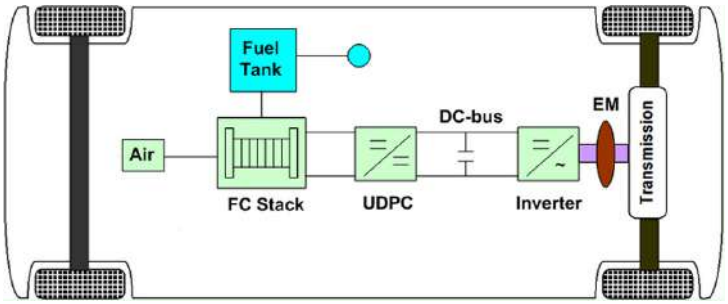

Figure 1.4: The drive train of a complete FCEV (Type I) [2]

1.3.3 Fuel Cell and Battery Hybridization

The most commonly used configuration for FCEV hybridization is the coordination of FC and battery units, called Type II . In this configuration, the FC is connected to the DC bus via a unidirectional DC-DC converter, while the battery is connected to a bidirectional DC-DC converter [38–41] , as shown in Figure 1.5. During the FC + battery hybridization operational process, initial start-up is facilitated by the battery to prevent the FC from operating in the low-efficiency range. This ensures that a high current is supplied to prime the electric motor [42]. Once the vehicle has been initially started, the FC is activated to keep the electric motor running. At the same time, the battery is charged to the required state of charge.

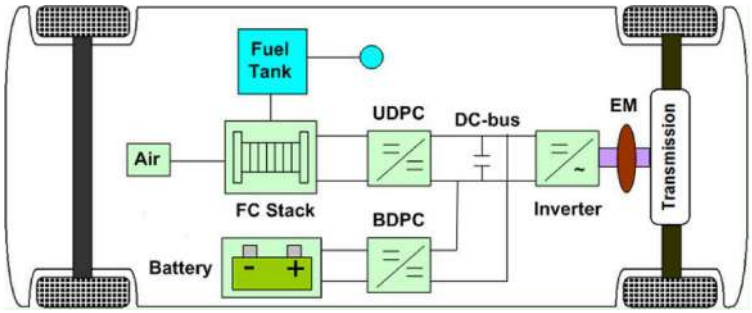

Figure 1.5: The FC + Battery combination drivetrain (Type II) [2]

1.3.4 Fuel Cell and Supercapacitor Hybridization

Instead of a battery, the Type III arrangement employs a supercapacitor as illustrated in figure 1.6 . The FC + supercapacitor combined typically serves to meet transitory power needs in emergency scenarios . Supercapacitors, however, are not ideal for long-term energy and power provision because to their poor energy density [43]. Voltage variations are common when charging and draining the supercapacitor. Impedance components must be introduced into the system to reduce these fluctuations while increasing the complexity of the system design. Furthermore, the increased complexity creates difficulties in regulating the power sources, limiting the practical uses of this architecture [44–46].

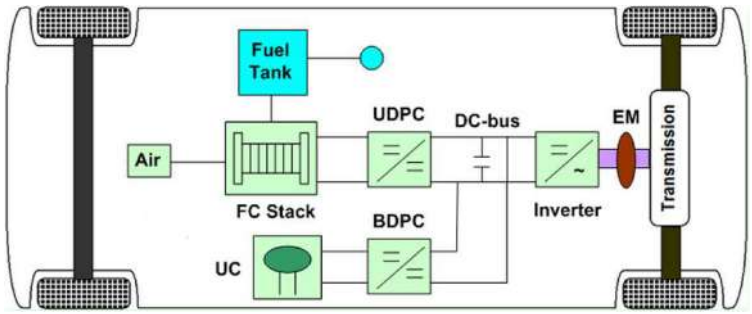

Figure 1.6: The FC + SC combination drivetrain (Type III) [2]

1.3.5 Fuel Cell ,Battery and Supercapacitor Hybridization

Differing from earlier hybrid configurations, the architecture involving FC + battery + supercapacitor (type IV) as illustrated in figure 1.7 features a primary power source (FC) alongside two supplementary components (battery and supercapacitor). This design combines the advantages of both FC + battery and FC + supercapacitor arrangements, ensuring a consistent power supply while also enhancing the FC's rapid response during transient conditions. Nonetheless, the diverse power sources necessitate intricate vehicle design and intricate control systems, which introduce complexity to the execution of this topology [47].

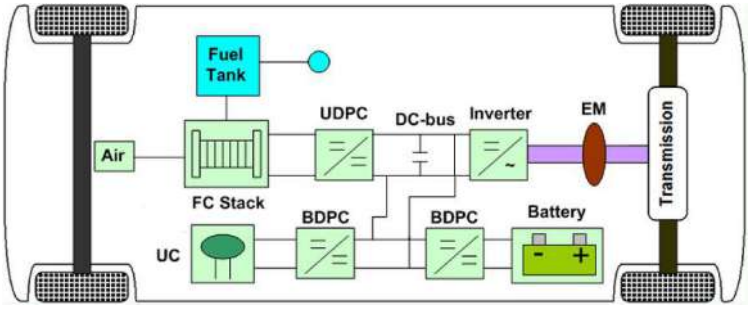

Figure 1.7: The FC + Battery + SC combination drivetrain (Type IV) [2]

1.3.6 Fuel Cell ,Battery and Photovoltaic Hybridization

Recently, photovoltaic panels have been combined with FC for FCHEVs. Photovoltaic panels provide electricity that varies according to the intensity of solar radiation, the temperature and the direction of the light. In this configuration, the FC acts as a primary energy source, while the photovoltaic panel acts as a supplementary energy source [48] [49].In addition, as shown in figure 1.8the DC bus connects the FC and the photovoltaic panel via unidirectional converters, while the DC bus connects the battery bidirectionally [48].In addition, the integration of photovoltaic (PV) panels, fuel cells (FC) and an auxiliary battery in a hybrid electric vehicle (HEV) enables high levels of energy and exergy efficiency to be achieved compared with systems without photovoltaic panels. As a result, this innovative vehicle power system has the potential to serve as an exemplary propulsion mechanism for environmentally conscious vehicles in the near future, addressing the concerns of technological progress and environmental preservation [50].The photovoltaic (PV) system, according to [51], recovers a total of 561 grams of hydrogen over a continuous driving time of 3 hours at a maximum power of 98.32 kW. This corresponds to around 11.2% of the tank's hydrogen storage capacity.

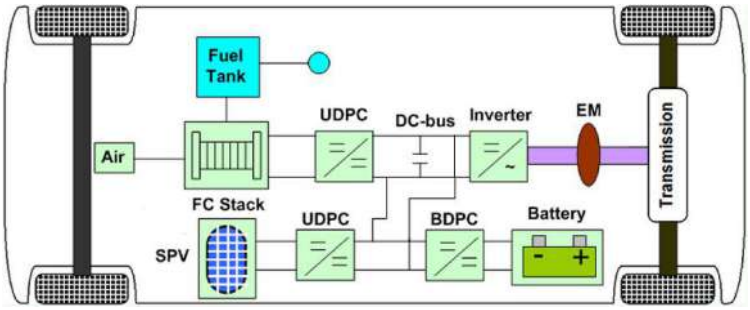

Figure 1.8: The FC + Battery + PV combination drivetrain (Type V) [2]

1.3.7 Fuel Cell and Flywheel Hybridization

In the comparative context of the previous topologies, Type VI presents a new FC + flywheel structure as illustrated in figure 1.9 . The current generator functions as the main energy source, as in the case of Type II, while the flywheel replaces the battery for energy storage. Flywheels offer higher charging speed, efficiency and performance than batteries [52].The Flywheel Energy Storage System FESS incorporates essential components like an electric machine, a bidirectional converter, a bearing, a DC link capacitor, and a substantial disk. Its principal advantage, setting it apart from other energy storage systems (ESS), resides in its impressive efficiency range spanning 90% to 95%. In the context of hybrid electric vehicles (HEVs) and electric vehicles (EVs), the flywheel functions as an energy reservoir, proving especially valuable during instances of demanding acceleration, particularly in scenarios involving steep inclines [50].The principal drawbacks of flywheels are as follows:

- Excessive weight and space requirements
- Inability to store energy over long periods of time

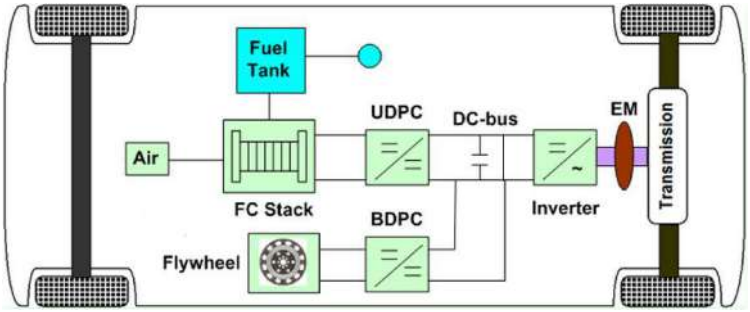

Figure 1.9: The FC + Flyweel combination drivetrain (Type VI)

1.3.8 Fuel Cell and Superconducting Magnetic Energy Storage System Hybridization

The powertrain of a FC + SMES hybrid (Type VII) is shown in Figure 1.10 . The Superconducting Magnetic Energy Storage System (SMES) uses a superconducting coil and direct current to generate a robust magnetic field for energy conservation [53]. A typical SMES installation comprises three fundamental elements: an energy conduction subsystem, a refrigeration and vacuum subsystem, and a unit containing the superconducting coil [54]. This technology relies on superconductors to eliminate resistance and enable efficient energy storage in the magnetic field. This approach enables efficient energy storage with short charge/discharge cycles and rapid energy conversion, making it a promising option for a variety of

applications [55].However, superconducting magnetic energy storage represents the most costly storage technology [56].

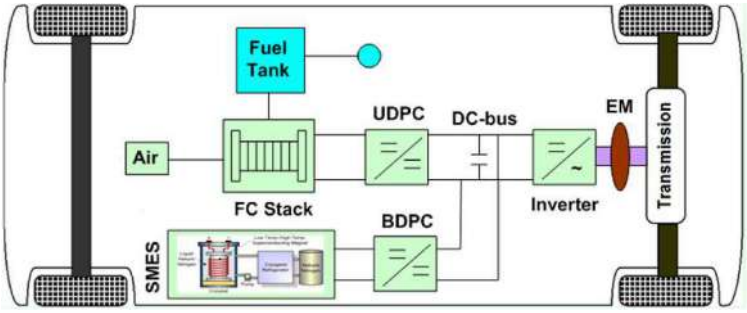

Figure 1.10: The FC + SMES combination drivetrain (Type VI)

1.4 Hybridization Hypothesis for Electrical Power Sources

The present work is concerned with demonstrating the hybridization structure of two or more electrical energy sources. Active and passive combination are the two approaches used to merge electrical energy sources into a system made up of several energy sources. This combination can be achieved using one or more converters . The integration of electrical energy sources in a multi-source system involves two approaches: active and passive combinations. This integration can be achieved by using one or more converters [57, 58]. The size of such an energy storage system is done based on unique operating conditions, taking into consideration many needs and establishing a balance between them. It is critical to guarantee that stored energy is used efficiently by avoiding divergent behavior of the energy storage system. To address these problems, hybrid energy storage systems containing several forms of energy storage have been created to better suit the diverse needs [59, 60]. In most instances, power is supplied by a single power source module that is directly linked to the powertrain through a DC bus, as seen in figure1.11a. Depending on whether a single traction motor or in-wheel motor systems are used, the power train may incorporate one or more inverters.Moreover, a large number of modules in series poses particular risks in terms of voltage balance. To reduce the number of modules, a DC-DC converter is usually installed between the power source and the drive train, as shown in figure 1.11b . This type of configuration also guarantees that the DC bus voltage is controlled by the DC-DC converter. The majority of systems studied in scientific research have been classified into two classes: passive hybrid energy storage systems (P-HESS) and active hybrid energy storage systems (A-HESS) .

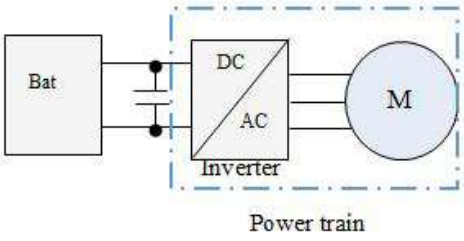

(a) without DC bus control

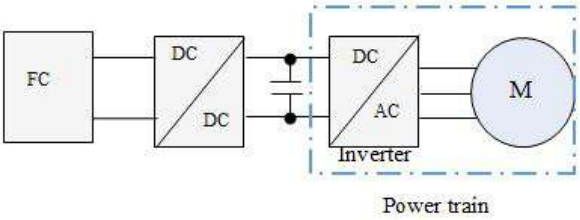

(b) with DC bus control

Figure 1.11: Configuration without an energy storage system

1.4.1 Passive Hybridization of Power Sources

The simplest hybridization solution involves combining two or more independent cell technologies directly in parallel. Figure 1.12 shows an example of this passive hybrid energy storage systems P-HESS using a combination of fuel cell storage and SC.The fuel cell and SC are passively coupled, without the need for an intermediate power electronic converter [44, 45].The sum of the piussance of both devices in the energy storage systemP_{fc} and P_{sc} is equivalent to the Power Load (P_{laod}) .In earlier studies [61, 62] HESS were investigated in which a SC is linked directly to a battery.The topology described is cost-effective, space-saving and lightweight, as it requires no additional power electronics. However, the dynamic response, voltage range and power distribution of the two power sources in this configuration are not optimized. [63]

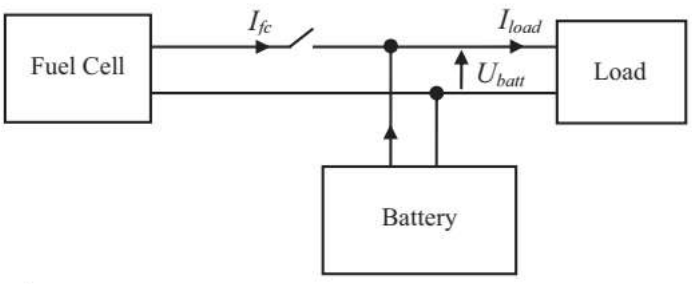

Figure 1.12: Exemple Passive hybrid energy storage systems [3]

1.4.2 Semi- Active- Parallel Topology

This configuration employs a single DC-to-DC converter associated to just one of the individual ESSs, with the other ESS directly connected to the DC- bus. An extra power electronic system increases the cost and takes up more space. This system, on the other hand, can regulate and release the energy required for applications [64–66]. A DC-DC converter is used to control the power output of the fuel cell with an appropriate control algorithm (see Fig. 1.13). The power exchanged by the HESS with this topology is given by:

$$p_{hess} = \kappa p_{fc} + p_{sc} \tag{1.1}$$

Here, κ refers to the HESS control factor and defines the power share of the supercapacitor.The system's peak power requirements is met by the supercapacitor and the remaining need is met by the fuel cell [67].. Despite providing some flexibility, it has certain drawbacks:

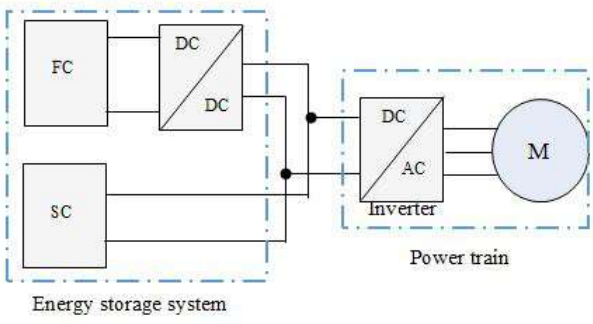

Figure 1.13: Semi active hybrid energy storage systems

- When a supercapacitor is directly coupled to the system, the DC bus voltage changes.
- When connected to a supercapacitor, the DC-DC converter must be built for mitigating high power peaks [67].

1.4.3 Active Hybridization of Power Sources

It is necessary to isolate the energy storage devices so that they operate as efficiently as possible and meet their individual specifications. DC-DC converters are used in this configuration in order to control both the fuel cell, known as the High Power Sourcehigh power source HPS, and the supercapacitor, known as the High Energy Source HES as shown in figure 1.14. This configuration allows for easier to operate both power generation systems, improving the energy supply control strategy and lowering operating costs. Furthermore, this architecture assures that the energy management approach may take use of the comple-

menting qualities of HPS and HES. Furthermore, energy management systems provide an opportunity to use a variety of control processes. All these benefits, nevertheless, come at the penalty of higher power conversion losses and higher converter prices [67]. The power transferred by HESS with this topology may be calculated as follows:

$$p_{hess} = \kappa p_{fc} + \beta p_{sc} \tag{1.2}$$

where κ and β denot the controllability of HPS and HES respectively. At present, this topology has been widely used in hybrid energy storage applications.There are two ways of using these converters: in parallel and in cascade [68].The architecture with parallel converters is more attractive in terms of efficiency. HPSpower flows through a single converter, whereas it has to pass through two converters in the cascaded converter architecture. Dimensioning in relation to the cascade converter structure is less advantageous than that of the parallel converter architecture.

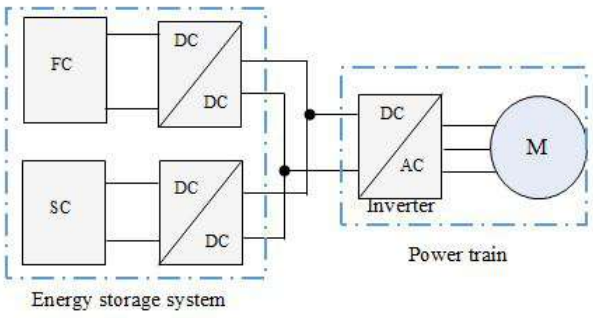

Figure 1.14: active hybrid energy storage systems

Electric traction applications have seen a considerable increase in the use of active parallel topology. This topology offers a number of advantages, including

- Greater adaptability thanks to independent control of high-power and high-energy sources.
- The possibility of applying a variety of control techniques
- Independence of ESS voltage levels from system voltage.
- The system can tolerate malfunctions by separating the ESS from the system via converters.

To facilitate the implementation of energy management methods, the use of a parallel architecture is desirable. Consequently, the hybrid systems analyzed will be built on this particular structure. Bidirectional DC-DC converters, in particular Buck-Boost converters, are used to interface with high-power sources. A boost converter is connected to the fuel cell, which serves as a high-power source. In this

study, particular attention is devoted to multi-source systems involving two independent power sources and adopting a parallel design.

1.5 Energy Management Strategies

The fuel cell hybrid system overcomes challenges such as the slow dynamic response and inability to recover braking energy encountered by conventional pure fuel cell vehicles [69]. The Energy Management System (EMS) is responsible for intelligently distributing the energy flow and pathways of each energy source. The fundamental roles of the EMS are to meet energy requirements for normal driving and to ensure equitable energy distribution. Consequently, it is essential to meticulously refine the design and control strategies of the energy management system to optimize the various objectives [70].

In fuel cell electric vehicles, energy management involves the management of DC-DC converters and the integration of fuel cells, batteries, supercapacitors and solar energy. These methodologies aim to distribute energy efficiently between these different sources, guaranteeing optimum vehicle performance and autonomy. They also help to manage fluctuations in energy demand and ensure a stable, consistent supply of the various components of the electric propulsion system [71].

In a recent review by Mohammed et al. [72], various Energy Management Systems (EMS) that have been widely acknowledged for achieving this objective are examined. Additionally, Li et al. [73] introduced a novel approach in their paper, integrating the EMS with the State Machine Strategy (SMS) to implement droop control for the FC-SC hybrid tramway. This innovative process not only enhances the system's hydrogen consumption but also significantly boosts its overall efficiency. In the paper [74], a comprehensive examination is provided for a Power Management Control (PMC) system developed specifically for electric vehicles. This system's crucial target is to guarantee a continuous power supply, and it contains two different algorithms. The first approach focuses on to controlling power flow via different storage sources, whilst the second algorithm is specifically designed to recover extra power from fuel cells. These results' practical importance has been shown by their effective implementation in real-time applications. In the paper [75], an FCEV design integrating a fuel cell, a supercapacitor and a battery is presented. The battery is directly connected to the DC bus and acts as an energy buffer. To distribute power between the different sources, the technique uses a frequency-division approach. The authors provide experimental results demonstrating the effectiveness of this online power distribution method. Considerable work has gone into exploring the efficiency that fuzzy logic control can bring to Hybrid Energy Storage Systems (HESS), in particular for their ability to integrate multiple energy storage technologies, thereby improving overall performance. In the paper by Naderi et al. [76], the researchers detailed the devel-

opment of a lab-scale Hybrid Battery-Supercapacitor Storage (HBSS) system and conducted an analysis of its experimental integration within a lab-scale hybrid microgrid. The study's outcomes offered valuable insights into the viability and practicality of HBSS in real-world power systems, particularly microgrids. As a result, this research contributes significantly to the existing literature on implementing energy storage systems in microgrids, which plays a crucial role in advancing sustainable and efficient power systems [77]. Fuzzy logic, renowned for its efficacy in controlling nonlinear and intricate systems, has gained widespread usage. In various applications, recent advancements in fuzzy logic controllers have emerged. For instance, the Fuzzy 1+Proportional+Derivative-Proportional +Integral F1PD-PI controller was introduced in a recent study by [78]. Another notable controller is the genetic-based fuzzy logic estimator proposed in [79], specifically designed to mitigate the impact of saturated-regulator operation in brush-less DC motors. Additionally, the Fuzzy Logic Estimator (FLE) was developed as an expert control approach to reduce the current ripple of the brush-less DC motor drive, as stated in [80]. The authors of the article [81] have proposed a series fuzzy control strategy SFCS, which uses fuzzy control to reduce the rate of load variation in FCs and limit their degradation. Based on the simulation results, SFCS is capable of maintaining the load changing rate of FCs within acceptable limits without compromising vehicle operating costs. The study also found that by optimizing fuzzy control, it is possible to enhance the fuel efficiency of vehicles.

In paper [82], an energy management technique for series-parallel hybrid electric vehicles was put forward. The strategy is based on intelligent fuzzy logic and considers torque demand, battery state of charge, and regenerative braking as primary inputs. By regulating torque, the engine and motor are maneuvered to operate efficiently. The study presents simulation and experimental results to support the proposed strategy. An adaptive energy management of a battery-supercapacitor energy storage system for electric vehicles is presented in [83]. The approach is based on flexible perception and a neural network and aims to reduce the operating cost of the hybrid battery/SC storage system while responding to real-time driving conditions. Simulation results show that the EMS can achieve a cost optimization efficiency of over 97% compared to offline benchmarks. the neural network element of the technique, on the other hand, necessitates a huge quantity of training data and is susceptible to overhead. A basic strategy for ensuring effective power distribution in fuel cell electric vehicles is the fuzzy logic controller. In paper [84] the usage of an FLC in connection with an EV is discussed, with motor current, DC link voltage, and SC voltage as inputs and battery power and SC power as outputs. A fuzzy technique was employed to achieve the battery/SC energy storage system. Moreover, a Back-stepping Direct Torque control BS-DTC method as well as a (Space Vector Modulation)(SVM) technique were presented to

enable decoupled torque and flux control of the PMSM machine.

Figure 1.15 provides a classification of the power management strategies involved .The following section reviews the objectives of process and the methods used to improve the efficiency of energy management systems.

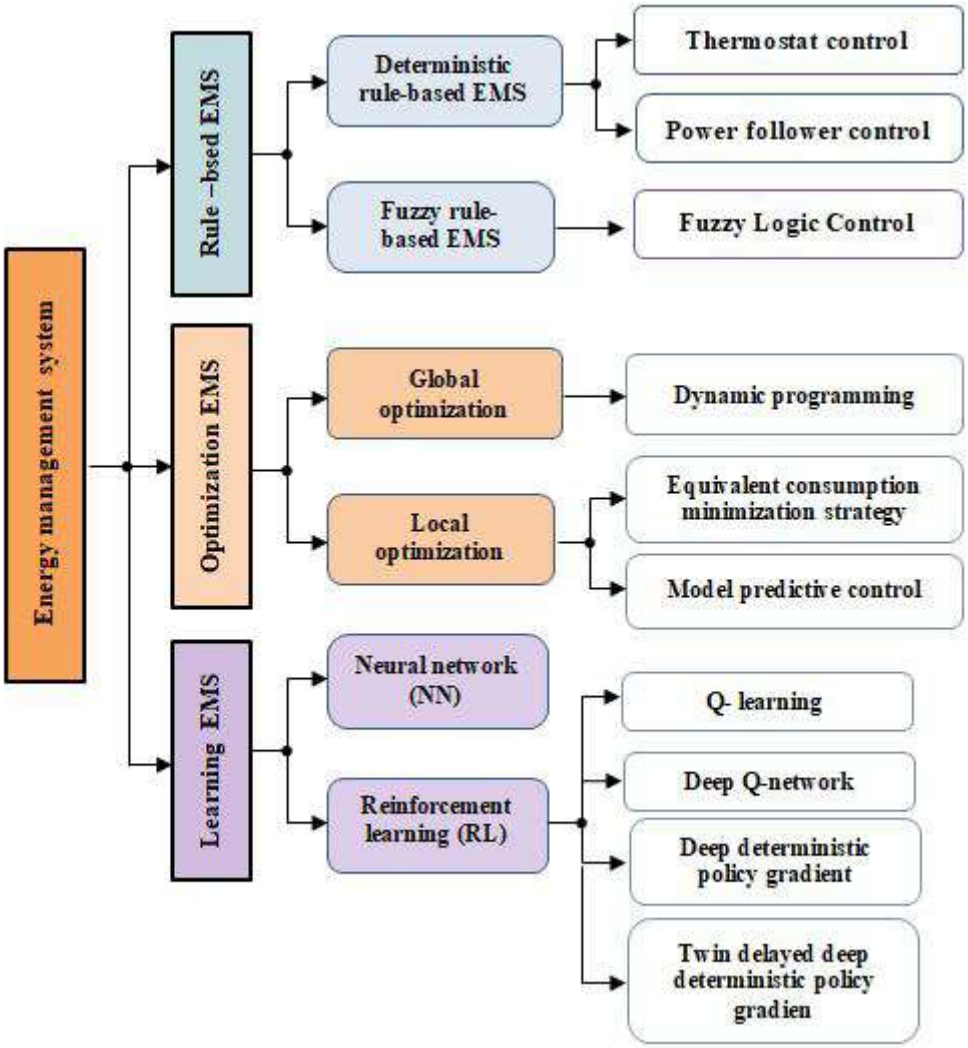

Figure 1.15: Classification of Energy Management Strategies

1.5.1 Rule-Based Methods

The rule-based methods (RBM) typically relies on a rule table and system state parameters to determine power distribution. The rule table is typically constructed based on experimental findings, engineering expertise, or mathematical models [85].Generally, this form of EMS offers benefits like low computational complexity, strong real-time performance, and independence from driving condition information [72].These advantages have contributed to the extensive adoption of rule-based EMS in commercial Fuel Cell Hybrid Electric Vehicles (FCHEVs), including models like Toyota Mirai [86]. Rule-based tech-

niques are further classified based on rule features into frequency separation methods (FSMs) [87] , fuzzy logic methods [88] , and deterministic approaches [89].

The Fuzzy Logic Control (FLC) method employs IF-THEN rules and membership functions, giving it the benefit of being model-independent and flexible. despite the absence of significant technical knowledge, control performance could have limitations and differentiate from desired outcomes. A rule-based Energy Management System (EMS) is suitable for real-time power generation and distribution, but it significantly relies on calibrating parameters and thresholds, limiting its usefulness in real-time conditions. Furthermore, because this rule-based EMS does not take into account a variety of operating situations, the fuel cell's lifespan is reduced [90].

In Energy Management Systems (EMS), the deterministic rule-based method generates control rules for input/output variables within a table, which it utilizes to govern energy flow . The thermostat control strategy TCS and power follower control PFC are two notable examples of this method. This deterministic rule-based technique is often regarded as the most practicable approach to energy management due to its simple rule construction.

The power frequency approach is centered around utilizing a series of frequency-based filters to effectively allocate traction power among the various sources within a vehicle. The determination of the cut-off frequency for these filters is rooted in the analysis of source responses. Once this allocation frequency is established, a reference signal is generated. The purpose of this signal is to maintain source responses within their prescribed limits, and this is achieved through the use of frequency separation methods [91]. In Literature [91], the authors propose and evaluate a new online Energy Management System (EMS) based on the improved power frequency method. This system's principal goal is a couple of things: first, to guarantee that load requirements are satisfied, and second, to increase the operating efficiency of a fuel cell electric vehicle (FCEV).Meanwhile, [87], on the other hand, focuses on a crucial component of energy management, notably the appropriate size of hybrid energy storage systems. This is done by implementing a strategic energy management method based on the frequency separation principle.

1.5.2 Energy Management Technique Based on Optimization

Due to the constraints of RBM, experts have decided to use an optimization-based energy management strategy OEMS in order to fulfill FCHEV's significant working objectives. Using the optimization-based energy management technique, an optimization framework consisting of one or more objective functions restricted by multiple operational constraints is commonly utilized [92].However, an optimization-based EMS becomes necessary when the ultimate objective is to decrease fuel consumption, alleviate fuel cell

deterioration, and even minimize the total operating expenses of the hybrid power system [90].This specific form of EMS essentially creates a target function by leveraging the operational traits of the hybrid electric system. It uses the system's state variables as constraints and then seeks to minimize this objective function through an optimization technique [93]. There are two main approaches: global optimization, which includes widely used methods like dynamic programming, and local optimization, which encompasses techniques like the standard equivalent consumption minimization strategy and model predictive control.

The use of Dynamic Programming (DP) as a global optimization technique for creating EMS in Fuel Cell Hybrid Electric Vehicles (FCHEVs) is common. DP is often applied to minimize fuel consumption and handle sources degradation in FCHEVs. However, it's acknowledged that DP is better suited for specific driving cycles with high predictability due to the computational burden and inconsistent performance when applied to various driving cycles [94].

At the local optimization , approaches such as Equivalent Energy Consumption(EEC), Pontryagin's Minimum Principle (PMP) and Predictive Horizon (PH) provide achievable methods for approximating the performance of global Optimal Energy Management Systems (GOEMS) . These local approaches of EMSs have easier topologies, lower processing requirements and are easier to deploy online [4].

1.5.3 Learning-Based Methods

The Energy Management System (EMS) that relies on learning incorporates neural networks (NN) and reinforcement learning (RL). To create the NN, NN-based EMSs must choose typical characteristics in various operating situations as model inputs and efficient power management as model outputs [90, 95].It is essential to guarantee a constant and reliable supply of data in a variety of driving conditions and environments. In addition, the systems would require sophisticated algorithms and computing capabilities [96–98].

In contrast to neural network-based energy management systems, reinforcement learning RL-based energy management systems are capable of rapidly deriving appropriate energy management systems, even when working with limited data [90]. The rise of Reinforcement learning as a notable trend in energy management, outranking conventional methodologies, emphasizes its emulation of human learning strategies and its dependence on accumulated experience to enhance the performance of decision-making systems [99]. When using the typical reinforcement-learning approach, the agent acquires its behavior through a process of trial and error in interactions with a dynamic environment. The agent receives feedback about the environment's state and then selects an action to produce as an output. This chosen action

Figure 1.16: In the reinforcement learning framework, an agent performs a sequence of actions, with each action resulting in both a reward and a new state

modifies the environment's state and is further reinforced by a value. The agent's task is to select actions that maximize the long-term sum of reinforcement values, and it can learn to do this through systematic trial-and-error processes and a variety of algorithms [100].The basic reinforcement learning process is shown in figure 1.16 .

The merits and demerits of the methods are summarised in Table 1.1 .

1.6 Fuel Cell Hybrid System Controllers

The Energy Management System (EMS) acts as a master controller, attempting to maintain the current performance of the FCHEV at an optimum level in terms of fuel utilization and source depletion. The converter controller, on the other hand, is responsible for ensuring stable and efficient vehicle performance [101]. This secondary control system provides accurate supervision of the EMS reference signals. Several control mechanisms are proposed, ranging from classical methods to approaches based on non-linear models.

1.6.1 Classical Methods

The hybrid power system encounters challenges due to the non-linear behavior of power sources, converters, and loads. While the EMS is responsible for generating traction power, it faces difficulties in addressing power flow concerns [102]. Consequently, researchers are actively exploring various control strategies for multi-source hybrid power systems. One such proposed linear control strategy, introduced in [103], implements a PID control strategy to regulate the output power of the battery and supercapacitor within the HESS. However, this approach has limitations as it does not consider the influence of temperature and polarization on the battery state, potentially leading to decreased control performance in scenarios where there are significant speed variations during vehicle operation due to local lineariza-

Table 1.1: Merits and Demerits of the approaches in existing literature

Methode		**Merits**	**Demerits**
Rule-based	Fuzzy logic	With real-time parameter-sthe robustness of the system is ensured	Extended operating time
		Effective for reasoning in physical frameworks	There are only a few input parameter
		Low hydrogen consumption	Requiring expert knowledge to define fuzzy rules
	Deterministic rule	Easy and simple to use control	A table of rules with human reasoning under perfect circumstances is needed
		Low initial cost	Lack of precision
Optimization based	Online	localize the total optimization issue	High computation times
		reduce fuel consumption	Requirement for an accurate cost function
		Appropriate for real-time analysis	
	Offline	Costs of fundamental techniques reduced	May not be suitable for complex powertrain systems
		Improved performance on complex problems	Not appropriate for real-time analysis
		Calculation costs reduced	Driving cycles data necessary
Learning-based	Learning	Unnecessary absolute knowledge model	Precise data mining is difficult and time-consuming

tion [104]. Designing a non-linear strategy can enhance effectiveness, particularly when integrated into a real-time controller [105].

1.6.2 Model Predictive Control Methods

For industrial applications, Model Predictive Control (MPC) has proved to be a wise choice among advanced control techniques, which go beyond standard PID control [106]. Indeed, MPC is now widely adopted in the industrial sector as an effective means of solving complex multi-variable constrained non-linear control problems [107]. Among the features of these controllers is the fact that they rely on a system model to predict the future behaviour of variables over a predefined time horizon, in order to guide optimal actions by minimising a cost function [106].One of the main advantages of MPC is its

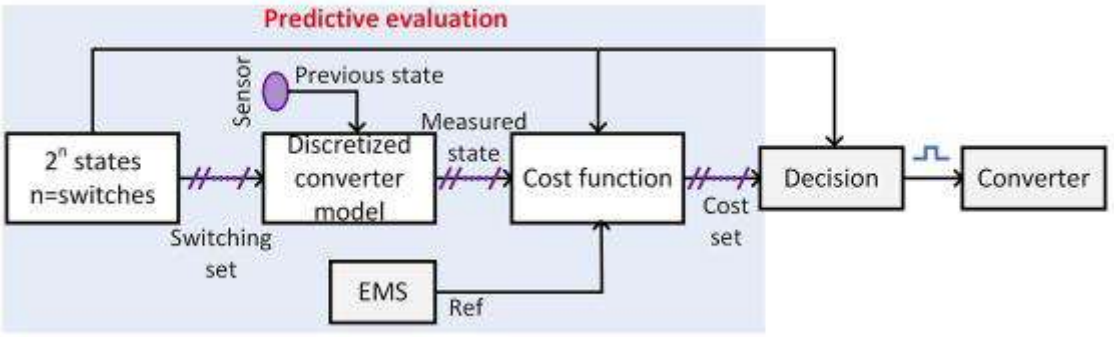

Figure 1.17: MPC operating concept entails employing a discrete converter model [4]

ability to function effectively despite the stringent constraints of a real controller. However, the downside of MPC's advanced algorithm is that it takes longer to operate when compared to other controllers [108]. The following steps should be followed to design a finite MPC control set for the control of a power converter [106]:

- Modeling of the power converter identifying all possible switching states and its relation to the input or output voltages or currents.
- Defining a cost function that represents the desired behavior of the system.
- Obtaining discrete-time models that allow one to predict the future behavior of the variables to be controlled.

Each switch comprises two switching states , and the combined number of all possible states is equal to the total number of switching states within the power converter.Typically, the total number of switching states N is:

$$N = x^y \tag{1.3}$$

where x represents the number of possible states for each converter leg, and y denotes the number of phases, or converter legs. as seen in Figure 1.17 The primary operating concept entails employing a discrete converter model to anticipate the states along the whole switching horizon ($2n$ switching states; n=switches). The cost function is calculated by comparing the measured states to the reference signals (from the EMS), allowing the least costly switching state to be selected in real time.

1.6.3 Nonlinear Methods

Various control design techniques rely on Lyapunov stability, and among them, the backstepping methodology stands out as a systematic approach for creating control tasks that track desired reference signals

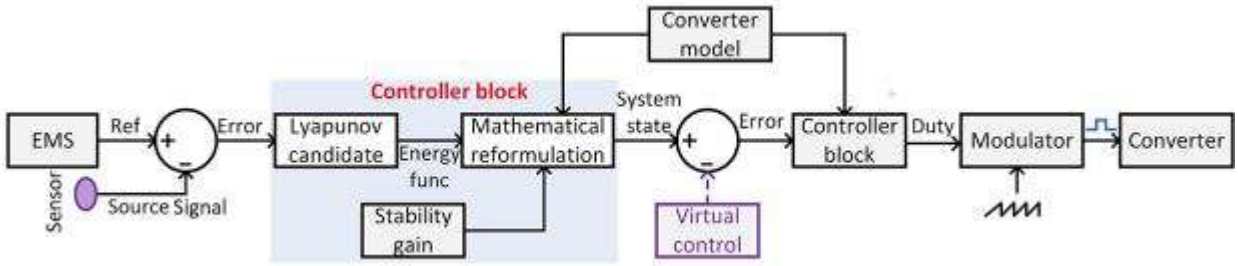

Figure 1.18: Typical backstepping concept employed as a secondary controller [4]

by selecting suitable Lyapunov function candidates [109]. To mitigate chattering, an undesirable behavior in numerous frameworks, a higher-order sliding mode controller called Super-twisting can be employed [110]. In paper [105], the authors used global sliding-mode integral control and a fast reaching law to derive the output of a boost converter interfaced with a PEMFC. Simulations were carried out, followed by experimental testing. The results showed that the integral global sliding-mode controller exhibited superior robustness to the other controllers tested during dynamic changes. This is evident in the better overshoot and undershoot values obtained by the global sliding mode integral controller. The paper [111] introduces a backstepping super-twist sliding mode control (BS STSMC) controller tailored for a four-phase interleaved boost converter (IBC) integrated with a proton exchange membrane fuel cell PEMFC. The controller comprises two loops: an inner loop employing a backstepping algorithm to ensure inductor current reference tracking, and an outer loop generating the reference current using a super-twisted sliding mode algorithm (STSMC). The sliding region is determined by the discrepancy between the output voltage and the reference voltage. Figure 1.18 displays a general representation of a backstepping-based secondary controller.As shown in Figure 1.18, a stabilized Lyapunov controller is first used to minimize the error between a reference signal and a controlled state, thus obtaining a corresponding residual state of the system. Next, a virtual controller is selected according to the system state, supported by an embedded controller. This total stabilization results in a viable duty cycle, which is modulated and converted into a digital signal before being fed into the matching converter.

1.7 Conclusion

In the end, this chapter has offered a thorough introduction to fuel cell electric vehicles (FCVs) and its complex properties. We began our investigation by explaining the fundamental architecture that defines FCVs. Following that, we explored the integration of hydrogen fuel cells with diverse energy sources, with a focus on electrical energy sources. The present chapter additionally reviewed several hybrid hydrogen vehicle design schemes and investigated potential interactions between hydrogen and simpler energy

sources. We also reviewed a simple integration of various electrical energy sources and provided a review of the current academic work on energy management systems. Additionally, we reviewed a number of potential control strategies, including both.As this research progresses, the following chapters will build on this foundation, delving deeper into these areas and offering useful insights into the current state of fuel cell electric vehicles. The aim is to contribute to the growth of knowledge in this field, while highlighting future prospects and problems.In the next chapter, we will give an overview of fuel cells and go into their detailed description. Practical applications and potential future developments will be presented.

Chapter 2

Overview of Fuel Cells and Supercapacitors

In this chapter, we embark on an fascinating path through the history and diverse applications of fuel cell technology. From early discoveries to cutting-edge developments, fuel cells continue to shine as the engine of sustainable energy for a greener, cleaner future.

Contents

2.1 Introduction

Three decades ago, hydrogen was recognized as a central and indispensable component of a decarbonized and sustainable energy system, offering safe, cost-effective and environmentally friendly energy solutions. Today, hydrogen is considered by energy experts to be the least secure and least influential factor in the global energy landscape. Despite its potential as a viable alternative fuel, hydrogen is perceived as having unfulfilled promises and limited tangible results. Nevertheless, hydrogen remains poised to play an important role in achieving low-carbon energy goals [112].

Both fuel cells and batteries transform chemical energy into electrical energy, require an electrolyte and an external load, and may be stacked to enhance power and voltage. Their key distinction is the type of their electrodes. Batteries employ metal anodes and metal oxide cathodes, whereas fuel cells use external agents and do not consume any of the cell's parts. Batteries must be recharged or replaced because their anode and cathode become empty, but fuel cells do not require recharging as long as the reactant is available. Because of the constant charging and discharging, batteries have a shorter lifespan than fuel cells [113].

2.2 History of Fuel cell

Fuel cells, batteries, and supercapacitors are crucial in meeting humanity's energy requirements. In order to gain valuable insights into the development of current and future energy technologies, a review of the history and progress of fuel cells will be presented in the following paragraphs.

2.2.1 19th Century: The Beginnings:

German chemist Christian Friedrich Scho nbein carried out the first scientific study of the fuel cell phenomenon in 1838, and his findings were published in the January 1839 issue of Philosophical Magazine. In contrast, the author claims in reference [114, 115] that Sir William Robert Grove invented the hydrogen fuel cell. Sir William Robert Grove experimented with electrolysis and discovered the possibility of producing electricity by reacting hydrogen and oxygen. The process of decomposing water into hydrogen and oxygen using electricity (water electrolysis) was identified years before the fuel cell, by British scientists Sir Anthony Carlisle and William Nicholson in 1800 [115].The Figure 2.1 above appear on page 272 of the Philosophical Magazine and Journal of Science, 1843, with William Grove's letter "On the Gas Voltaic Battery." [116]

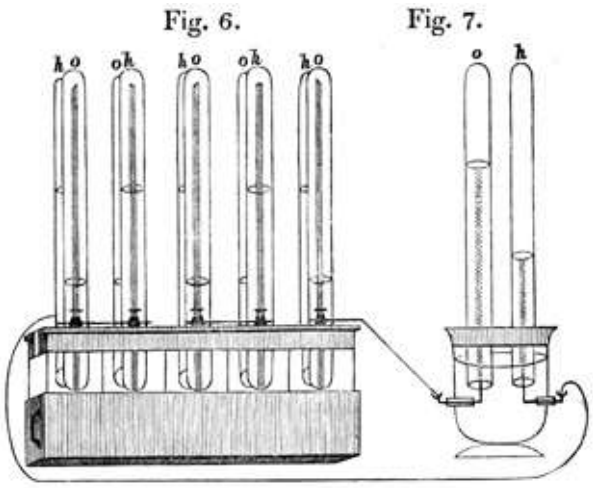

Figure 2.1: William Grove's drawing of an experimental "gas battery" from an 1843 letter [5]

2.2.2 The Evolution of Fuel Cell Technology in the 20th Century

In the late 19th and early 20th centuries, William W. Jacques and Emil Baur were two leading researchers in the field of fuel cells. In 1921, Baur achieved a first milestone by building the first molten carbonate fuel cell. Meanwhile, Jacques focused on the development of high-power systems, including a 1.5 kW fuel cell . In the 1930s, Baur conducted experiments on high-temperature solid oxide electrolytes. Their contributions played a key role in the advancement of fuel cell technology at that time [115].

At the beginning of 1933, the advances made by Thomas Francis Bacon marked a milestone in the development of the fuel cell. Bacon succeeded in developing the first functional fuel cell using hydrogen and oxygen to generate electricity in a practical way. This electrochemical device converts oxygen and hydrogen directly into electricity. Bacon's research initially focused on alkaline fuel cells, establishing the foundations for this promising technology [115]. In 1955, Thomas Grubb, a scientist at the General Electric Company (GE), improved on the initial idea of the fuel cell. His method involved using a membrane of ion-exchange sulfated polystyrene as the electrolyte. Three years later, Leonard Niedrach, another GE scientist, devised a method for placing platinum on the membrane [115].

The work of G.V. Elmore and H.A. Tanner introduced a phosphoric acid fuel cell in 1961.The electrolyte composition included 35% phosphoric acid and 65% silicon dust fixed on Teflon. They found that, compared with acid batteries, electrochemical degradation did not build up during operation of the fuel cell itself. Moreover, the fuel cell can be powered by air instead of pure oxygen. They claim that their phosphoric acid fuel cell can function for 6 months at 90 mA/cm2 and 0.25 V without any apparent deterioration [115]. In 1960, when NASA was looking for an alternative energy source for space flight, the development of proton exchange membranes marked the renaissance of fuel cells. The first fuel cells

faced difficulties such as their small size, high cost and limited availability. Despite this, NASA's interest and the energy crisis of 1973 revitalised fuel cell research and paved the way for their successful implementation in a variety of applications [117]. NASA's Jet Propulsion Laboratory, jointly developed in 1990 in conjunction with the University of Southern California, features a battery of methanol [115].

2.2.3 The 21st Century: Present Day

Numerous companies are now working on applying fuel cell technology in numerous areas, notably automotive applications [113]. Fuel cells are widely utilized in aircraft, ships, trains, buses, automobiles, motorcycles, trucks, and even forklifts. Furthermore, the market for fuel cells in mobile phones, laptops, and other portable electronic equipment is expanding. Furthermore, larger-scale organizations such as hospitals, police stations, and banks are using fuel cell systems to produce electricity on their arguments [115].

2.3 The Different Applications of Fuel Cell Technology

Fuel cell technology has found numerous applications in a variety of sectors. Indeed, fuel cells are revolutionizing the way energy is produced, whether in vehicles, portable appliances or high-volume construction. In addition to reviewing the many uses of fuel cell technology, the following section describes some of the ways in which fuel cells are being used in the automotive, communications, electronics and infrastructure sectors.

2.3.1 Stationary Power Plants

Fuel cells are critical in power production for residence, commercial, and industrial uses. They are utilized for both grid-independent (stand-alone) and turbine-assisted power generation. Stationary fuel cells are used in emergency power supply , and distributed generation of energy or steam [118]. figure 2.2 show a Convion C50 biogas Solid Oxide Fuel Cell (SOFC) system has been installed at Collegno, Italy, marking the commencement of Convion's demonstration of their fuel-flexible C50 SOFC co-generation unit at an industrial biogas facility. This milestone represents a significant step towards the commercialization of the product.The SOFC is expected to produce approximately 175 kW of electricity. It will be deployed at the SMAT Collegno Waste Water Treatment Plant [1]in the Turin area and will provide around 30% of the site's electrical consumption and almost 100% of its thermal requirements [6, 119].

[1]The Collegno waste water treatment plant is a medium sized facility serving a population of approximately 180 000

Figure 2.2: First Convion C50 SOFC module [6]

2.3.2 Transportation Applications

The transport industry is one of the key factors in the advancement of green energy technologies. Indeed, the transportation sector is responsible for 17% of global greenhouse gas emissions each year. It is predicted that over 50% of new public and freight vehicles will be powered by fuel cells and batteries. However, given current technical complexity, the production cost of a medium-sized FCEV is still around 50% higher than that of its internal combustion engine equivalent [120].During the previous 30 years, most manufacturers have been actively involved in fuel cell car research and development . Because of autonomous control and optimal operating points and the cold start capabilities of fuel cells under low-temperature settings , the proton exchange membrane fuel cell appears to be the ideal option for car applications [121]. Hyundai, Toyota, and Honda, among others, have stated that they will produce a large number of FCEVs in 2020. Hyundai Nexo produced 63% of total sales in 2019, Toyota Mirai 32%, and Honda Clarity Fuel Cell under five percent. In the applications in the public transportation the bus is the most potential vehicle type for large-scale adoption of fuel cell technology in the automotive industry.Figure 2.3 provide a cutaway model of the popular fuel cell vehicles on the market, the Toyota Mirai and the Hyundai Nexo fuel cell electric vehicle. The key advantages of buses over automobiles are their power requirements, operation schedule, available space, and proximity to refueling stations. Because of

the large size of a conventional bus, massive volumes of hydrogen may be easily stored onboard, often on the roof [121].

(a) A cutaway model of the Toyota Motor Corp. Mirai fuel cell electric vehicle. Photographer: Toru Hanai/Bloomberg

(b) A cutaway model of the Hyundai Nexo fuel cell electric vehicle

Figure 2.3: Fuel cell vehicles models

2.3.3 Portable Applications

The rising importance of telecommunications, computers, the Internet, and social networks in today's society, highlighting the necessity for a steady electrical supply. Because of its advantageous properties such as high energy density, durability, and cost-effectiveness, fuel cells have been recognized as potential portable power systems. Portable fuel cell applications are primarily focused on two markets: Portable power production for personal outdoor activities and consumer electronics. The major markets are personal outdoor activities, modest commercial purposes, and disaster relief operations. Fuel cells are a greener alternative to typical generators, with no environmental effect and noise pollution. Fuel cells are

seen as potential in the second market for powering numerous consumer electrical devices in the future because to their versatility and high energy density [122]. Today, fuel cell-powered systems have proved extremely useful for a variety of drone applications as shown in figures 2.4 and 2.5, due to their greater reliability than small internal combustion engines. These mechanisms also offer other advantages, including lower maintenance requirements and enhanced safety measures, enabling them to fly longer than battery-powered drones.

Figure 2.4: surveillance drones

Figure 2.5: Scan Eagle3 UAV [7]

2.4 Fuel Cell Types

Fuel cells are classified according to electrolyte material, operating temperature, fuel type and application location (stationary or mobile). The most popular categorization approach, however, is based on

electrolyte material.The following are the most prevalent commercial types of electrolyte-based fuel cells:

- Proton Exchange Membrane Fuel Cell (PEMFC), $\sim 80°C$
- Alkaline Fuel Cell (AFC), $\sim 100°C$
- Phosphoric Acid Fuel Cell (PAFC),$\sim 200°C$
- Molten Carbonate Fuel Cell,$\sim 650°C$
- Solid Oxide Fuel Cell (SOFC),$\sim 650e1000°C$
- Direct Methanol Fuel Cell (DMFC),$\sim 80°C$

2.4.1 Proton exchange membrane

PEM is classified into two types: high-temperature PEM and normal-temperature PEM. The significant benefit of high-temperature PEM is that the Top can reach temperatures of $120°C$ or more. As water exists as a gas in an atmosphere of over $100°C$ (1atm), it completely eliminates the problems created by the presence of liquid water in the FC, and water management is no longer necessary. However, the proton conductivity of high-temperature PEMs is currently quite low, and their lifetime is very short.As a result, the PEM on the market today is normal temperature PEM. Because the electrochemical reaction produces water, there is a high volume of liquid water in the FC at room temperature, making water management a critical challenge in the development of PEMFC [123].

2.4.2 Alkaline Fuel Cell

Bacon invented the first Alkaline Fuel Cell alkaline fuel cellAFC in 1939 [124]. Power output can range from 1-5 kW, however recent findings of stationary fuel cell testing have reached 200 kW . Alkaline fuel cells are no different from proton exchange membrane fuel cells (PEMFC). The general operating principle of an alkaline fuel cell, which uses a liquid or polymer electrolyte [125]. Alkaline fuel cells (AFCs) are gaining popularity as the first practical and efficient fuel cell capable of supplying sufficient power, which has greatly improved the field of transportation. In fact, it delivered electrical power to the Apollo missions to the Moon, the Space Shuttle orbiter and the Gemini spacecraft [126].

2.4.3 Phosphoric Acid Fuel Cell

The electrolyte in a Phosphoric Acid Fuel Celll cell (PAFC) is concentrated phosphoric acid. Platinum or similar metals are often used as electrodes, acting as catalysts in the creation of electricity [121, 127].Fig-

ure 2.6 gives an illustration of the phosphoric acid fuel cell concept. A high operating temperature is necessary to ensure good electrolyte conductivity, as the chemical stability of phosphoric acid decreases above $225°C$. This type of fuel cell has similar characteristics to high-temperature PEMs, including the risk of acid loss and a limited service life due to the high risk of chemical corrosion. In addition, PAFC fuel cells are also sensitive to traces of sulfur and require careful temperature monitoring [128].However, what prevents the future use of PAFCs requires intervention. PAFCs, for example, are characterized by low power density and an unstable electrolyte, both of which are major obstacles that need to be overcome [121].

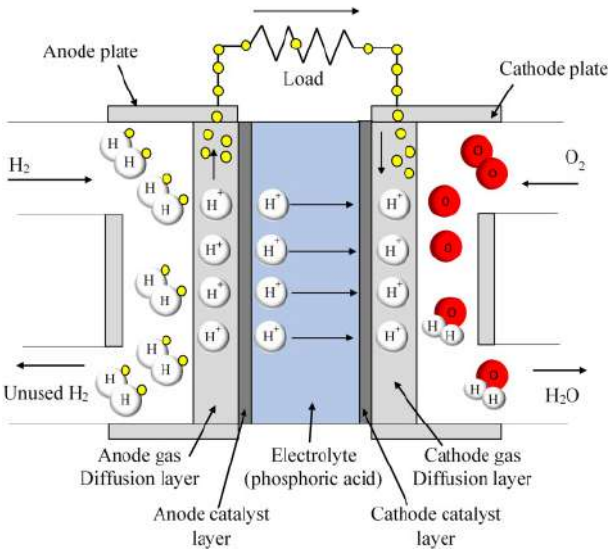

Figure 2.6: Phosphoric acid fuel cell concepts [8]

2.4.4 Solid oxide Fuel Cell *SOFC*

A typical SOFC consists of a cathode, an anode and an electrolyte that form a single cell. These single cells are stacked to form a larger unit that produces more energy. SOFCs can operate at higher temperatures in the range 600 to 1200 degrees Celsius, creating high-quality heat as a by-product, actively stimulating rapid electrocatalysis with non-precious metals and enabling internal restructuring. In addition to O2 ion transport, the SOFC can operate with high-purity hydrogen for proton transport [129].

2.4.5 Molten Carbonate Fuel Cell *MCFC*

Researchers have focused on the molten carbonate fuel cell (MCFC), because of its high-temperature operation($650°C$), fuel flexibility, long-term operational stability and efficiency for high-capacity stationary applications. However, these advantages are not offset by MCFC's poor performance, limited service life and high production and operating costs [130]. The MCFC can be practically applied for a service life

exceeding 40,000 hours. However, because of the rapid evaporation of the carbonate electrolyte, damage to the cell structure and depletion of the electrode material at such high operating temperatures, it is impossible to meet this target [130].The following electrochemical procedures take place via the MCFC electrodes [131]:

Anode

$$H_2 + CO_3^{-2} \rightarrow H_2O + CO_2 + 2e^- \tag{2.1}$$

Cathode

$$CO_2 + 1/2O_2 + 2e^- \rightarrow CO_3^{-2} \tag{2.2}$$

2.4.6 Direct Methanol Fuel Cells *DMFC*

Direct methanol fuel cells (DMFCs), in particular, could be suitable for small, portable devices. As liquid methanol can be fed directly to the anode, a fuel treatment device is not required. Methanol is less expensive than hydrogen, has a lower energy density and is easier to store and transport . A perfluorosulfonic acid (Nafion) polymer membrane is now used in DMFCs. Nafion stands out for its chemical and mechanical stability, as well as its excellent proton conductivity at temperatures of around 80°C [132]. The operating principle of this fuel cell involves the direct oxidation of a solution containing methanol as fuel and oxygen as oxidant. The physico-chemical reaction of this process can be described as follows:

Anode

$$CH_3OH + H_2O \rightarrow CO_2 + 6H^+ + 6e^- \tag{2.3}$$

Cathode

$$\frac{3}{2}O_2 + 6H^+ + 6e^- \rightarrow 3H_2O \tag{2.4}$$

Total reaction

$$CH_3OH + \frac{3}{2}O_2 \rightarrow CO_2 + 2H_2O \tag{2.5}$$

Table 2.1 provides an overview of the primary fuel cell types and their fundamental characteristics. Among these fuel cell types, PEM fuel cells exhibit considerable potential due to their high efficiency

Table 2.1: Principal fuel cell technologies [15]

	PEMFC	PAFC	SOFC	MCFC	AFC
Electrolyte	Polymer	Phosphoric acid	Ceramics	Molten carbonate	Potassium hydroxide
Primary fuel	H_2 reformed	H_2 reformed H_2	H_2 biogas methane	H_2 biogas methane	cracked ammonia
Mobile ion	H^+	H^+	O^{2-}	CO_3^{2-}	OH^-
Temperature $°C$	-40120	$150-200$	$500-1000$	$600-700$	$50-200$
Efficiency (%)	up to 65 - 72	up to 45	up to 65	up to 60	up to 70

(reaching up to 65-72), low operating temperature, and safe handling. Additionally, PEM fuel cells offer high power density and rapid start-up times, making them user-friendly.

2.5 Fuel Cell Modules

The primary element within a PEM fuel cell is known as themembrane electrode assembly MEA. This assembly consists of a polymer electrolyte membrane positioned between the anode and cathode electrodes. These electrodes consist of three layers: the Catalyst Layer (CL), the Microporous Layer (MPL MPL), and the Gas Diffusion Layer (GDL). To create the fuel cell, the MEA is sandwiched between two Bipolar Plates (BP), which have grooved or placed gas flow channels (GFC) [133]. You can see the main components of a PEM fuel cell illustrated in Figure 2.7.

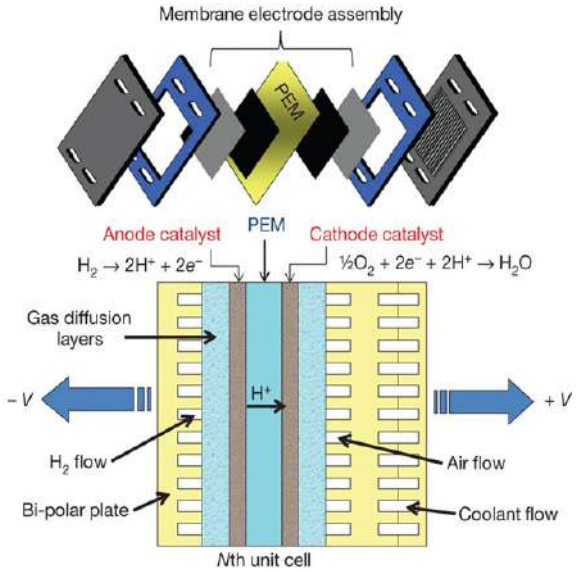

Figure 2.7: Ingredients of a fuel cell: A view of the Nth individual cell in a fuel cell technology stack, displaying the various parts of an expandedMEA [9]

2.5.1 The Bipolar Plate

In proton exchange membrane fuel cells (PEMFCs), the bipolar plate, also known as the current collector plate, is critical. It facilitates gas movement, prevents hydrogen and oxygen collisions, and creates a current route between the anode and cathode. Bipolar plates make for a major amount of the entire volume and cost of the PEMFC stack, determining the technology's large-scale industrial applicability. As a result, limiting thickness to a minimum is critical for reducing volume and saving money. Furthermore, the bipolar plate flow field design is critical since it has a direct influence on the power production, longevity, water consumption, and thermal management of PEMFCs [134]. The following points are essential considerations for the bipolar plate in a PEMFC [134]:

- The bipolar plate plays a crucial role as the structural backbone of the entire PEMFC, providing mechanical support to the MEA. As a result, it is essential for the plate to possess adequate strength. Moreover, for enhanced power density, it is advisable to opt for materials with higher specific strength.
- The surface of the bipolar plate must incorporate a processing flow field to act as a conduit for gas and water. Therefore, maintaining a high standard of processing performance is essential.
- Since the bipolar plate is responsible for collecting and conducting current, it is imperative for it to exhibit excellent conductivity.
- To prevent contact between the oxidizer and the reducing agent, the bipolar plate needs to effectively segregate them, necessitating low gas permeability.
- Due to the PEMFC's acidic electrolyte, the bipolar plate must have commendable chemical and electrochemical corrosion resistance to ensure a prolonged service life.

2.5.2 Electrodes

Electrodes are composed of up of two layers: the gas diffusion layer (GDL) and the catalyst layer (CL). The GDL is composed of two layers: a macroporous layer (MPL) comprising carbon powder and hydrophobic/hydrophilic agents, and a carbon paper or carbon fabric backing layer. The electrodes must constantly enable electrons to pass from the anode to the cathode in addition to functioning as electrochemical reaction areas [135] the electrode structure is presented in figure 2.8 . Electrodes must therefore address three important aspects.

- the electrode must contain appropriate pores for the reagents.

- the electrode must have a chemical catalyst capable of breaking links between fuels, producing more reactive ions to develop.
- the electrode must transfer electrons to the external circuit.

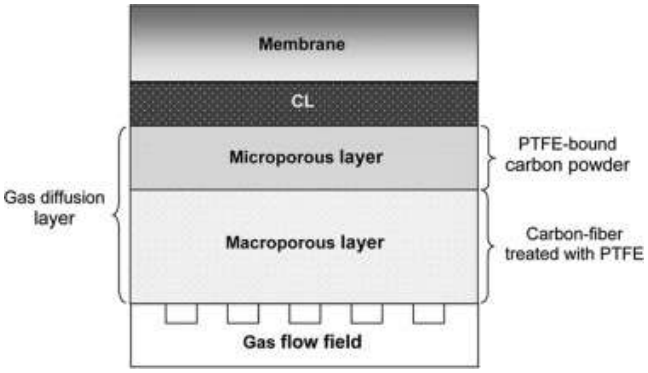

Figure 2.8: The simple design of a PEMFC electrode

2.5.3 Gas Diffusion Layer

PEMFCs contain the GDL as one of their main components. Located midway between the BP and the CL, and linking them together, the GDL supports not only the AME, but also the flow of reagents; the GDL must meet the criteria mentioned below [136].

- The gas diffusion layer (GDL) in proton exchange membrane fuel cells (PEMFC) is distinguished by its high gas conductivity and pore structure.
- The the GDL has to let gas to pass along in order for the catalysts on each side of the membrane to function effectively in the electrochemical process.
- the GDL must be well hydrated to maintain high proton conductivity.
- The GDL must also have excellent electrical and thermal conductivity to decrease ohmic losses and contact resistance, as well as quickly dissipate heat generated during cell operation.
- The GDL additionally needs to have enough rigidity to support the stack assembly and protecting concerning elements.

2.5.4 Catalyst layer

Typically, catalyst layers have been joined along both sides of the membrane, functioning as anodic and cathodic electrodes. The basic function of the CL is to accomplish two essential tasks. Firstly, it improves

the passage of reactants and products through the porous electrode. Secondly, it modulates electrochemical processes within the LC, promoting hydrogen oxidation on the anode side and oxygen reduction on the cathode side. Furthermore, the CL is also responsible for monitoring the mobility of protons and electrons inside the MEA [137–139].

At the anode and cathode, the catalytic layers consist of platinum (Pt) particles or Pt-based catalytic composites, combined with carbon grains. This latter usually takes the form of Pt/C masses enveloped by ionomer thin films. To enhance the mechanical strength of Pt particles, a carbon support is commonly added [140] . Figure 2.9 shows the microstructure of the catalyst layer in schematic form.

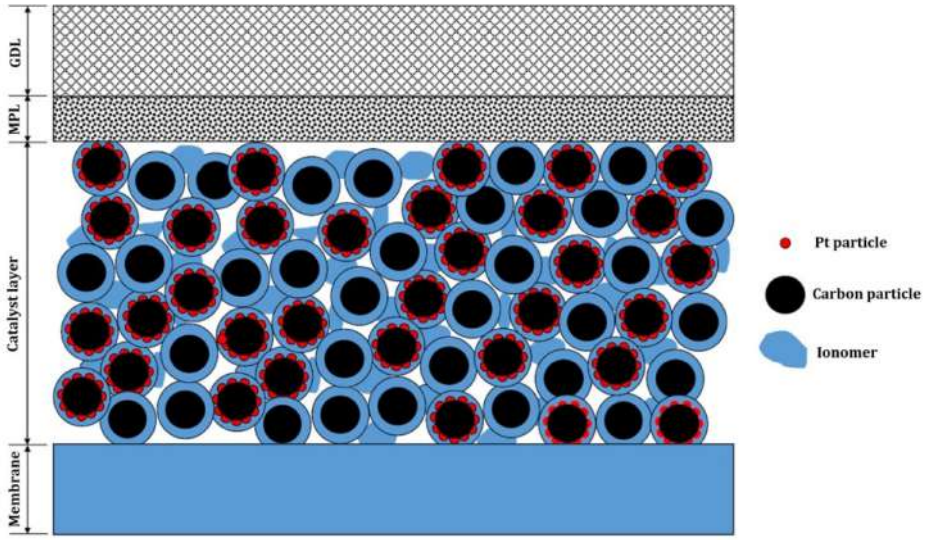

Figure 2.9: microstructure of the catalyst layer

2.5.5 A membrane

In the operational concept of a membrane (acid) fuel cell, protons are generated by the breakdown of hydrogen. These protons then pass through the ionomer membrane and proceed to the cathode, where they engage in the reduction of oxygen. Simultaneously, electrons flow through the external circuit. In accordance with this notion, the membrane material must exhibit minimal resistance to proton transfer, ensuring high ionic conductivity [133]. A thin layer of electrolyte, measuring 10 to 100μm in thickness, acts as the membrane, facilitating the conduction of protons from the anode to the cathode. The necessary membrane materials possess high ionic conductivities, preventing electron transfer and the crossover of oxygen reactants from the cathode and hydrogen fuel from the anode [141].

2.6 PEMFC Subsystems

PEMFC systems are often separated into five subsystems: fuel cell stacks, hydrogen supply systems, air supply systems, heat management systems, and humidification systems [10]. As shown in Figure 2.10, a typical PEMFC system is applied for fuel cell vehicles.Within this framework, the PEMFC cell plays a decisive role in energy conversion, while other subsystems provide the operating conditions required for efficient electrochemical reactions. All these subsystems work harmoniously together to ensure the overall stability and efficiency of the PEMFC system [142].

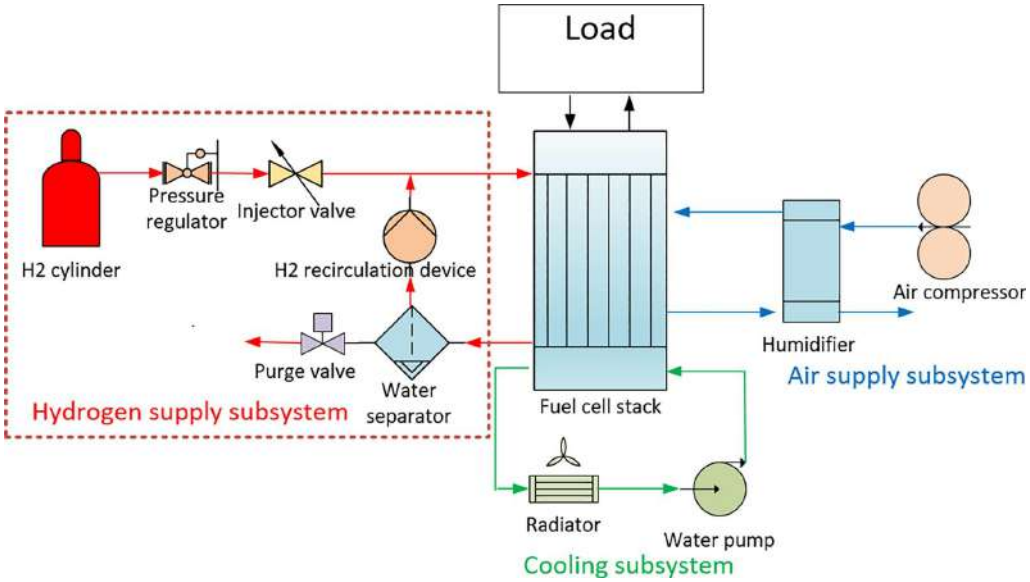

Figure 2.10: PEMFC system layout for fuel cell vehicles [10]

2.6.1 Proton Exchange Membrane Fuel Cell Stack

The economic viability of PEMFC systems depends on their dynamic characteristics and durability. Automotive applications, for example, require a service life of 5,000 hours, even under harsh conditions [143]. Problems with electrodes and catalysts have a direct impact on PEMFC lifetime. Degradation occurs due to poor water and heat management, fuel and oxidant shortages, and reactions within the components [144]. To improve durability, various strategies such as designing corrosion-resistant bipolar plates or replacing weak graphite plates with more robust composite plates can be implemented. By optimizing operating parameters and taking into account dynamic characteristics such as load variations, fuel cell life can be considerably extended [145]. In addition, water and heat management play a crucial role in improving PEMFC durability and performance [146].

Impact of Stack Temperature

PEMFC performance is degraded at both low and very high temperatures, leading to dehydration of the proton exchange membrane and reduced ionic conductivity. The upper limit of fuel cell operating temperatures is restricted by the thermal characteristics of the materials. To ensure high efficiency and minimal degradation while reducing hydrogen consumption and extending cell life, effective heat management strategies are essential for PEMFC cell operation [147, 148].

Impact of Stack Pressure

The stability of hydrogen and oxygen pressure is crucial for the overall performance of a fuel cell system. Undesirable pressure fluctuations can adversely affect the system's efficiency and effectiveness [149].

Changes in the system pressure directly impact the current-voltage characteristic and the overall performance of the fuel cell (refer to Fig. 3.15). The current-voltage characteristic is influenced by variations in oxygen partial pressure resulting from changes in total pressures. The oxygen partial pressure, governed by the Nernst equation, can be adjusted, in part, by controlling the cathode stoichiometric ratio. Additionally, the current-voltage characteristic is affected by the water-holding capacity within the cathode, which, in turn, depends on the total air pressure. This directly impacts the humidity inside the fuel cell, thereby defining the membrane resistance and corresponding ohmic loss. The humidity levels can be managed by adjusting the temperature and/or cathode stoichiometric ratio [150]. A study by [151] investigated the impact of reaction gas pressure on PEMFC performance. According to their findings, the electrical power of the cell increases with increasing pressure, as well as the energy consumption of the compressor.

2.6.2 Hydrogen Supply System

The main purpose of the hydrogen supply system is to consistently deliver hydrogen gas to the fuel cell stacks at the appropriate pressure. In PEM fuel cell systems, hydrogen gas is commonly sourced from high-pressure tanks. To enhance the performance of PEM fuel cells, the depleted hydrogen can be recycled through recirculation. Additionally, the water in the anode channel can be effectively managed by controlling the hydrogen flow rate [152]. Indeed, the fuel supply system has a significant effect in terms of hydrogen consumption rate. There are four anode-based hydrogen supply systems, most of which are applicable to proton exchange membrane (PEM) fuel cell systems [11]

Flow-through method Figure 2.11(a), is a dead-end design that is simple but does not allow for uniform distribution of hydrogen, limiting its effectiveness.

Dead-end with period purge method Figure 2.11(b) depicts a configuration where hydrogen flows through the structure, but this leads to high fuel losses due to the viscous forces of water droplets.

Ejector recirculation with period purge method The active anode recirculation configuration, illustrated in Figure 2.11(c), addresses this issue by using a recirculation pump to circulate unused hydrogen back to the fuel cell inlet, resulting in more efficient utilization of hydrogen.

Compressor recirculation with period purge method Figure 2.11 (d) shows the passive anode recirculation configuration, which also circulates unused hydrogen back to the fuel cell inlet, but it does so using an ejector.

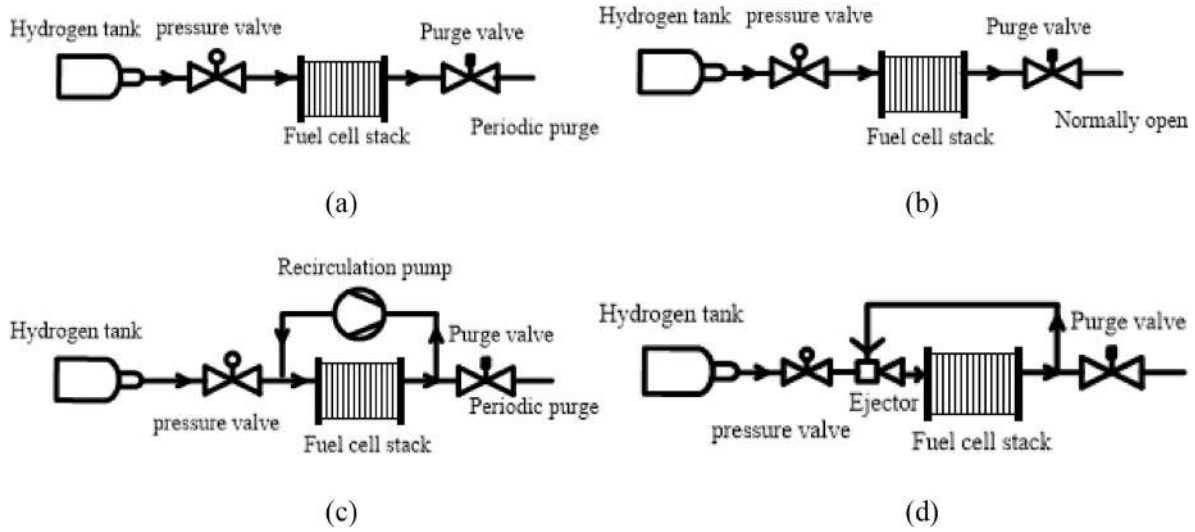

Figure 2.11: The anode configuration diagrams [11]

2.6.3 Air Supply System

As a fuel cell is based on an electrochemical process of oxygen and hydrogen, oxygen can be obtained from the air. The air supply system is an essential subsystem in PEM fuel cell systems. The main roles of the air supply system are listed below:

- **Air purification:** Any particles (solid or oil) or substances that can harm the catalyst and membrane should be removed from the air before it enters the fuel cell. Therefore, the air must pass through filters to ensure its cleanliness and protect the fuel cell.
- **Air delivery:** The air supply system must efficiently deliver an adequate amount of the reagent (oxygen) to the fuel cell. The mass flow rate of the air supply system significantly impacts the oxygen concentration within the fuel cells.
- **Pressurization:** In all scenarios, air is provided at a pressure higher than atmospheric pressure to

compensate for the flow loss within the fuel cell stacks. The air pressure plays a crucial role in determining the performance of PEM fuel cells.

- **Humidification:** To achieve optimal performance, the polymer membrane must remain fully hydrated. In certain systems, the air is humidified before it enters the fuel cell to ensure the membrane's proper hydration level. The air supply system must carefully manage water consumption to maintain this balance.

2.6.4 Heat Management System

The energy conversion efficiency of PEMFC can be as high as 50% [153]. However, this high efficiency also results in the generation of a significant amount of heat. To maintain the optimum operating temperature of the fuel cell, a sophisticated cooling system is required, capable of coping with complex and dynamic conditions [154]. Three cooling technologies are used to meet the challenges of fuel cell thermal management: air cooling, liquid cooling and phase change cooling [155]. Due to their exceptional thermal conductivity and heat capacity, liquid cooling is being increasingly employed in high-power PEMFC cells, allowing for efficient heat dissipation. The heat generated by the PEMFC is effectively dissipated by this cooling method, ensuring that optimal cell operation is achieved within the desired temperature range [156].Illustration of the cooling system diagram in Figure 2.12.

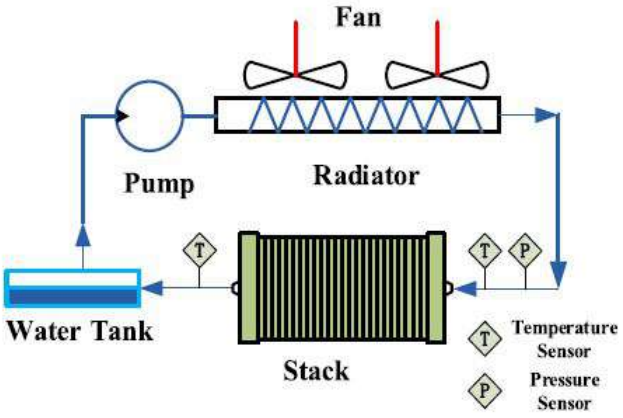

Figure 2.12: cooling system diagrams [12]

2.6.5 Humidifcation System

The proton conductivity of the membrane has a significant impact on energy conversion in a PEMFC. Increasing the water content of the membrane promotes proton transport and enhances fuel cell performance. However, too much water can overload the channels and prevent gas movement, whereas too

little water results in high proton resistance and membrane breakdown. As a result, water control is critical for maximizing PEMFC performance. This may be achieved by humidifying both the anode and cathode gases; however, investigations have shown that the cathode gas outperforms the anode gas. As a result, fuel cell membrane water management should concentrate on humidifying the supply of air/oxygen [157, 158]. At present, various fuel cell humidification technologies are available, including self-humidification [159], internal humidification, and external humidification. Among these, external humidification stands out as an easily controllable, installable, and maintainable method, making it a popular choice for high-power fuel cell stack humidification systems. The commonly used hydrogen humidification system employs a membrane humidification approach. Proton exchange membrane fuel cells exhibit a high hydrogen utilization rate, resulting in a low water content after the reaction. As a consequence, the recovered hydrogen is insufficient to fully humidify the hydrogen inlet, and liquid water is typically employed for this purpose. Ongoing research on fuel cell humidification systems primarily focuses on studying the humidity characteristics of fuel cells or low-power fuel cell stacks and aligning the humidification technology with the specific stack characteristics [160]

2.7 Description of a Supercapacitor

Supercapacitors are high-performance, extremely dynamic electrostatic storage technologies. The earliest technological advances in supercapacitors, also known as Electric Double Layer Capacitors EDLC , were made in 1957 [161].Today, numerous supercapacitors are already available on the market, with capacities ranging from a few farads to 9,000 farads and a variety of unique features. Several electrical system manufacturers and power electronics research centres are investigating the potential use of these components for applications requiring high power peaks, such as electric and hybrid vehicles, energy storage for homes and energy recovery systems for cranes and lifts [162].

2.7.1 Basic Principle of Operation

Supercapacitors are devices designed to store electrical energy, which is stored in the form of electrostatic charges confined in small devices. These devices are made up of pairs of conductive plates separated by a dielectric medium. The development of supercapacitor technology is due to a simple but significant improvement in the specific surface area of the electrodes. This increase in specific surface area allows charges of opposite sign to come closer together, even at the molecular level. By using materials with a high specific surface area, such as activated carbons, supercapacitors can increase specific surface area values by up to 100,000 times more than smooth materials with a lower specific surface area. The result

is capacities around 1 million times greater than those of capacitors of similar size and weight [163]. The structure of supercapacitors resembles that of batteries, consisting of an electrolyte and two electrodes. A semi-permeable substance is used to separate the electrodes, allowing for the passage of electrolyte ions while preventing a short circuit. When a difference in potential is applied, a gradient in the density of charge is established between the plates, causing ions to move to the surface of the electrode and attach to the interface. Each interface between the electrode and electrolyte functions as a capacitor, and thus the entire cell can be viewed as two capacitors connected in series [164] as shown in Figure 2.13.

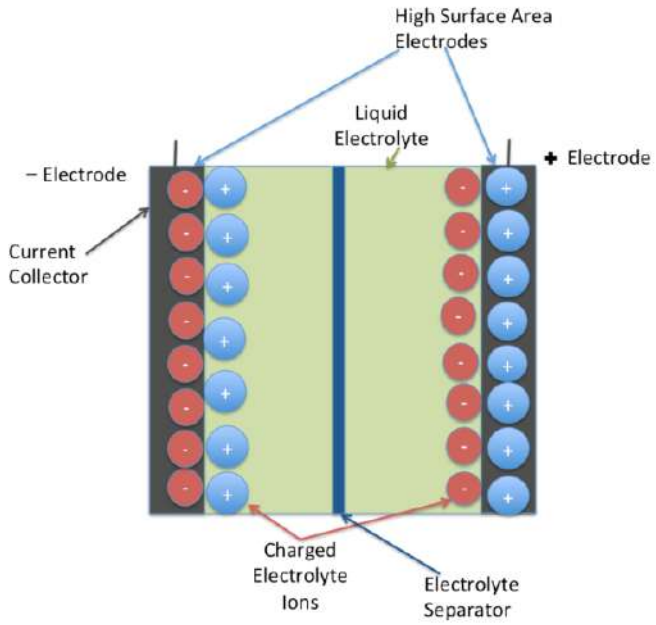

Figure 2.13: Charged Electrochemical Double Layer Capacitors EDLCillustration

2.7.2 Examining the Performance of Supercapacitors Compared to Other Storage Devices

Super capacitors (SCs) outperform batteries and electrolytic capacitors in terms of energy and power density while also being more compact and lightweight [165].Supercapacitors provide a notably extended lifespan compared to batteries, capable of enduring up to 500,000 cycles. This renders them an appealing choice for augmenting the energy storage capabilities of electric vehicles, particularly when employed alongside lithium-ion batteries. Consequently, there has been extensive exploration into their capabilities [166].Table 2.2 presents the performance data for supercapacitors utilized as energy storage systems.

2.7.3 Advantages and Properties

The following are the primary benefits of supercapacitors over conventional energy storage solutions:

Table 2.2: The Performance of Supercapacitors [16]

Storage device characteristics	**Supercapacitor**
Charging time	1 – 30 s
Discharging time	1 – 30 s
Energy density (Wh/kg)	1 – 10
Life time (Cycle number)	10^6
Power density (W/kg)	10,000
Charge / discharge efficiency	0.85– 0.98

- High mass power, which enables for charging and discharging cycles at extremely high currents (several hundred amperes)
- Very excellent efficiency in charging and discharging.
- Almost minimal chemical reaction during operation, allowing for very extended life spans.Under typical operating conditions, a supercapacitor may be charged and discharged a millions of times.
- A relative simplicity of electrical behavior and relative temperature stability compared to batteries.

However, these devices have the disadvantage of having insufficient energy density, of the order of 1 to 10 Wh/kg, whereas lithium-ion batteries have an energy density of 265 to 280 Wh/kg [167].

Supercapacitors have a number of key qualities that considerably enhance their performance. In particular, they have low equivalent series resistance (ESR), with a minimal leakage current, as well as a long service life and a wide operating temperature range.

2.7.4 Application of Supercapacitors in Renewable Energy

Solar Energy Applications

Solar energy, also known as photovoltaic energy, is a renewable and clean energy source that provides power on a periodic or fluctuating basis, depending on environmental and climatic conditions [168].Batteries are currently widely used to store large quantities of electricity generated by photovoltaic (PV) cells. However, power supply fluctuations and irregular energy use can reduce battery life. Consequently, this can potentially reduce the overall efficiency of the energy storage system.One way to solve battery challenges is by using hybrid energy storage systems that combine batteries with supercapacitor technologies. This approach not only helps to balance the inconsistent nature of solar power generation but also reduces the stress on batteries [169].

Supercapacitors' Application in Traction Systems

For applications that require large amounts of energy for vehicles, supercapacitor technology is proving to be promising, especially for high-power activities such as acceleration and start-up. Conventional energy sources like batteries and fuel cells are not well-suited for applications that demand rapid power peaks, mainly due to their size and weight and slow dynamics. Supercapacitors enhance energy delivery, prolonging the lifespan of batteries or fuel cells and allowing for the addition of new features to mobile devices [170].

Supercapacitors are currently the principal power source in the flash chargers of the newest ABB TOSA bus, substituting lithium-ion batteries because of the capacity to effectively generate high-power surges [171].Figure 2.14 show supercapacitor applications in transportation and industry.

(a) Flash chargers using supercapacitors are provided at ABB TOSA bus stops.

(b) Supercapacitors are also utilized in forklifts for efficient energy storage.

Figure 2.14: Supercapacitor applications in transportation and industry.

Application in Automatic Guided Vehicle

Supercapacitors are finding an increasingly popular application in the field of Automated Guided Vehicles (AGVs). Traditionally relying on batteries, AGVs have encountered problems of reliability, limited service life, sub-optimal power and extended recharging intervals. By contrast, supercapacitor-based so-

lutions for AGVs offer a lighter alternative with significantly increased operational longevity, improved reliability, increased power capacity suitable for lifting tasks, and accelerated recharging capabilities compared with conventional battery systems [13].

Figure 2.15: Hybrid Supercapacitor Powered Automated Guided Vehicles [13]

2.7.5 Approaches to Representing Supercapacitor Circuits

Having a reliable mathematical representation of supercapacitors (SCs) is crucial for accurately predicting their behavior and assessing potential disturbances caused by non-linear loads during transient events. Furthermore, it is essential for optimizing the power system structure and determining the most efficient energy management strategies. While there are several models available in the literature, the choice of the most suitable model depends on factors such as the specific application, the design phase, and the available resources [172]. Some publications, such as [173], have used basic equivalent circuit models to demonstrate the overall behavior of supercapacitors.A capacitance, denoted as C, and an equivalent series resistance ESR form the components depicted in Figure 2.16a.To mitigate delayed self-discharge losses in Figure 2.16b, it is recommended to add an equivalent parallel resistance EPR to the capacitance.Using these circuits, it is possible to establish the best design of a power system. Additionally, they make it easier to simulate reliable charging and discharging cycles, especially at low usage rates. Furthermore, the circuits are especially designed to be simple to use, with their settings available immediately from the manufacturer's description data sheet.

The idea of a multi-branch equivalent circuit for supercapacitors is shown in Figure 2.17a. Each branch includes a combination of capacitance and resistance in series. In this multi-branch circuit model, each branch can represent a different behavior of the supercapacitor at different times.The accuracy of the multi-branch equivalent circuit model improves as the number of branches grows. However, creating a multi-branch comparable circuit model with many branches would be difficult . As a result of their simplicity, two- or three-branch equivalent circuit models have been widely used in practice [174].

(a) (b)

Figure 2.16: Basic representations of supercapacitors: 2.16a with ESR 2.16b with EPR

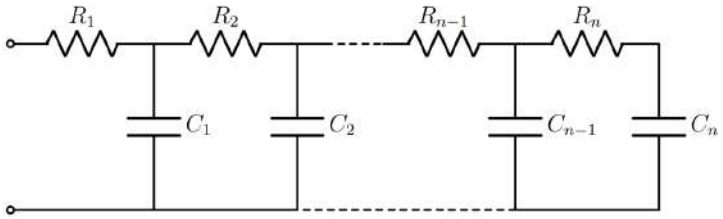

(a) Supercapacitor with several branches in series.

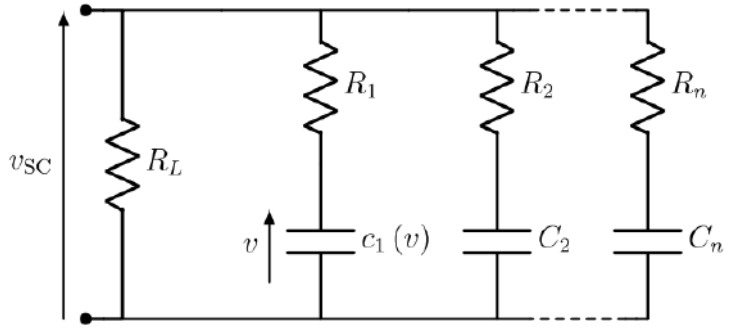

(b) Supercapacitor with several branches in parallel.

Figure 2.17: Supercapacitors with different configurations.

2.8 Conclusion

Fuel cell technology has undergone remarkable advancements since its inception in 1839. Researchers and scientists have persistently pushed the boundaries of this technology, driving its evolution forward. From Sir William Grove's visionary concept to the practical utilization of Bacon's fuel cell, and the advancements in PEMFC and SOFC, this progress has been marked by ingenuity and determination [175].

Fuel cells have been used in a wide range of industries, including transportation, stationary power generation, and portable technology. Their exceptional efficiency positions them as a viable solution in the quest for cleaner and more sustainable energy sources. As the demand for environmentally-friendly energy options continues to rise, fuel cells present a compelling and competitive alternative for building a greener future.

In this chapter, we explored the key components of PEMFCs, understanding how the Membrane Electrode Assembly, bipolar plates, gas diffusion layers, and electrodes work together to drive the ef-

ficient conversion of hydrogen and oxygen into electricity. Furthermore, a comprehensive overview of PEMFC systems revealed the significance of managing subsystems such as fuel cell stacks, hydrogen supply systems, air supply systems, heat management systems, and humidification systems to ensure optimal performance.

The latter part of this chapter provides information on the history, composition, and applications of supercapacitors. It also discusses their advantages and limitations in comparison to other energy sources. Furthermore, it explores their operational principles, changes in properties, and methods for illustrating supercapacitor circuits.

Moving on to the following chapter, various models for the components of the multi-source system are described. These components comprise electrical energy sources like supercapacitors and fuel cells, static converters, as well as a powertrain consisting of a three-phase voltage inverter and a permanent magnet synchronous machine (PMSM).

Chapter 3

Exploring Essential Elements of the Design Process

The aim of this chapter is to introduce diverse models for the different elements comprising the multi-source system. These elements include the electrical energy sources (such as supercapacitors and fuel cells), the corresponding static converters, and the drive train, which encompasses a three-phase voltage inverter and a permanent magnet synchronous machine (PMSM). The multi-source system is designed to utilize the PMSM as the motor responsible for propelling the vehicle forward.

Contents

3.1 Introduction

The purpose of this chapter is to present various models for the different components of the multi-source system. These components include electrical energy sources such as supercapacitors and fuel cells, static converters associated with the sources.In previous discussions, we have already explored the use of power sources in electric vehicles, specifically focusing on PEM fuel cells and supercapacitors. Now, we will shift our attention to the modeling and numerical simulation of these power sources. This modeling process is crucial as it allows us to fully understand and exploit the potential of these sources in the context of electric vehicle applications, optimizing their performance.

By introducing these diverse models, we aim to establish a comprehensive understanding of the multi-source system and its interconnected elements. This chapter will provide valuable insights into the functioning and integration of the various components, enabling us to make informed decisions for enhancing the overall performance and efficiency of electric vehicles.

3.2 Desired System Configurations

Figure3.1 depicts the FCHEV's drive train construction. The energy sources, which are primarily the fuel cell model, and the supercapacitor model, are coupled to the wheels through an inverter and electric motor. The FCHEV's drive system comprises mostly of DC/DC converters, a DC/AC inverter, and a motor, as well as the vehicle model. Under this research, the FC is the primary source of energy for the creation of typical power requirements. To keep a constant voltage, the principal energy storage device, a supercapacitor, is permanently interfaced to the DC link. It can also offer more energy as the vehicle accelerates and use recuperative energy while the vehicle is parked.

3.3 Mathematical Models for PEM Fuel Cells:

Fuel cell models can be classified as either transient or steady-state, depending on their consideration of dynamic effects. Steady-state models, which ignore transient effects, offer significant simplifications in modeling and result in cheaper computing costs. These models are useful for analyzing and optimizing the performance of fuel cells at critical operating points. However, they are unable to represent transient operation phases such as fuel cell starting or the influence of varying operating circumstances. Additionally, steady-state models cannot be used to investigate control techniques, as they require the use of transient models. [176, 177].

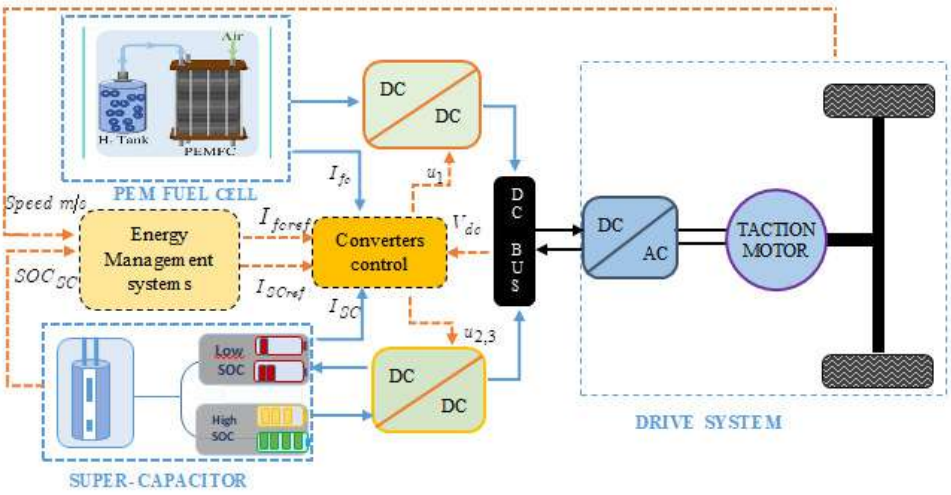

Figure 3.1: Powertrain topology of FCHEV

Anode reaction:

$$H_2 \rightarrow 2H^+ + 2e^- \tag{3.1}$$

Cathode reaction

$$2H^+ + 2e^- + 1/2O_2 \rightarrow H_2O + heat \tag{3.2}$$

These, half-reactions are catalysed, often with platinum, to improve the kinetics of the reactions, which are extremely slow at low cell operating temperatures.Through the figure 3.2, the fuel cell is illustrated in schematic form.

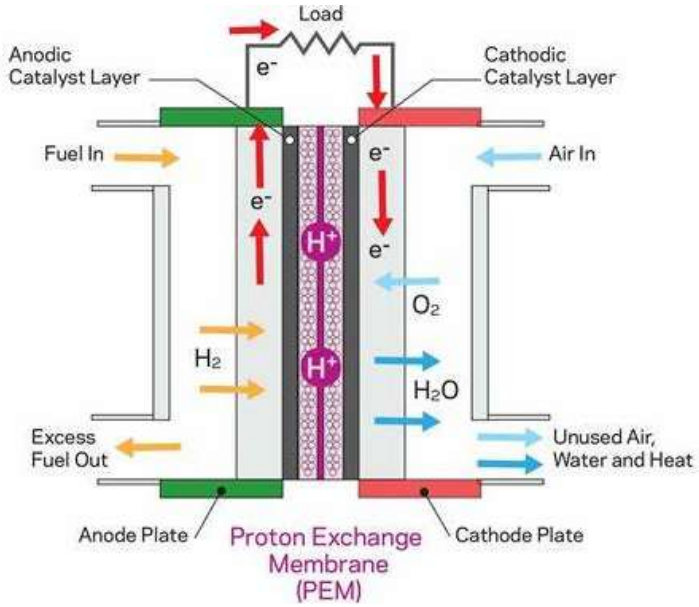

Figure 3.2: PEM fuel cell schematic

3.3.1 Hypotheses for Simplification:

The following hypotheses have been formulated to expedite the analysis.

- The stack is well designed, ensuring uniform performance across all cells. This allows them to be grouped together as a single stack.
- All gases has a uniform distribution and satisfies with the ideal gas law's rules.
- The cell temperature is evenly distributed and maintained by a reliable control system during operation, ensuring that the temperatures of the hydrogen in the anode and the oxygen in the cathode match the stack temperature.
- Inside the cell, the partial pressures of gas are assumed to remain constant, without considering any pressure decreases caused by interactions between the gas and the membrane in the gas distribution channels. Similarly, the pressure at the inlets of the anode and cathode compartments is assumed to be constant, just like the temperature.
- The airflow is regulated, and a constant cathodic stoichiometric ratio is maintained.
- Only liquid water is produced as a result.

3.3.2 Energy , Open Circuit Voltage and Nernst Equation:

Fuel cell operation involves the direct conversion of chemical energy into electrical energy. The resulting electrical power depends on the product of the voltage and current supplied. However, one of the main advantages of fuel cells over traditional chemical combustion systems is their exceptionally high potential energy efficiency. In specific applications, such as combined heat and power generation, achievable efficiencies can be significantly improved, particularly with the use of high-temperature fuel cells. This underlines the appeal of fuel cells as a potentially valuable technology for optimizing energy use in a variety of applications. [178].

Figure 3.3 shows the inlets and outlets of the fuel cell. At the anode, hydrogen dissociates into protons and electrons. The electrons move through an external circuit, establishing an electric current. At the same time, protons migrate through the electrolyte to the cathode. At the cathode, they combine with oxygen and electrons, producing water and heat. This electrochemical process illustrates the fundamental mechanism by which a fuel cell generates electricity [179].

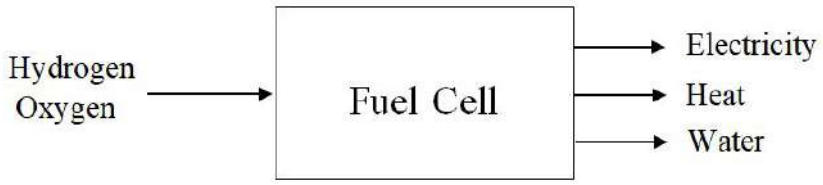

Figure 3.3: Inlets and outlets of the fuel cell

Energy:

Assuming the stoichiometry of the reactions, it is confirmed that each hydrogen molecule generates two electrons. The electrical work, represented as follows:

$$W_{el} = -E \cdot q \tag{3.3}$$

where q is the total charge produced per mole of hydrogen in coulombs and E the electric potential difference in volt .

such as

$$W_{el} = -E \cdot n \cdot F \tag{3.4}$$

The number of electrons exchanged in moles is indicated by n while F stands for Faraday's constant. It's crucial to know that electric work is achieved through the consumption of hydrogen fuel. In particular, for every mole of H_2 consumed, the number of transferred electrons n is equal to 2 moles.

The possibility of producing useful work or electricity from a chemical reaction is measured by the Gibbs free energy change of the process. To put it another way, $\Delta \bar{g}_f$ represents the thermodynamic potential that is accessible for producing electrical energy or carrying out work during a chemical process [180].Here is a definition of free energy in an electrochemical process:

$$W_{el} = -\Delta \bar{g}_f \tag{3.5}$$

Consequently, the ideal reversible potential E_{rev} for a fuel cell process involving n electrons can be derived from:

$$E_{rev} = \frac{-\Delta \bar{g}_f}{n \cdot F} \tag{3.6}$$

The standard potential depends on temperature and can be calculated using the following equation [181]:

$$E^0(T) = \frac{-\Delta\bar{g}_f^0(T)}{n \cdot F} \tag{3.7}$$

and

$$\Delta\bar{g}_f^0(T) = a \cdot T - b \tag{3.8}$$

In the case of liquid water, the constants a and b have values of $160.778 Jmol - 1K^{-}1$ and $284972 Jmol^{-}1$, respectively, between $298K$ and $500K$.The computed values of $\Delta\bar{g}_f^0$ and E^0 traveling $303.15K$ to $353.15K$ are shown in Table 3.1.

Table 3.1: Calculated $\Delta\bar{g}_f^0$ andE^0

T/K	303.15	313.15	323.15	333.15	343.15	353.15
$\Delta\bar{g}_f^0/j \cdot mol^{-1}$	-236232	-234624	-233017	-231409	-229801	228193
E^0/V	1.224	1.216	1.208	1.2	1.191	1.183

The Nernst Equation and Open Circuit Voltage:

The voltage produced by a fuel cell with no electrical load attached is called the open circuit voltage (OCV). As the current discharges to zero, the thermodynamic cell voltage indicates electrochemical equilibrium. The Nernst equation is used to calculate the electrode potential in an electrode reaction based on the concentration of reactants and products in the cell, resulting in the equilibrium cell voltage. The Nernst equation is expressed in its general form as follows:

$$E = E^0 - \frac{RT}{nf} ln(Q) \tag{3.9}$$

The reaction quotient,Q is determined by dividing the product of all product activities by the product of all reactant activities.

A Simulink model is subsequently used to calculate the open circuit voltage of a single PEM fuel cell.

$$E = -\frac{\Delta\bar{g}_f^0}{2F} + \frac{RT}{2F} ln\left(\frac{\gamma\beta^{\frac{1}{2}}}{\delta} P^{\frac{1}{2}}\right) \tag{3.10}$$

This calculation is based on the change in the molar specific energy of water's Gibbs free energy of generation, denoted as $\Delta\bar{g}_f^0$. The concentrations of hydrogen, oxygen, and steam are considered, denoted respectively as γ, β, and δ, along with the system pressure P. The model also incorporates the molar gas constant R, which is equal to $8.314 JK^{-1}mol^{-1}$, the temperature T, and the Faraday constant F. The Faraday constant represents the charge of one mole of electrons, which is equivalent to $96,485 coulombs$.

3.3.3 Overpotential:

The voltage of the cell when it is under a current load will be lower than the theoretical equilibrium voltage. This is because of voltage losses that occur within the cell, which are caused by polarization of the electrodes. Therefore, in order to address terminology issues and enhance everyday language in relation to electrochemical experiments, the authors [182] propose multiple definitions of polarization.

Definition 1 (polarization)**.**

- *Polarization occurs in an electrode at equilibrium when the potential deviates from its equilibrium value due to the flow of current from an external power source.*
- *Polarization in any electrode refers to the manipulation of the electrode by externally applying a specific potential, current, or a predefined time function.*
- *In an electrochemical cell with a defined electrochemical equilibrium, polarization occurs when the cell voltage deviates from the electromotive force of the same cell due to the current passing through the cell.*
- *Polarization at the interface of two immiscible electrolyte solutions can refer to either the change in potential difference across the interface caused by current from an external source, or the establishment of this potential difference.*

Polarization can be caused by activation losses, concentration or mass transport losses, and ohmic loss. Activation and concentration or mass transport losses contribute to total polarization, whereas ohmic loss is the voltage drop caused by current passing through the cell and between the electrodes. As a result, the cell's voltage may be described as follows:

$$\begin{aligned} V = \text{Open circuit voltage} - \text{cathode activation losses} - \text{anode activation losses} \\ - \text{ohmic losses} - (\text{concentration and mass transport losses}) \end{aligned} \tag{3.11}$$

The polarization curve represents the relationship between cell voltage and current density. Figure3.4 provides a visual representation of this curve, including schematic representations of the different potential losses.

3.3.4 Activation Loss:

Voltage Loss Caused by Overpotential The activation overpotential, which refers to the extra potential needed for charge transfer because of activation energy, is impacted by the electrode kinetics at the reaction site. This includes the electrochemical kinetics as well as the movement of protons and electrons.

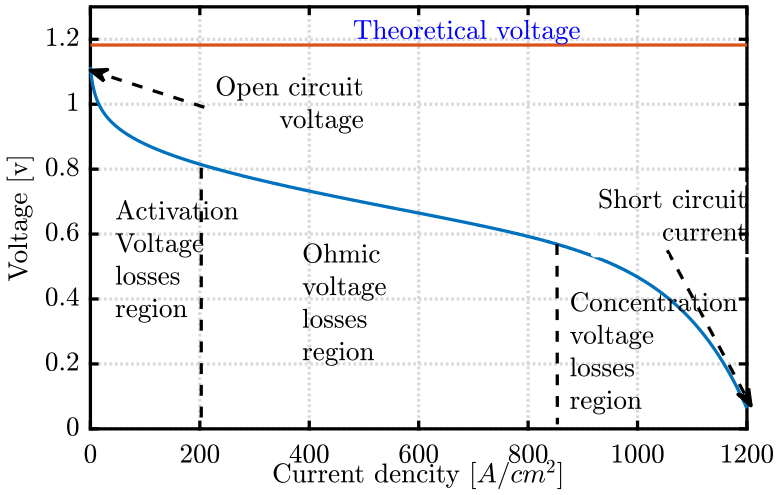

Figure 3.4: Representation of the negative impact of fuel cell polarization.

Tafel equation:

When reactant transport constraints are not present, electrode systems' behavior usually expresses an exponential connection between the current and the overpotential, $\Delta V_{fuel+crossover}$.The Tafel slope and the exchange current density are two significant physical characteristics that are often obtained from the Tafel analysis. The following Tafel connection has been thoroughly verified empirically [183] :

$$\Delta V_{fuel+crossover} = a + b \cdot ln(i) \tag{3.12}$$

By plotting overpotential against $ln(i)$, we can determine the Tafel slope, represented by b. The Tafel equation for the cathodic reaction in a fuel cell is then formulated using the exchange current density.

$$\Delta V_{fuel+crossover} = \frac{RT}{2\alpha F} \ln i_0 - \frac{RT}{2\alpha F} \ln i \tag{3.13}$$

Furthermore, to put it another way:

$$\Delta V_{fuel+crossover} = \frac{RT}{2\alpha F} \ln \left(\frac{i + i_n}{i_0} \right) \tag{3.14}$$

Here, α represents the transfer coefficient, while f stands for F/RT (where F denotes Faraday's constant, R represents the universal gas constant, and T signifies the absolute temperature), and i_0 refers to the exchange current density.The constants include Faraday's constant, $F = 96500\,\mathrm{C\,mol^{-1}}$, the gas constant, $R = 8.314\,\mathrm{J\,mol^{-1}\,K^{-1}}$, temperature T, the electron transfer coefficient, $\alpha = 0.25$.

PEM cell properties that simply take activation losses into account, is shown in Figure 3.5.

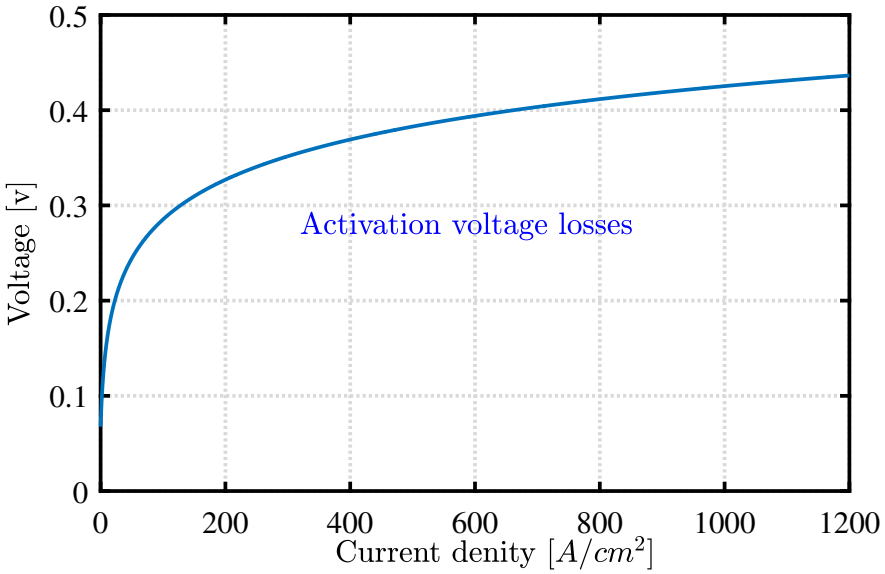

Figure 3.5: PEM cell characteristic considering only activation losses

3.3.5 Ohmic Loss:

(Voltage Loss Related to Charge Transport) As charge flows through conductors, cell voltage decreases due to natural resistance. This resistance, known as ohmic polarization, is caused by the electrical resistance in different parts of the cell. The main cause of the voltage drop in the fuel cell is internal ohmic losses. This decrease in voltage is called ohmic loss.

Ohmic polarization follows Ohm's law:

$$\Delta V_{Ohm} = ri \tag{3.15}$$

In this particular context, internal electrical resistance is designated by the symbol r_{ohm}, which is measured in $\Omega \cdot cm^2$. It's important to specify that this resistance includes electrical resistance(R_{ele}) , that is the resistance for transport of electrons in contact wires, connections and electrodes. The term also encompasses ionic resistance (R_{ion}), that is the resistance to the transfer of protons from the anode to the cathode. Research findings show that ionic resistance plays a key role in ohmic losses, even more so than electronic resistance. Consequently, the collective impact of electrical and ionic resistances shows a linear increase with increasing current density.The ionic component may be described as follows:

$$R_{ionic} = \frac{l_m}{A\sigma_m} \tag{3.16}$$

in the equation, l_m and σ_m are the membrane thickness and conductivity respectively. Experiments have shown that the temperature T and water content λ of the membrane affect its conductivity as:

$$\sigma_m = a \cdot \lambda - b \tag{3.17}$$

and

$$\lambda = c_m \frac{M}{\rho_{dry}} \tag{3.18}$$

the terms of M, ρ_{dry} and c_m in the aforementioned relationships correspond to the membrane equivalent weight,water concentration, and membrane density under dry conditions, respectively.The PEM cell characteristic, which only takes into account ohmic losses, is shown in Figure 3.6.

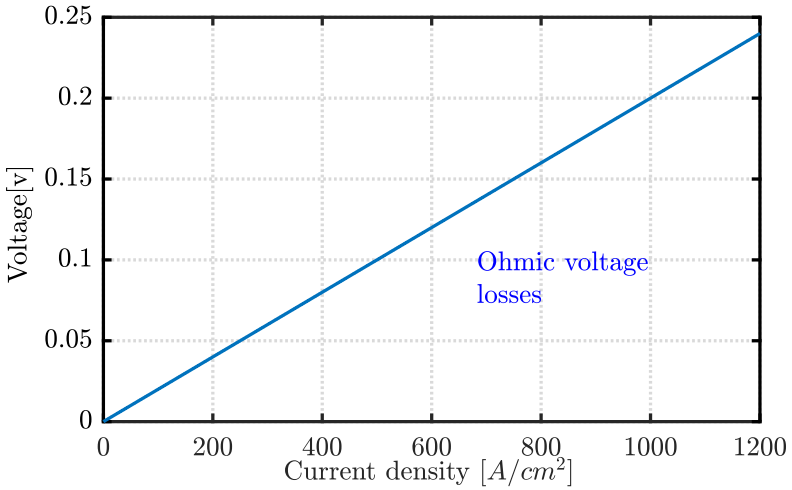

Figure 3.6: PEM cell characteristic considering only ohmic losses

3.3.6 Concentration Loss

A lot of chemical processes involve concentration polarization, also known as mass transport loss. Concentration polarization occurs when a decrease in oxygen concentration at the surface of the cathode catalyst leads to a decrease in cell voltage. This voltage decrease highlights the importance of progressive oxygen mass transfer in causing this drop in voltage. The concentration polarization becomes more significant as the power load increases. Although these processes occur at both electrodes, the hydrogen concentration polarization is often ignored in practice. This is because of the high rate of hydrogen diffusion and the frequent use of pure hydrogen on the anode [184, 185].The typical polarization curve illustrated in figure 3.4 shows a distinct range where mass transport losses begin to dominate, particularly at higher current densities. This occurs in particular as the oxygen content at the electrode surface

decreases. Figure 3.7 shows the characteristics of a PEM cell based only on mass transfer loss.

Examination of the conventional polarization curve in figure 3.4 have revealed a distinct range where mass transport losses become more significant, particularly at higher current densities. This occurs in particular as the oxygen concentration at the electrode surface decreases. Concentration loss in the PEMFC is expressed by the equation below.

$$\Delta V_{Trans} = m \exp^{ni} \tag{3.19}$$

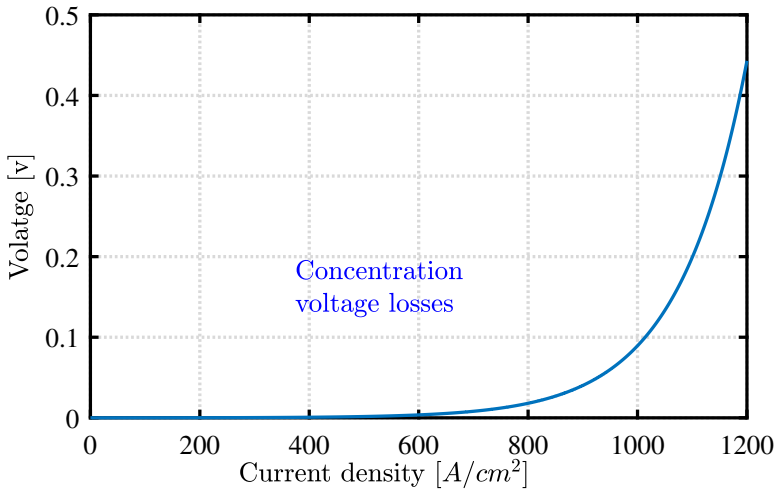

Figure 3.7: PEM cell characteristic considering only mass transport loss

3.3.7 Terminal Voltage

The equation below can be used to determine the terminal voltage of the fuel cell [186]:

$$V_{fc} = E - \Delta V_{fuel+crossover} - \Delta V_{Ohm} - \Delta V_{Trans} \tag{3.20}$$

therefore 3.3.7 has the new form below:

$$V_{fc} = E - \frac{RT}{2\alpha F} \ln\left(\frac{i+i_n}{i_0}\right) - (r \cdot i) - \left(m \cdot \exp^{ni}\right) \tag{3.21}$$

The symbols E, $\Delta V_{fuel+crossover}$, ΔV_{Ohm}, and ΔV_{Trans} represent open-circuit voltage, activation, ohmic, and concentration losses, respectively.Table 3.2 comprises the specifications and amounts applied in the simulink model for the aforementioned equation constants.

The voltage of a fuel cell is represented by the estimated voltage v_{fc}. To form a stack, multiple cells

Table 3.2: Description of estimations for the over-potentiality equation parameters

Symbol	Description	Value
m	Coefficient	$0.00003V$
n	Coefficient	$0.008cm^2mA^{-1}$
r	Area specific resistance	$0.0002K\Omega cm^2$
i_n	Internal current density	$3mAcm_{-2}$
i_0	Exchange current density	$1mAcm^{-2}$
α	Charge transfer coefficient	0.25

are stacked in sequence. The stack voltage v_{st} is obtained by multiplying the cell voltage with the number of cells N and the stack current i, which is equal to the cell current.

$$v_{st} = N \cdot v_{fc} \tag{3.22}$$

To calculate the current density j, divide the stack current by the active cell area A.

$$j = \frac{i}{A} \tag{3.23}$$

3.3.8 Power and Efficiency of PEMFC

The fuel cell's specific power density, denoted as P_{sfc} and measured in W/m^2, can be calculated as follows:

$$P_{sfc} = v_{fc} \cdot j \tag{3.24}$$

Fuel cell operating efficiencies are lower than theoretical values due to activation, ohmic, and mass transport overvoltages [187]. Fuel cell efficiency is essentially determined by the ratio of usable energy generated to the total energy supplied to the system over a given time period [188]. In an ideal situation, all the energy from the previous reaction (3.1)and (3.2) could be converted into electrical energy. The thermodynamic efficiency of the fuel cell reaction is shown below. In this context, $\Delta\bar{h}$ represents the total amount of energy available in the process, while $\Delta\bar{G}$ indicates the potential amount of energy that can be converted into electrical energy.

$$\eta_{Theo} = \frac{\Delta\bar{G}}{\Delta\bar{h}} \tag{3.25}$$

By replacing $\Delta\bar{G}$ by its value in equation (3.25) the thermodynamic efficiency is represented by

$$\eta_{Theo} = \frac{-2E \cdot F}{\Delta\bar{h}} \tag{3.26}$$

Here, $\Delta\bar{h}$ represents the change in enthalpy per mole of hydrogen in the reaction.

On the contrary, the presence of excessive voltage at the electrodes and resistance in the electrolyte leads to a decrease in the potential v_{fc}. If we assume that the efficiency of the fuel cell is equivalent to that of a basic cell, the efficiency value, η_{fc}, is then determined as follows:

$$\eta_{Theo} = \frac{-2v_{fc} \cdot F}{N_{cell}\Delta\bar{h}} \tag{3.27}$$

Note that N_{cell} is the number of elementary cells in the stack.

The change in enthalpy for steam is not equivalent to that of liquid water. As a result, the potential output values for a reaction can vary depending on the state of the output. The following table 3.3 presents the $\Delta\bar{h}$ values for reaction (3.2).

Table 3.3: Enthalpy Changes,Gibbs free energy and Calorific (Heating) Values for Various Water States

Output State	**Value**	$\Delta\bar{g}$ **(kJ mol^{-1})**	$\Delta\bar{h}$**(kJ mol^{-1})**	**Calorific value (MJ Kg^{-1})**
Liquid Water	LHV	223	241.83	120.21
Steam	HHV	237.1	286.84	142.18

When defining the heating value of a reaction, it is important to distinguish between the High Heating Value (HHV) and the Lower Heating Value (LHV) The HHV is a higher number, resulting in the production of steam, while the LHV is a lower number resulting in the production of Liquid Water. it is likely that the LHV has been used, as it provides a higher efficiency value [189]. The efficiency of the PEMFC system, represented as η_{FC}, can be calculated using the following equation:

$$\eta_{FC} = \frac{P_{FC}}{\dot{M_{FC}} H_{LHV}} \tag{3.28}$$

with

$$\dot{M_{FC}} = \frac{N_{cell} \cdot M_{H_2} I_{fc}}{2F} \tag{3.29}$$

in which $\dot{M_{FC}}$ is the fuel consumption rate of the PEM fuel cell stack, $H_{LHV} = 120MJ/kg(33.33kWh)$ is the specific energy or lower heating value of hydrogen, M_{H_2} and N_{cell} are respectively the molar mass of hydrogen and the number of cells.

3.3.9 Capacitance Double-Layer Charge Effect:

In addition to the impact of load current, pressure, and temperature on fuel cells, their dynamic response is also influenced by their capacity to store electric charge. This characteristic, found in most fuel cells, causes them to function like a substantial capacitor [190].This behavior is referred to as the *double layer of charge* and refers to the accumulation of both positive and negative charges at the interfaces between the electrolyte and electrode [14, 191].

In Figure 3.8a, the movement of oxygen ions represented as negative charges can be seen crossing the electrolyte from the cathode to the anode.The double layer charge functions similarly to an electric capacitor, as illustrated in Figure 3.8b. It can be charged or discharged based on the current's direction or the load applied.

$$C = \varepsilon \frac{A}{l} \tag{3.30}$$

where l represents the distance between the layers,A represents the effective surface area shared by the electrolyte and electrode, and ε represents the electrical permittivity of the electrolyte. In real fuel cells, l is extremely small (measured in nanometers), whereas A is significantly larger due to the porous nature of the electrodes. As a result, the capacitance (which can range from hundreds of microfarads to a few farads) is significantly high [192].

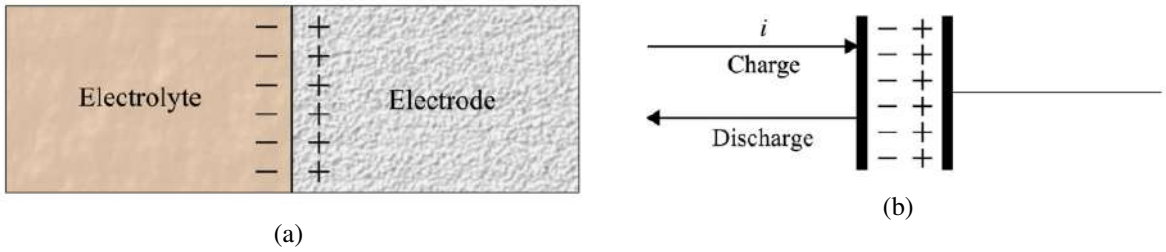

Figure 3.8: The double layer of charge at the electrode-electrolyte interface is shown in3.8a , capacitor that represents the double layer of charge's charging and discharging is shown in3.8b [14]

An effective approach to improving the accuracy of the fuel cell model is to incorporate the influence of the electrochemical double layer. This can be done by adding a capacitor to the activation and concentration resistors, which introduces a time delay between the voltage and current responses of the fuel cell. Figure 3.9, part 3.9a, shows the electric circuit equivalent model of a Proton Exchange Membrane Fuel Cell (PEMFC) without the electric double layer capacitor. In contrast, Figure 3.9, part 3.9b, presents an enhanced model that includes the double layer capacitor, resulting in a more comprehensive representation of the fuel cell dynamics.In this context, the equivalent resistance is defined as the ratio between each

polarization and the electric current.

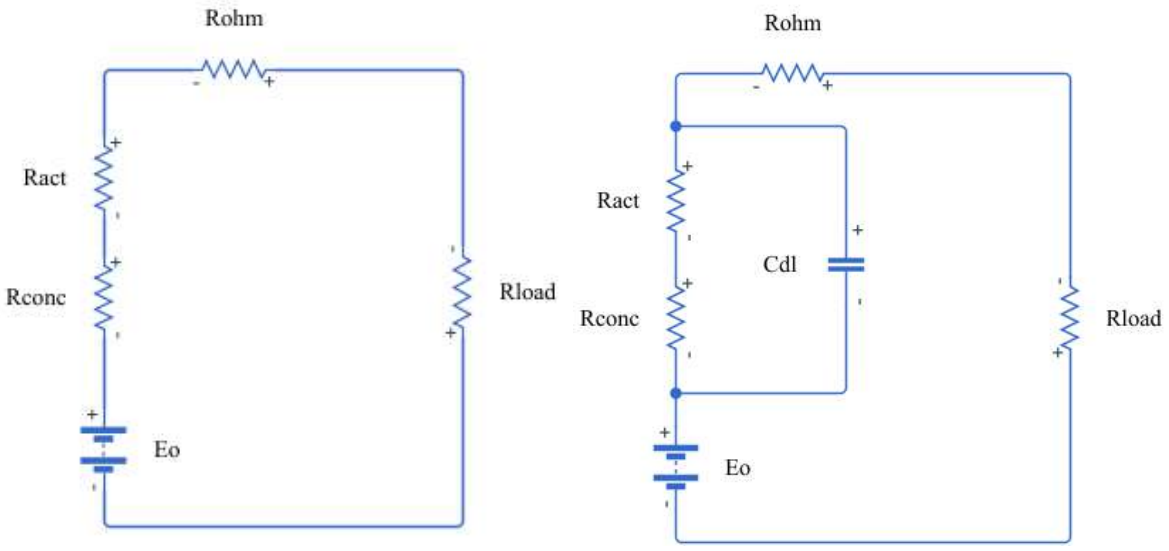

Figure 3.9: Schema for a simple and equivalent fuel cell circuit

Activation :

$$R_{act} = \frac{\Delta V_{act}}{i} \tag{3.31}$$

Concentration:

$$R_{con} = \frac{\Delta V_{Trans}}{i} \tag{3.32}$$

Ohmic:

$$R_{ohm} = \frac{\Delta V_{ohm}}{i} \tag{3.33}$$

R_{act}, R_{con}, and R_{ohm} represent the activation, concentration, and ohmic equivalent resistances, respectively.The overvoltage of the capacitive double layer can be described by first-order dynamics, as follows:

$$\frac{dv_d}{dt} = \frac{1}{C} i_{cell} - \frac{1}{(R_{act} + R_{conc})C} v_d \tag{3.34}$$

where v_d is the dynamical voltage through the equivalent capacitor associated with C, representing the membrane capacitance owing to the influence of the PEM fuel cell output voltage, and R_{act}, R_{conc} are the activation and concentration resistors, respectively.

This analysis focuses on the time required for the double-layer effect to stabilize as consumption fluctuates. The time constant τ of the corresponding circuit can be determined using the following calculation

$$\tau = (R_{act} + R_{conc})C \tag{3.35}$$

When calculating the operating voltage of a PEM fuel cell (PEMFC), the voltage drop v_d across the charge double layer is considered an irreversibility, similar to ohmic polarization. Essentially, the double layer polarization is subtracted from the Nernst potential to determine the fuel cell's operating voltage.

$$v_{cell} = E - V_{ohm} - v_d \tag{3.36}$$

Results of Dynamic Behavior Simulation

In this model, a time-step current is utilized to simulate a specific level of stress while observing the behavior of fuel cell properties. Figure 3.10a shows how the fuel cell output voltage dynamically responds to changes in load current. At $t = 10s$, as the current increased from $10A$ to $20A$, the output voltage decreased from $0.69V$ to $0.6V$. This change immediately caused a voltage drop across R_{ohmic}, which depends on R_{act} and capacitor C. Within $0.11s$, the voltage stabilized at $0.6V$ and remained constant. Conversely, when the current decreased to $10A$ at $t = 15s$, the output voltage increased from $0.6V$ to $0.69V$ and continued at this level until the simulation ended.

The plot in Figure 3.10b shows the evolution of the cell's output power and power consumption as the load current varies. The output power starts at $6.83W$ and peaks at $13.23W$ when the current is increased from 10 to $20A$ at $t = 10s$. It then returns to $6.83W$. The power consumption starts at $5W$, rises to $11.57W$ with increasing current, and then returns to $5W$ after 15 s. When the current drops to $10A$ at $t = 15s$, the output power falls from $12.24W$ to $5.56W$. After $1s$, it gradually increases back to $6.83W$. Power consumption drops from $11.57W$ to $5.075W$ and remains at this level until the end of the simulation.

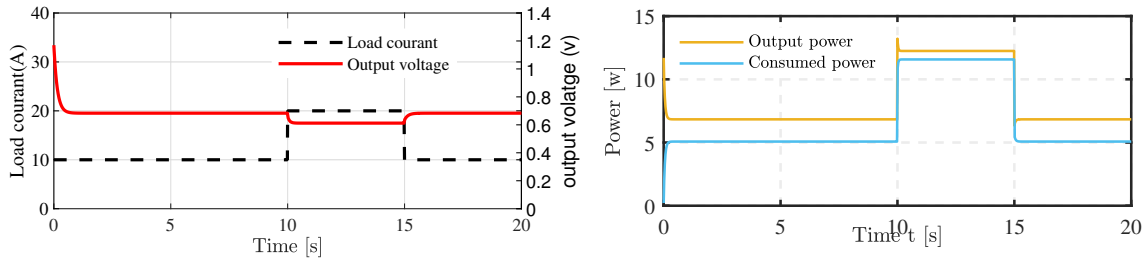

(a) (b)

Figure 3.10: The cell's dynamic output voltage response3.10a, The cell's dynamic output power and consumed power response3.10b

The figure 3.13 illustrates the variations in the output power of a Proton Exchange Membrane Fuel Cell (PEMFC) in response to different capacitance values associated with the double-layer charging effect.

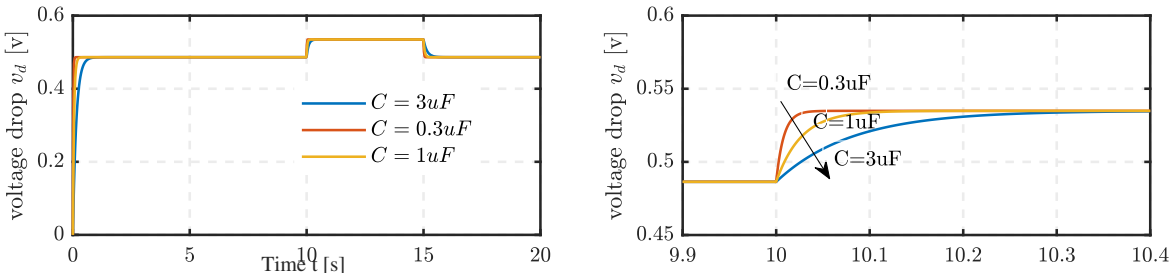

(a) (b)

Figure 3.11: Voltage drop polarization 3.12a,Zoom voltage drop polarization 3.12b

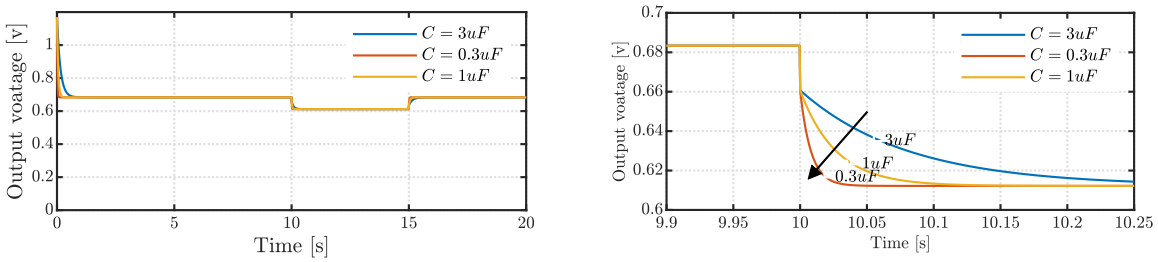

(a) (b)

Figure 3.12: Dynamic voltage response of the PEMFC model in relation to the double-layer charge effect. 3.12a,and thair Zoom 3.12b

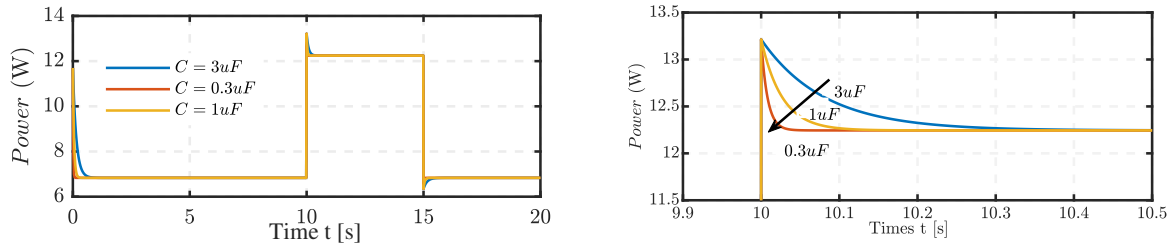

(a) (b)

Figure 3.13: Fuel cell due to capacitance of double-layer charge effect: Cell output power 3.13a, Zoom of cell output power 3.13b

3.3.10 Exchange Currents Effect:

Figure3.14a and Figure3.14b show the polarization curve and power of PEMFCs were plotted for a range of current densities at an operating temperature of cell 80°C and 1bar air pressure at defferent exchange currents. As shown in Figure 3.14 the impact of the proton exchange current on the cell is easily noticeable and has a significant influence on its performance. When there is an increase in the proton exchange current i_o, it has a substantial effect on power generation, which is relatively dependent on it. As the proton exchange current rises, the energy production and voltage also increase, resulting in reduced losses within the PEMFC.

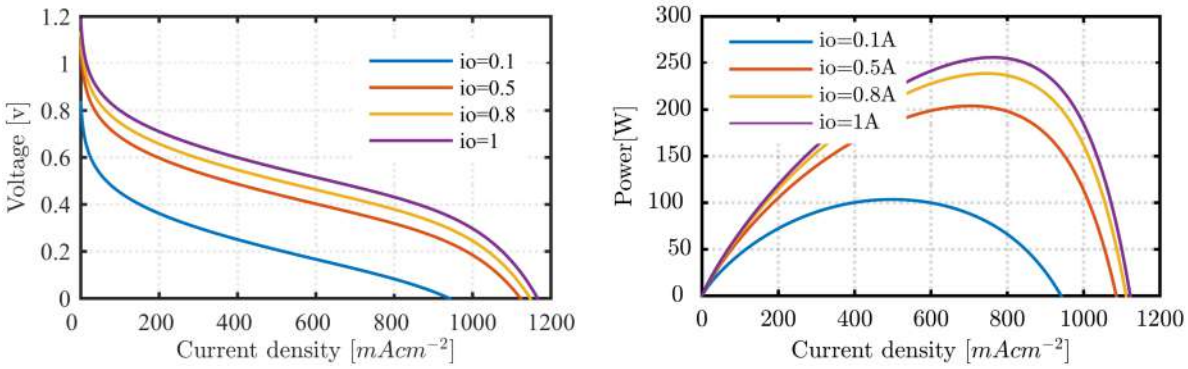

(a) (b)

Figure 3.14: 3.14a: One cell voltage and 3.14b : Fuel cell power against current density performance for a typical fuel cell operating at around 80°C, 1bar air pressure, with variable exchange currenti_0

3.3.11 Pressure Influence:

Figure 3.15 presents polarization curves, activation curves, ohmic and concentration overvoltages at different pressures for 80°C. The pressure effect corresponding to hydrogen and oxygen at the fuel cell inlet is measured for the flooding fault. As the pressure of hydrogen and oxygen increases, activation losses decrease, resulting in a reduced increase in current density, as shown in Figure 3.15b. Moreover, increasing pressure reduces concentration losses and improves current density, as illustrated in Figure 3.15c.On the other hand, ohmic resistance remains unchanged, as shown in Figure 3.15d . In summary, increasing the inlet pressure enhances fuel cell voltage and power density, as demonstrated in Figure 3.15a. During normal fuel cell operation, the pressure is maintained at 1 bar. However, in the event of flooding, the inlet pressure automatically increases, leading to cell failure . Therefore, effective cell monitoring is crucial to ensure reliable cell operation.

3.3.12 Temperature Influence:

The reversible cell potential from (3.14), (3.15) (3.19) is used in a fuel cell that consumes H_2 and O_2. As the temperature rises, the activation losses decrease because of the Tafel constant. This, in turn, increases the cell current density. The voltage drop under these conditions is non-linear. Figure 3.16b displays the activation voltage as it changes with temperature. Figure 3.17b shows the ohmic overvoltage as it changes with temperature. These losses occur due to the ohmic resistance caused by the electrolyte, cell interconnections, and bipolar plates. Figure 3.17aillustrates the impact of temperature on concentration voltage losses, which occur due to reactant consumption at the electrode. Here, temperature and losses are inversely proportional. Additionally, figure 3.16a presents the cell voltage loss and power density for varying temperatures. In general, increasing the temperature has a positive effect on fuel cell operation

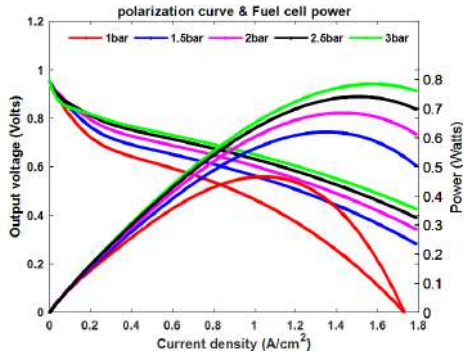

(a) Polarization curves for a fuel cell operated at different pressure

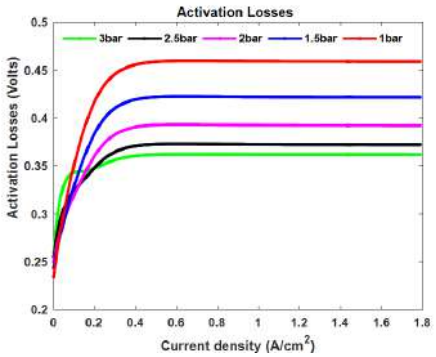

(b) Effect of pressure on the Activation loss

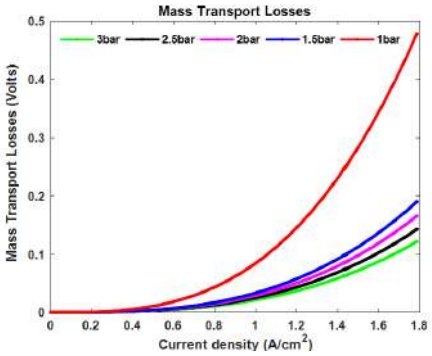

(c) Effect of pressure on the concentration loss

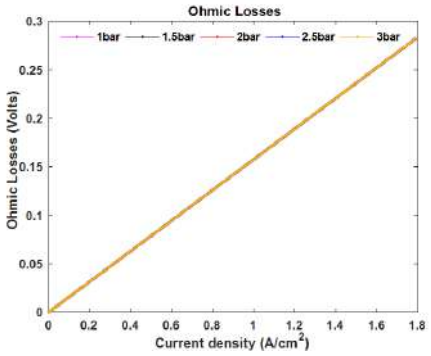

(d) Effect of pressure on the ohmic loss

Figure 3.15: Comparison of fuel cell performance at different pressures

and performance, reducing activation and concentration losses. However, higher temperatures have a minimal effect on improving cell performance and can even result in cell degradation and early failure.

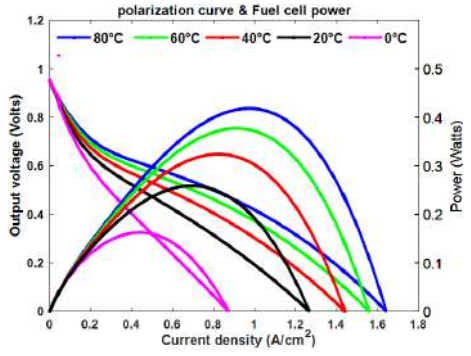

(a)

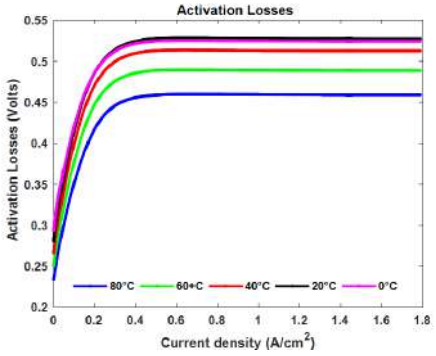

(b)

Figure 3.16: Various temperature effects: 3.16a on the polarization curve , 3.16b on the Activation loss

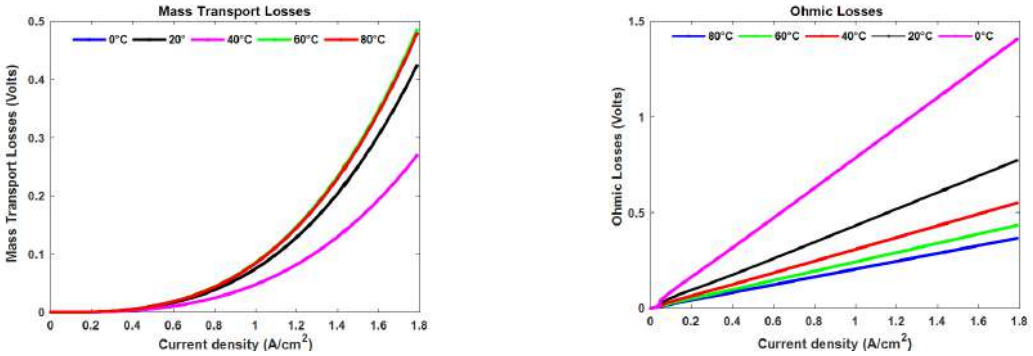

(a) (b)

Figure 3.17: Various temperature effects: 3.17a on the concentration loss and 3.17b on the ohmic loss

3.4 Supercapacitor and their Mathematical Model

Below, the model and dimensions of the supercapacitor are discussed. The equivalent circuit model frequently used is known as the RC model, which consists of a resistor R (also known as an equivalent series resistor or ESR) and a capacitor C. Widely used for energy regulation in embedded systems, this simple RC model effectively captures the energy characteristics of a supercapacitor, including its storage capacity [193, 194], as illustrated in figure 3.18.

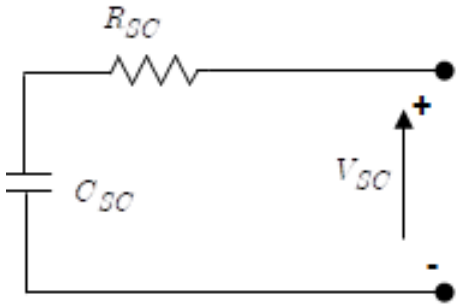

Figure 3.18: RC Model of the super capacitor

Because the connection between residual capacity and voltage level is relatively proportional, the super capacitor's SOC has always been applied to represent residual energy, it may be stated as:

$$SOC_{SC}(\%) = \frac{V_{SC} - V_{min}}{V_{max} - V_{min}} \tag{3.37}$$

in the following, the super-capacitor voltage V_{SC} as a function of SC current i_{SC} is calculated:

$$V_{SC} = -\frac{Q_t}{C_{SC}} - R_{SC} i_{SC} \tag{3.38}$$

where, Q_t denotes the amounts of electricity stored in a cell.

Using the power of a supercapacitor as a storage element in an electric vehicle necessitates the building of a stack of numerous cells, N_S of which are linked in series and N_P are coupled in parallel.

The following is the SC rated capacitance:

$$C_{SC} = C_{elem}\frac{N_P}{N_S} \tag{3.39}$$

the maximum equivalent series resistance of SC is provided by :

$$R_{SC} = R_{elem}\frac{N_S}{N_P} \tag{3.40}$$

the stack voltage is given below :

$$V_{SC} = V_{elem}N_S \tag{3.41}$$

the current of the supercapacitor can be written in the following manner :

$$I_{SC} = I_{elem}N_p \tag{3.42}$$

The energy saved in the capacitor develops as the voltage rises throughout charging as follows:

$$E_{cap} = \frac{1}{2}C\left(U_{Max}^2 - U_{Min}^2\right) \tag{3.43}$$

the capacity can then be computed using:

$$C = \frac{mv^2}{\left(U_{max}^2 - U_{min}^2\right)} \tag{3.44}$$

The discharge profile of a supercapacitor is shown in figure 3.19.The process starts by discharging the supercapacitor. Then, it is charged with a constant current I_c until it reaches the specified rated value, v_{rated}. After that, the supercapacitor's voltage is kept at v_{rated} for 5 seconds. Lastly, the supercapacitor is discharged by applying a constant current I_d where $I_d = I_c$.

When a charge or discharge current is applied, the resulting voltage deviation is used to determine the resistance R (or ESR).

$$\text{ESR} = \frac{V_{ESR}}{I_d} \tag{3.45}$$

where ESR represents the Equivalent Serial Resistance in V, I_d is the discharge current A, and V_{ESR}

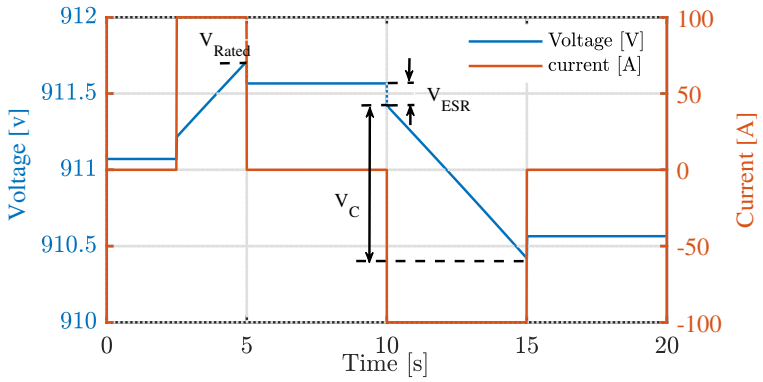

Figure 3.19: Constant current discharge profile

denotes the voltage drop V.The voltage drop V_{ESR} is calculated as the difference between V_{rated} and the value on the voltage tangent at the start of discharge.

3.5 Design and Development of DC/DC Converter Models

DC/DC converters are essential in hybrid power systems. They help control and adjust the current and voltage.

- **Boost Mode**: This mode increases the voltage from the PEMFC to match the higher voltage on the DC bus side, based on the power needs of the load.
- **Bi-directional Buck-Boost Mode**: This mode allows easy voltage conversion between the supercapacitor (SC) and the DC bus in both directions. During discharge, the boost mode is used, and the buck mode is used for charging.

There are two main types of DC/DC converter models used in simulations:

- **Average-Value Model**: This model replaces the switching component with controlled voltage/current sources. While it's quicker and ignores some switching effects, it doesn't capture all the converter's dynamics.
- **Switching Model**: This model considers switching harmonics and converter losses. It's mostly used for experimental setups with PWM control. This model provides a detailed understanding of switching conditions and converter dynamics within a specified time. In our study, we use the switching model to design a robust control loop that creates control signals for the switching components.

The structures of DC/DC converters based on the switching model are shown in Figure 3.20. Figure3.20a illustrates the electrical design of the boost converter, while Figure 3.20b demonstrates the arrangement of the bidirectional buck-boost converter. In terms of switching, the IGBT is chosen because it offers voltage control, fast switching speed, low conduction voltage drop, high blocking voltage, and a favorable switched power/cost ratio. It is a power semiconductor device that combines the advantages of the MOSFET and the bipolar transistor.

3.5.1 Converter Sizing Guidelines

At the time of sizing the converter, the values of the smoothing inductors L_{fc} and L_{sc} are specified (figure 3.20). These are used to adjust the current ripple in both the converter and the power source. In addition, it is necessary to determine the value of the filter capacitor C_{BUS}, which is designed to minimise the voltage ripple due to switching at the output of the converter [195].

$$L_{fc} = \frac{V_{bus}}{4 \cdot f \cdot \Delta I_{L_{\max}}} \tag{3.46}$$

$$C_{BUS} = \frac{I_L}{4 \cdot f \cdot \Delta V_{bus-max}} \tag{3.47}$$

$$L_{sc} = \frac{V_{bus}}{4 \cdot f \cdot \Delta I_{sc\max}} \tag{3.48}$$

where f is the switching frequency of the converter, I_L and $\Delta I_{L_{\max}}$ are respectively the current and the maximum current ripple in the boost inductor (figure , $\Delta I_{SC_{\max}}$ is the maximum ripple in the inductor of the biderctional buck-boost converter, and $\Delta V_{\text{bus}-\max}$ is the maximum voltage ripple across the capacitor. A DC bus handled the energy between the storage units of the fuel cell hybrid electric vehicle (FCHEV). Although the DC voltage delivered by the PEMFC changes greatly depending on the power requirements of the vehicle, a well-regulated DC voltage is necessary.

3.5.2 Modeling of Fuel cell Converter

Because the FC is not reversible, you must operate it with a unidirectional converter. The unidirectional converter is expressed in this study using the canonical mean-state theory, which is as follows:

$$\frac{di_{fc}}{dt} = \frac{v_{fc}}{L_1} - \frac{R_1}{L_1} i_{fc} - (1-u_1)\frac{v_{dc}}{L_1} \tag{3.49}$$

$$\frac{dv_{dc}}{dt} = (1-u_1)\frac{i_{fc}}{C_0} - \frac{i_1}{C_0} \tag{3.50}$$

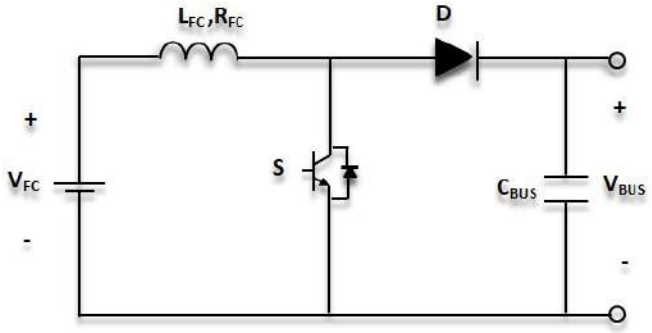

(a) Fuel cell DC-DC converter

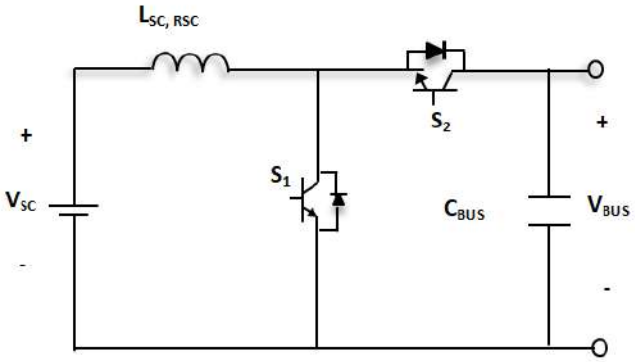

(b) SC bidirectional mode (buck-boost) DC-DC converter

Figure 3.20: The switching model of DC/DC converters with boost mode 3.20a and bidirectional mode 3.20b

where i_{fc},v_{fc} ,v_{dc} and i_1 represent the FC current, FC voltage, DC link voltage, and output current of the boost converter, respectively. The residual resistance of inductance, L_1 is represented by R_1 , and the duty ratio signal is u_1 applied to the switch, S_1 .

3.5.3 Modeling of Supercapacitor Converter

On the SC side, a bidirectional DC-DC converter facilitates charging and discharging of the SC while changing operational modes [196]. The mathematical expression for the SC current in the discharge process is as follows:

$$\frac{di_{sc}}{dt} = \frac{v_{sc}}{L_2} - \frac{R_2}{L_2} i_{sc} - (1-u_2)\frac{v_{dc}}{L_2} \tag{3.51}$$

$$i_2 = (1-u_2)\, i_{sc} \tag{3.52}$$

where v_{dc} is the DC connection voltage, and The SC current and voltage are represented by *isc* and *vsc*, respectively. Therefore, the linear connection is used to describe the relationship between i_{sc} and i_2 . The following expression determines the mathematical model and the link with the converter current and the

SC current:

$$\frac{di_{sc}}{dt} = \frac{v_{sc}}{L_2} - \frac{R_2}{L_2} i_{sc} - u_3 \frac{v_{dc}}{L_2} \tag{3.53}$$

$$i_2 = u_3 i_{sc} \tag{3.54}$$

where $u_3 = 1 - u_1$

An additional drive signal can be used to build a full converter design:

$$u_{23} = [H(1-u_2) + (1-H)u_3] \tag{3.55}$$

with $H = \begin{cases} 1 & if \quad i_{scref} > 0 \\ 0 & if \quad i_{scref} < 0 \end{cases}$ where H is the changeover mechanism and i_{scref} is the set-point current of the supercapacitor. Figure 3.21 depicts the structure of the two sources of energy and their associated DC/DC converters. The global state model of hybrid energy storage system (HESS) is given:

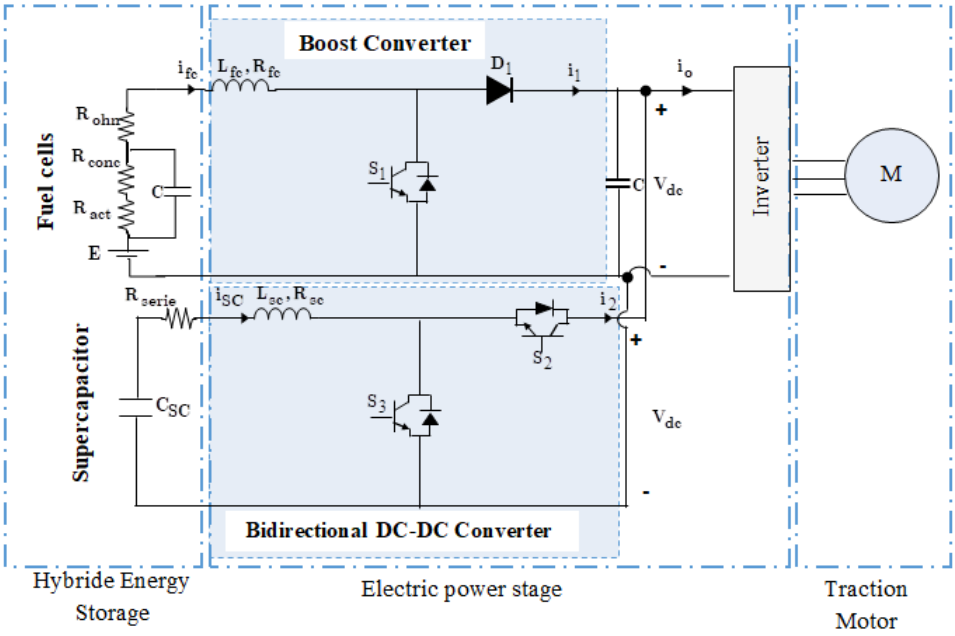

Figure 3.21: Diagram of the proposed hybrid power system

$$\begin{cases} \dot{x}_1 = \frac{v_{fc}}{L_1} - \frac{R_1}{L_1} x_1 - (1-u_1)\frac{x_3}{L_1} \\ \dot{x}_2 = \frac{v_{sc}}{L_2} - \frac{R_2}{L_2} x_2 - u_{23}\frac{x_3}{L_2} \\ \dot{x}_3 = (1-u_1)\frac{x_1}{C_0} + u_{23}\frac{x_2}{C_0} - \frac{i_0}{C_0} \end{cases} \tag{3.56}$$

with $i_0 = i_1 + i_2$

The subsequent alternatives are applied:

$$[x_1, x_2, x_3,] = [i_{fc}, i_{sc}, v_{dc}] \tag{3.57}$$

3.6 Three Phase Current System Configuration

To gain a comprehensive understanding of motor control methods, let us commence with an examination of the three-phase current configuration. Figure 3.22a serves as an illustration of how power systems utilize a three-axis coordinate system to depict this technique, rendering it more accessible to visualize the arrangement of three-phase currents. While this approach employs a complex frame of reference, Figure 3.22b presents a more straightforward alternative for visualizing the steady-state system.

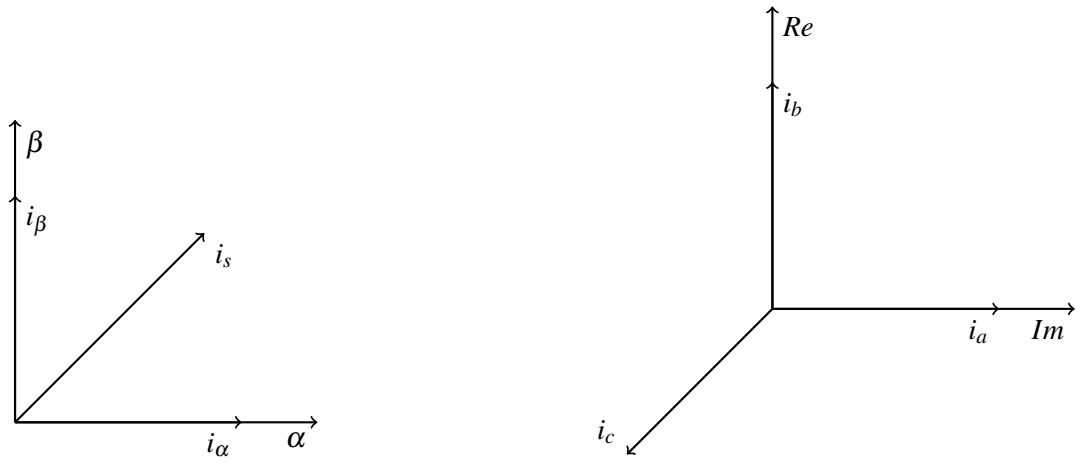

(a) Complex reference frame $\alpha\beta$ (b) Current System in a three axis coordinate abc

Figure 3.22: Rotate coordinate

A three-phase electrical system having an angular frequency w_0 can be represented within a stationary three-phase coordinate framework as outlined below:

$$i_a = I \cdot \sin(w_0 \cdot t) \tag{3.58}$$

$$i_b = I \cdot \sin\left(w_0 \cdot t + \frac{2\pi}{3}\right) \tag{3.59}$$

$$i_c = I \cdot \sin\left(w_0 \cdot t + \frac{4\pi}{3}\right) \tag{3.60}$$

The transition from a three-phase to a two-phase system is determined by the following expressions:

$$i_s = i_a + a \cdot i_b + a^2 \cdot i_c \tag{3.61}$$

$$\begin{cases} a & = e^{j\cdot\frac{2\cdot\pi}{3}} = \frac{-1}{2} + j\cdot\frac{\sqrt{3}}{2} \\ a^2 & = e^{j\cdot\frac{4\cdot\pi}{3}} = \frac{-1}{2} - j\cdot\frac{\sqrt{3}}{2} \end{cases} \tag{3.62}$$

The vector i_s can be represented in complex coordinates by applying the Clarke transformation.

$$i_s = i_\alpha + j\cdot i_\beta \tag{3.63}$$

$$i_\alpha = \frac{2}{3}\cdot\left(i_a - \frac{1}{2}\cdot i_b - \frac{1}{2}\cdot i_c\right) \tag{3.64}$$

$$i_\beta = \frac{2}{3}\cdot\left(\frac{\sqrt{3}}{2}\cdot i_b - \frac{\sqrt{3}}{2}\cdot i_c\right) \tag{3.65}$$

The symbols α and β signify the utilization of a complex frame of reference. In this scenario, the matrix structure can be employed to represent i_α and i_β as follows:

$$\begin{bmatrix} i_\alpha \\ i_\beta \end{bmatrix} = \frac{2}{3}\cdot\begin{bmatrix} 1 & -\frac{1}{2} & -\frac{1}{2} \\ 0 & \frac{\sqrt{3}}{2} & -\frac{\sqrt{3}}{2} \end{bmatrix}\cdot\begin{bmatrix} i_a \\ i_b \\ i_c \end{bmatrix} \tag{3.66}$$

Park's transformation is applied to transition from $\alpha\beta$ coordinates to rotating dq coordinates. As the dq coordinates rotate by an angle θ with respect to the $\alpha\beta$ system, the relationship between the two coordinate systems is described below:

$$\begin{pmatrix} i_d \\ i_q \end{pmatrix} = \begin{pmatrix} \cos(\theta) & \sin(\theta) \\ -\sin(\theta) & \cos(\theta) \end{pmatrix}\begin{pmatrix} i_\alpha \\ i_\beta \end{pmatrix} \tag{3.67}$$

The Park transformation also facilitates the inverse transition from dq coordinates back to $\alpha\beta$ coordinates in the following manner:

$$\begin{pmatrix} i_\alpha \\ i_\beta \end{pmatrix} = \begin{pmatrix} \cos(\theta) & -\sin(\theta) \\ \sin(\theta) & \cos(\theta) \end{pmatrix}\begin{pmatrix} i_d \\ i_q \end{pmatrix} \tag{3.68}$$

3.7 Mathematical Model for Permanent Magnet Synchronous Machine

As illustrated in Figure 3.23 , the propulsion system primarily comprises a (PMSM), a power converter, a drive circuit, and a circuit for current sampling [197, 198] [199] .The Permanent Magnet Synchronous Motor (PMSM) is mathematically represented in the rotational coordinate framework $d-q$ in the follow-

ing manner:

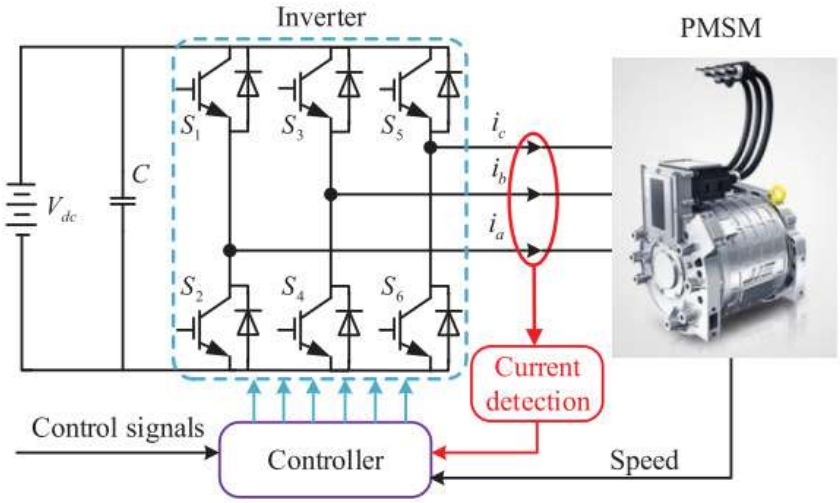

Figure 3.23: PMSM propulsion mechanism used in the FCEV.

$$\begin{cases} v_d & = R_s i_d + L_d \frac{di_d}{dt} - w_e L_q i_q \\ v_q & = R_s i_q + L_q \frac{di_q}{dt} + w_e (L_d i_d + \phi_f) \end{cases} \tag{3.69}$$

$$T_e = \frac{3}{2} p \left((L_d - L_q) L_d L_q + \phi_f i_q \right) \tag{3.70}$$

The inductances on the $d-q$ axes of the Permanent Magnet Synchronous Motor (PMSM) being used are equivalent. Hence, Equation 3.71 can be expressed as:

$$T_e = \frac{3}{2} p \left(\phi_f i_q \right) \tag{3.71}$$

where the mechanical and electrical rotor speeds are denoted as n and $w = \frac{2\pi p}{60} n$, respectively.In the $d-q$ coordinate frame, i_d and i_q represent the stator currents, while v_d and v_q denote the stator voltages. R_s stands for the armature winding resistance, L_s signifies the stator inductance, and ϕ_f represents the permanent magnet flux. p indicates the number of pole pairs, and T_e represents the electromagnetic torque.

The mechanical dynamics of the PMSM can be described as follows:

$$\frac{\mathrm{d}w_m}{\mathrm{d}t} = \frac{1}{J} \left[T_m - T_e - f_w \right] \tag{3.72}$$

here w_m represents the motor speed, J stands for the analogous inertia, f_w denotes the rotor's viscous friction, while T_m indicate the load torque.

The torque and power versus speed curve depicted in Figure 3.24 illustrate two modes of opera-

tion for electric motors: constant torque mode and constant power mode.In constant-torque mode at low speeds, the machine can provide a constant rated torque , and the rotor power increases proportionally with speed.When in constant-power mode, the machine can deliver a constant rated power when operating above rated speed, and the available rotor torque decreases inversely with rotor speed.

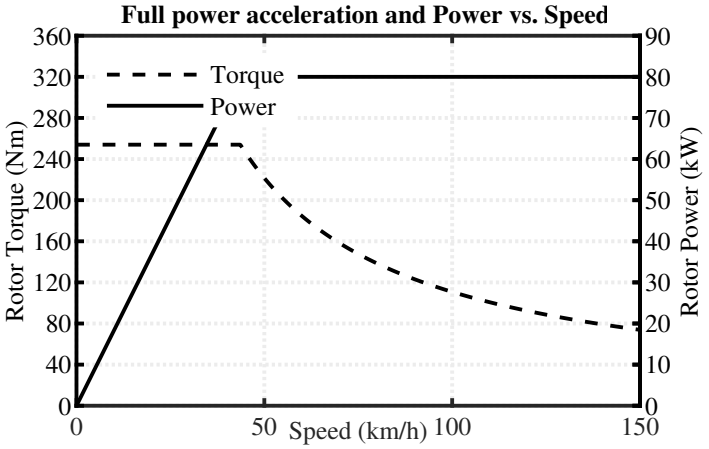

Figure 3.24: Full power acceleration and Power vs. Speed

Table 3.4: PMSM Parameters

Parameter	Value	Units
Rated power (Pr)	50	kW
Stator resistance (Rs)	6.5	mΩ
Stator inductance (Lsd, Lsq)	8.35	mH
PM magnet flux ϕ_f	0.1757	Wb
Number of pole pairs (p)	4	-
Motor inertia (J)	0.089	kg.m^2
Viscous damping (f)	0.005	N.s/m

3.8 Two-Level Voltage Source Inverter - Model

Figure 1(a) depicts a schematic representation of a 2L-VSI-PMSM drive system. The illustration displays the switching signals for the top and bottom inverter arms of phases A, B, and C, specifically identified as S_{ap}, S_{bp}, S_{cp}, S_{an}, S_{bn}, S_{cn}.

Due to the corresponding structure of its top and bottom arms, the 2L-VSI can alternate between eight modes. Consequently, these eight states produce six fixed amplitude and phase position space vectors for the output line voltage.S_a, S_b, and S_c are the gating signals that control the switching states of the converter. They are shown in the following manner:

$$S_{ij} = \begin{cases} 1 & \text{if } S_{ap} \text{ on and } S_{an} \text{ off} \\ 0 & \text{if } S_{ap} \text{ off and } S_{an} \text{ on} \end{cases} \tag{3.73}$$

where $i = a, b$ and c and $j = p, n$

The switching states can be expressed by the vector as following:

$$S = \frac{2}{3}\left(S_a + aS_b + a^2 S_c\right) \tag{3.74}$$

where $a = e^{j2\pi/3}$.

Similar to the described three-phase current system above, the output voltage space vectors genergated by this two-level voltage source inverter are defined by:

$$v = \frac{2}{3}\left(v_a + av_b + a^2 v_c\right) \tag{3.75}$$

where $v_{a,b,c}$ denotes the phase to neutral voltages of the inverter. This voltage vector v is related to the switching state S by

$$v = V_{dc} S \tag{3.76}$$

Considering all possible combinations of the switching signals $S_{a,b,c}$, there are in total eight reasonable different switching states. These are presented in Fig. 2.2(b). The equivalent of $v_0 = v_7$ results in only seven different voltage vectors.

In this work, the inverter is considered as a nonlinear discrete system with seven different states as possible outputs, because only the direct control methods are focused.

Table 3.5: Summary of Voltage Vectors with Switching States concerning the VSI

$(S_a\, S_b\, S_c)$	Voltage Vectors v	$(S_a\, S_b\, S_c)$	Voltage Vectors v
(0, 0, 0)	$V_0 = 0$	(0, 1, 1)	$V_4 = -\frac{2}{3}V_{dc}$
(1, 0, 0)	$V_1 = \frac{2}{3}V_{dc}$	(0, 0, 1)	$V_5 = -\frac{1}{3}V_{dc} - j\sqrt{\frac{3}{3}}V_{dc}$
(1, 1, 0)	$V_2 = \frac{1}{3}V_{dc} + j\sqrt{\frac{3}{3}}V_{dc}$	(1, 0, 1)	$V_6 = \frac{1}{3}V_{dc} - j\sqrt{\frac{3}{3}}V_{dc}$
(0, 1, 0)	$V_3 = -\frac{1}{3}V_{dc} + j\sqrt{\frac{3}{3}}V_{dc}$	(1, 1, 1)	$V_7 = 0$

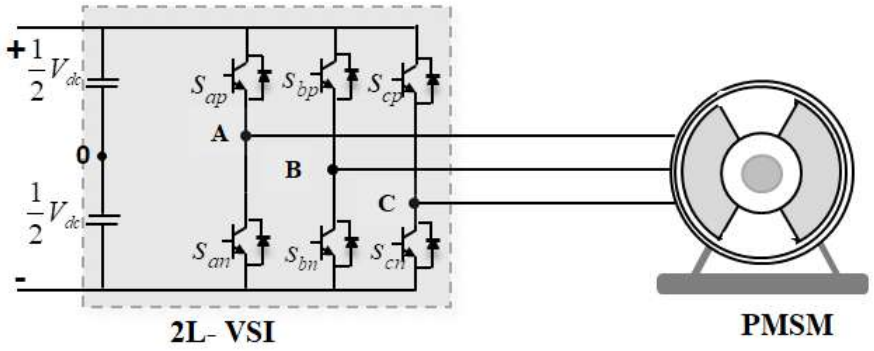

(a)

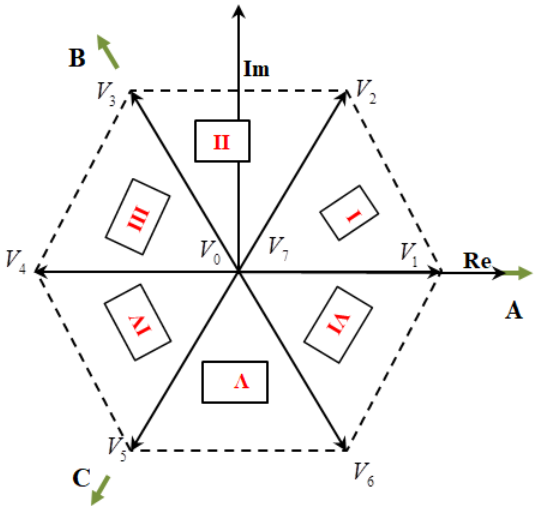

(b)

Figure 3.25: Illustration of Two-Level Three-Phase Voltage Source Inverter (VSI) 3.25a and their Voltage Vector Configuration 3.25b

3.9 Conclusion

This chapter focuses on the importance of power sources, in particular PEM fuel cells, supercapacitors and power converters, examining their definitions, analyses and modeling. These components play an essential role in vehicle operation and propulsion. In addition, the importance of modeling and numerical simulation of these components was highlighted in order to fully exploit their capabilities. By creating accurate models, it was possible to better understand their behavior and improve the performance of electric vehicles. This modeling process was essential to ensure the effective and efficient use of PEM fuel cells and supercapacitors, resulting in improved performance of fuel cell electric vehicles. The next chapter will focus on the development and improvement of energy management across the different energy sources and their controls, as well as exploring new possibilities for improving their performance for EVs.

Chapter 4

Essential Components of Control Design

In this chapter, we explore energy management strategies for multi-source electric vehicles. Our primary objective is to provide a comprehensive review of the various approaches and methods available to enhance energy management in multi-source electric vehicles.More specifically, we are focusing on the complex interaction between two essential energy sources: the fuel cell and the supercapacitor. We will study how energy can be efficiently transferred and distributed between these two sources. The key role of energy management is to improve system performance, increase overall efficiency and ensure a smooth and comfortable driving experience which is our main objective throughout this chapter.Furthermore, we will also discuss the specific challenges and promising opportunities related to power management in the context of multi-source electric vehicles.

Contents

4.1 Introduction

To facilitate energy exchange and power distribution, we introduce a dedicated power electronics interface, which includes both unidirectional and bidirectional power converters.The primary advantage of an active hybrid power exchange system through a power electronics interface, as opposed to a passive structure, lies in its ability to monitor and control energy flow in real time.Subsequently, we employed non-linear backstepping controllers to regulate the output voltage of the power sources, allowing for both step-down and step-up operations. These controllers exhibited exceptional performance, ensuring voltage stability with minimal ripple current.

However, the current chapter has highlighted specific challenges stemming from the highly non-linear behavior of the fuel cell. These challenges have led to current ripples both at the fuel cell outputs and within the hybrid system. Additionally, a fuzzy logic controller is employed to generate the reference current, further enhancing overall control performance and effectively managing the system's non-linear characteristics. As a complement to the main controller, we have proposed a robust non-linear control strategy. This strategy combines backstepping with super-twist sliding mode control to effectively address these issues in the boost converter outputs.

4.2 Driving Cycle

A driving cycle is a standardized driving model used to evaluate various aspects of a vehicle's performance, such as fuel efficiency, emissions and range, among others [200]. It is essentially a sequence of data points that graphically describe a vehicle's speed over a given period. These cycles are carefully designed to closely simulate real-world driving conditions, and are widely used by automakers, organizations and researchers to evaluate and analyze vehicle performance. They provide valuable information on a vehicle's operational characteristics and its impact on fuel consumption and emissions in typical driving scenarios [201]. Cycles can be categorized according to the following indicators [202]:

- Load situation: This includes periods of continuous or variable speed.
- Context of use: This refers to urban, suburban, or motorway environments.
- Proposed vehicle mission profile: This may include bus service, private passenger transport, or commercial delivery.

For emissions testing and certification in Europe, a chassis dynamometer test is conducted. This test includes one Extra Urban Driving Cycle (EUDC 4.1b), which simulates highway driving, and four ECE

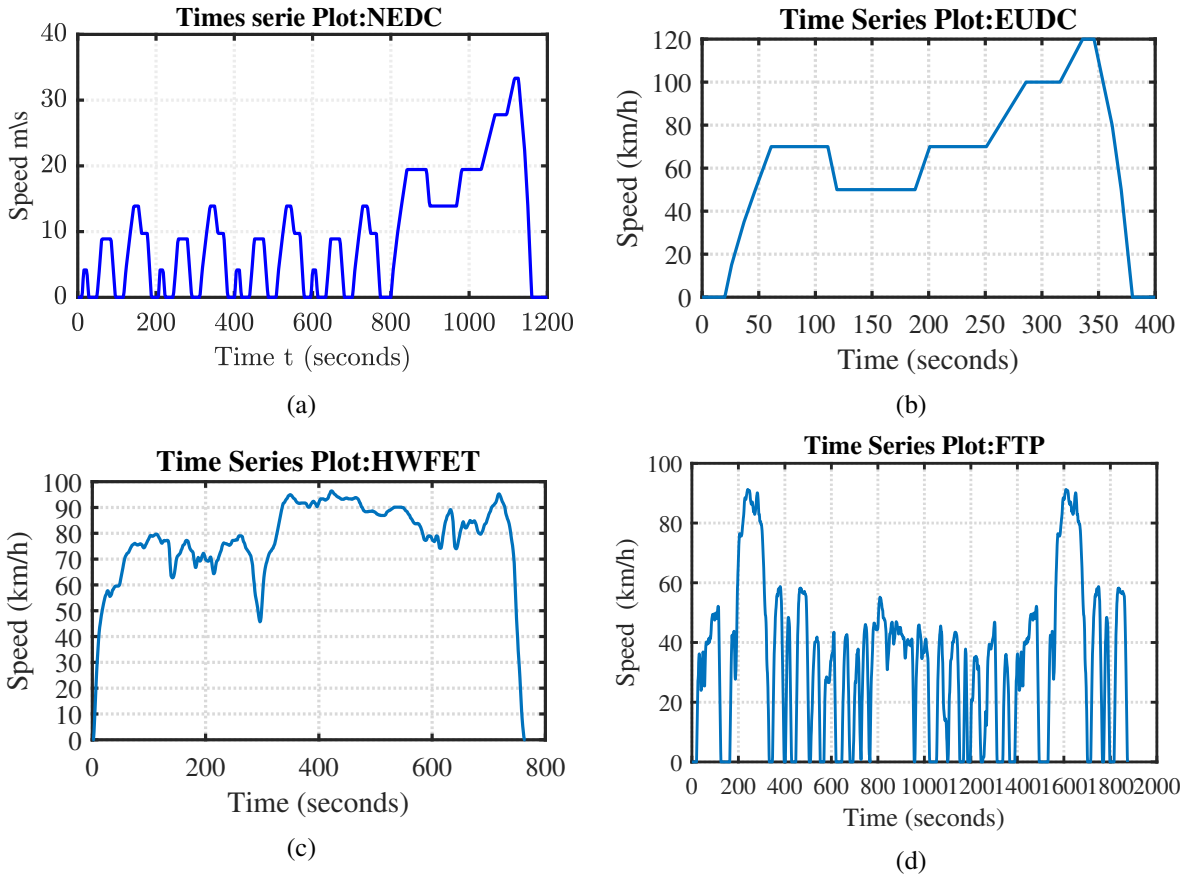

Figure 4.1: Time series plot :NEDC4.1a EUDC 4.1b ,HWET4.1c,FTP4.1d

Urban Driving Cycles that replicate real urban driving conditions. The cold-start variant of this test, known as the New European Driving Cycle (NEDC figure 4.1a), was implemented in 2000 [17].

Table 4.1: Comparative Analysis of Parameters Employed in the NEDC, EUDC, and ECE Driving Cycles [17]

Characteristics	Unit	ECE 15	EUDC	NEDC
Distance	km	0.9941	6.9549	10.9314
Total time	s	195	400	1180
Average speed (incl. stops)	km/h	18.35	62.59	33.35
Maximum speed	km/h	50	120	120
Average acceleration	m/s^2	0.599	0.354	0.506
Maximum acceleration	m/s^2	1.042	0.833	1.042

4.3 Power Demands Determination

A fuel cell, a supercapacitor, or both could be used as the main power source in a hybrid electric vehicle to provide the power needed at all times [203]. Indeed, the vehicle's power requirements at each phase of the driving cycle are crucial to the efficient sizing of both energy sources [204]. The quantity of mechanical energy dissipated by a vehicle while adhering to a specific driving pattern is determined by

three fundamental factors: aerodynamic friction losses, rolling friction losses, and energy dissipated via the braking system [205, 206].As a vehicle moves forward, it encounters a number of resistive forces. Figure 4.2 provides a visual representation of these forces acting on the vehicle.

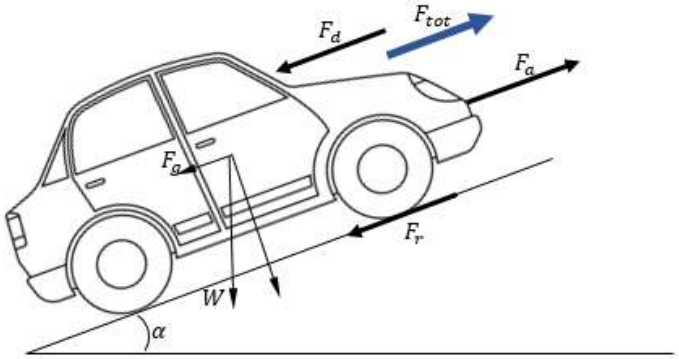

Figure 4.2: Forces applied on a vehicle

In this context, the force acting on the vehicle F_{tot} is the sum of accelerating force F_a ,drag force or Aerodynamic force F_d,gravitational force or grade force F_g and rolling force F_r as the following and their brief descriptions are presented in Table 4.2:

$$F_{tot} = F_a + F_d + F_g + F_r \tag{4.1}$$

Aerodynamic force (F_d) is generated by a vehicle's motion through the air and is influenced by factors such as the vehicle's size and forme. It is directly related to air density ρ, the vehicle's frontal area A , the aerodynamic drag coefficient C_D, and the square of its speed $V(t)$. The aerodynamic drag coefficient C_D represents the object's resistance to air movement for a given frontal area.

$$F_d = \frac{1}{2} C_D A \rho V^2(t) \tag{4.2}$$

Gravitational force (F_g) is relevant when the road is inclined. This force become stronger as the slope of the road increases and the vehicle's mass becomes greater.

$$F_g = M_v g sin(\alpha) \tag{4.3}$$

where M_v determines the vehicle's weight, g apply gravitational acceleration,the slope of the road α is considered zero .

Rolling Force F_r The term rolling resistance, also known as rolling drag or rolling friction, refers

to a force that resists the movement of a vehicle [207]. This resistance is mainly due to several factors, including the aerodynamic drag acting on the vehicle, the resistance generated during acceleration due to inertial forces, and the frictional resistance within the tires [208]. It is conventionally expressed using the following mathematical notation [209]:

$$F_r = M_v g f cos(\alpha) \tag{4.4}$$

where f represents the rolling resistance constant.

Acceleration force (F_a): The acceleration of a vehicle caused by a net external force is directly proportional to the force in a direction parallel to that force and inversely proportional to its mass, according to Newton's description of the Second Law of Motion [210].This force, called the acceleration force, is typically expressed as :

$$F_a = M_v \frac{dV}{dt} \tag{4.5}$$

Table 4.2: Forces Affecting Vehicle Movement

Symbol	Description
F_{tot}	Total tractive force required to move the vehicle.
F_a	Accelerating force required to overcome the inertial effect.
F_d	Drag force due to aerodynamic resistance of air.
F_g	Grading force required to overcome the slopes of the road.
F_r	Frictional load due to the movement of tires over the road.

The equation for the balance between the driving force and the vehicle resistance can therefore be written as follows:

$$F_{tot} = mgf + \frac{1}{2} C_D A \rho V^2(t) + \delta m \frac{\mathrm{d}V}{\mathrm{d}t} \tag{4.6}$$

where δ represents the rotating mass weight constant.

The necessary power can be computed as described below:

$$P_{laod}(t) = \frac{1}{\eta_{motor} \eta_{DC/AC} \eta_{DC/DC}} V(t) \left(mgf + \frac{1}{2} C_D A \rho V^2(t) + \delta m \frac{\mathrm{d}V}{\mathrm{d}t} \right) \tag{4.7}$$

The efficiency of the motor, the DC/AC converter, and the DC/DC converter is represented by η_{motor} , $\eta_{DC/AC}$ and $\eta_{DC/DC}$ respectively. In addition, the following result was obtained :

$$P_{laod} = P_{fc} + P_{sc} \tag{4.8}$$

where P_{fc} denotes the power of the fuel cell, while P_{sc} denotes the power of the supercapacitors.The vehicle's essential characteristics are shown in table 4.3.

Table 4.3: The vehicle's essential characteristics

Characteristic	Value
Mass	$800kg$
Frontal projected area	$2.59m^2$
Air drag coefficient	0.35
Air density	1.29
Roll resistance coefficient	0.014

4.4 Energy Management System

The main objective is to continuously meet the energy requirements of the powertrain while using the least amount of hydrogen possible. It is crucial to determine the limitations set by the size of the system's components and prioritize keeping the storage element charged to maximize the overall efficiency of the system. The main challenge lies in the unpredictable route taken by the hybrid vehicle. Consequently, the energy management system needs to be capable of promptly responding to immediate energy demands without prior knowledge of the future energy profile. Since achieving an optimal solution in this scenario is impossible, the goal is to develop a solution that closely approximates the desired outcome [211].

4.4.1 Effective Scheme for Current Sharing and Frequency Regulation

The hybrid power system control system, which is based on the frequency sharing approach, effectively handles transient and steady-state power issues. It achieves this by supplying the fuel cell and supercapacitor (SC) with the appropriate setpoint currents. This ensures a stable bus voltage and rapid recovery.

With this management method, the charging requirements of the fuel cell, whether regular or low-frequency, are taken into consideration. As a result, the supercapacitor only responds to short charging pulses. This not only prolongs the service life of the fuel cell, but also protects it from harmful current peaks. Additionally, the supercapacitors are valuable for maintaining and restoring bus voltage, thus ensuring a continuous power flow. Figure 4.3 illustrates the distribution of load power in the hybrid power system using the LPF approach.

Figure 4.4 illustrates the decoupling of power between the fuel cell and supercapacitor (SC) power setpoints. The objective is to allocate each power source an appropriate current, taking into account their technical characteristics and operational limitations. The low-pass filter (LPF) used is defined as

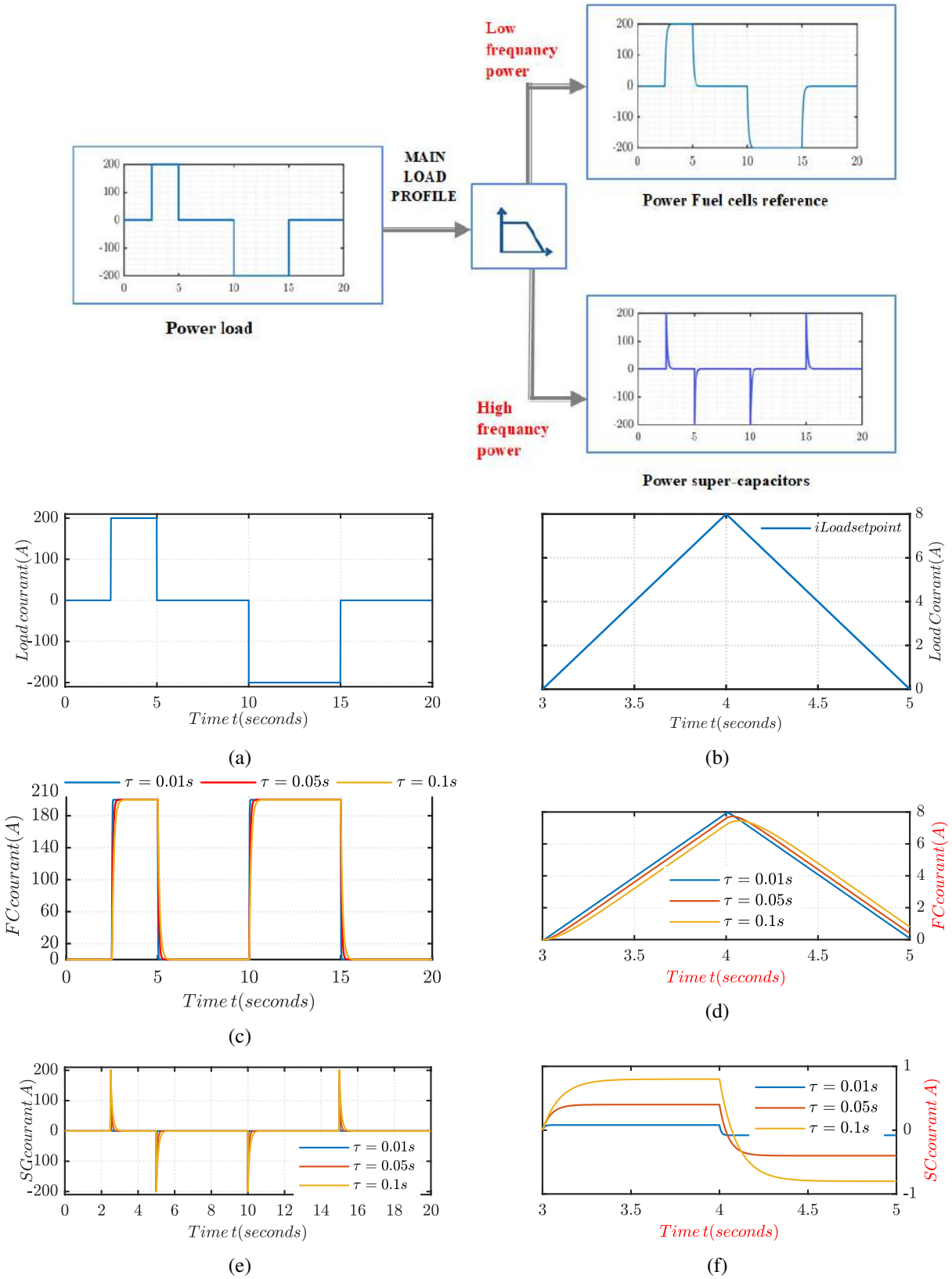

Figure 4.3: The process of Frequency Splitting in Power Systems

$\frac{1}{\tau \cdot s+1}$, where τ represents the time constant (0.01, 0.05, and 0.1). This filter attenuates high-frequency SC currents while allowing lower-frequency fuel cell currents to pass through.The use of higher time constants is suggested for improved filtering [212]. The desired output power of the fuel cell can be

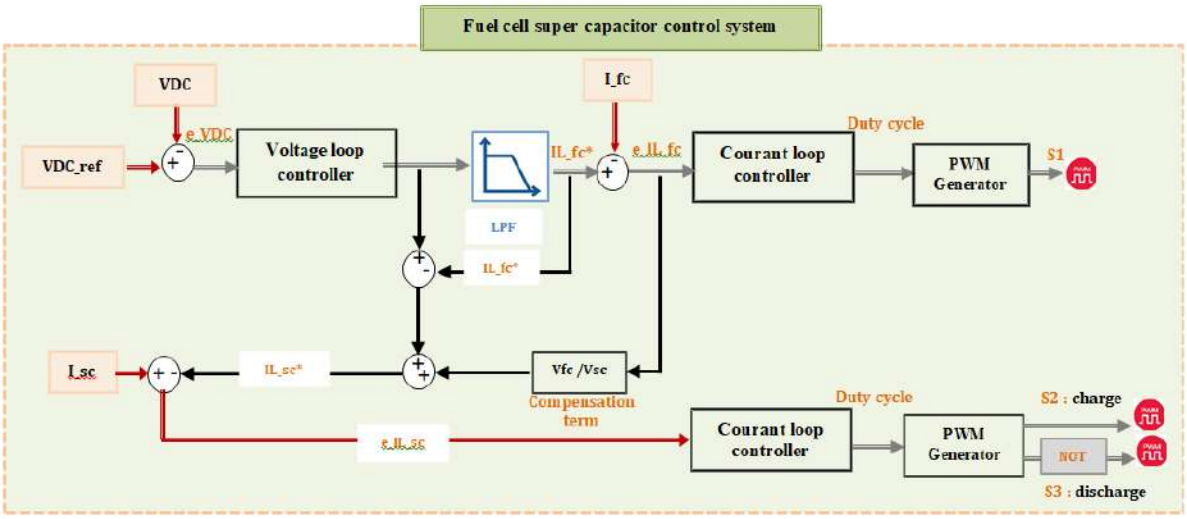

Figure 4.4: Lowpass filter based power management strategies for fuel cells and supercapacitors power Systems

determined on the basis of the Low Pass Filter:

$$P_{\text{fc}} = \frac{1}{\eta(\tau s+1)} P_{\text{load}} \tag{4.9}$$

The output net power of the FC system, denoted as P_{fc}, is influenced by the efficiency of the EV system represented by η, and the filter time constant of the FC, indicated by τ.

4.4.2 Energy management based Fuzzy Logic Methode

The purpose of the core layer control is to determine the appropriate allocation of power supplied by the storage device as a function of speed. It is intended to make this system work properly and maintain the power allocation from the demand side to the supply side in order to satisfy the load demand while rejecting power shortages and excesses.In order to satisfy the energy needs of the load. A fuzzy inference system (FIS) was created to provide an indicator called K_{ε}, which is an additional parameter used to make the adjustment between the main source power and the load power, This adjustment was based on the following expressions:

$$i_D = i_{scref} + i_{fcref} \tag{4.10}$$

and

$$i_{fcref} = K_\varepsilon i_D \tag{4.11}$$

Furthermore, the desired current of the supercapacitor can be written as follows:

$$i_{scref} = (1 - K_\varepsilon)\, i_D \tag{4.12}$$

where i_D denotes the demand current

4.4.3 Fuzzy Logic Controller

In this work, the objective is to maximize the performance of the vehicle by holding the SOC at as a high level as possible.

Figure 4.5, shows a fuzzy logic based power management system (PMS).The FLC's two input variables are the speed and the change in the supercapacitors's state of charge SOC_{SC} . The value of the first input variable velocity is arranged in three modes for fuzzification: Low L , Medium M, and High H, with a numerical limit of $[0km/h \quad 60km]$. Equally, the other input signal has three modes: Low L , Medium M ,and High L , with a numerical range of $[0\% \quad 100\%]$.The output of the K_ε factor is classified into four modes: Very Small VL, Small L , Medium M, and Very Large VL , with a numerical limit of $[0.5 \quad 1.5]$.

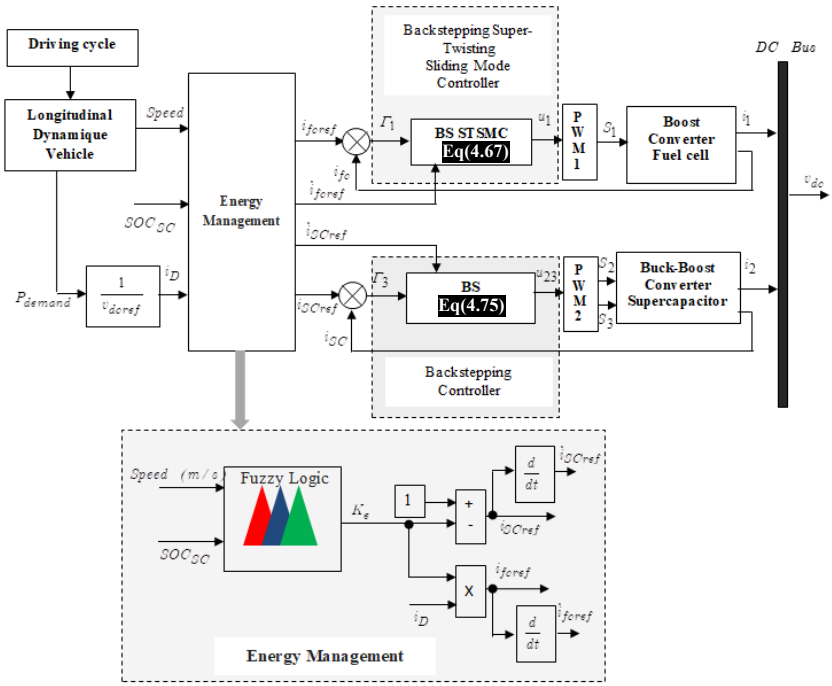

Figure 4.5: Fuzzy logic based power management system (PMS)

4.4.4 Membership Function Selection for Input and Output Variables

A crucial aspect of fuzzy logic modeling is the selection of membership functions. Because it has the ability to approximate any piecewise continuous linear function using membership functions such as triangular and trapezoidal functions and central mean defuzzification, fuzzy logic is a powerful tool in engineering applications.The process involves three steps: first, the input data is converted into a fuzzy form to optimize decision-making; second, an inference engine applies a set of rules; and finally, the defuzzification step is carried out as shown in Figure 4.6.

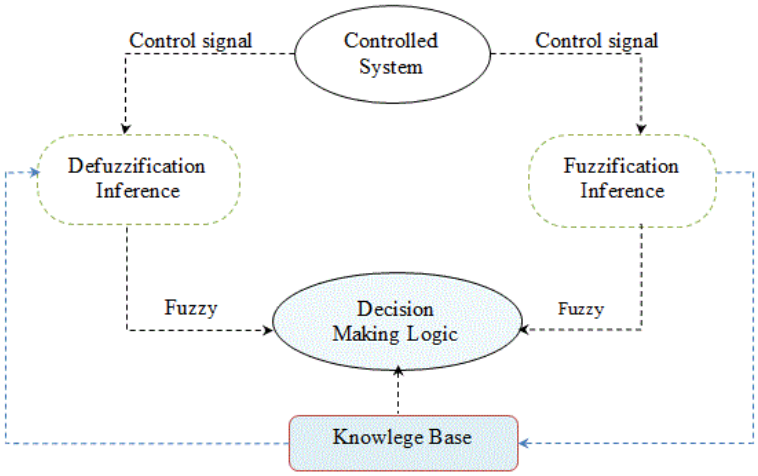

Figure 4.6: Fuzzy logic steps

Due to their simplicity of representation and computational efficiency, triangular and trapezoidal functions are used in this context, making them suitable for real-time applications. Semantic rules must be used to create a membership function for each language value. Therefore, each value of the linguistic variable *speed*, *SOC* and the output K_ε has its own membership function.

The referential rule must specify a membership function for each linguistic data value. Figure 4.7 shows the membership functions which highlight the source feedback mechanisms. For defuzzification, Mamdani's fuzzy inference approach as well as the centroid method are used.

The trapezoidal membership functions have been chosen to specify the degree of membership of a numerical input to a linguistic variable, as well as the possible operating domains of all input values; they are specified by :

$$trap(x,a,b,c) = \begin{cases} 0 & , \quad x < a \\ \frac{x-a}{b-a}, & a \leq \quad x \leq b \\ \frac{d-x}{d-c}, & c \leq \quad x \leq d \\ 0 & , \quad x \geq d \end{cases} \tag{4.13}$$

where (a), (b), (c) and (d) represent the possible range of variation of the input value.The blue curves shown in Figures 4.7a and 4.7b low limit variation of inputs value, the red ones for the medium rang variation, and finally the orange one gives the high rang of variation .

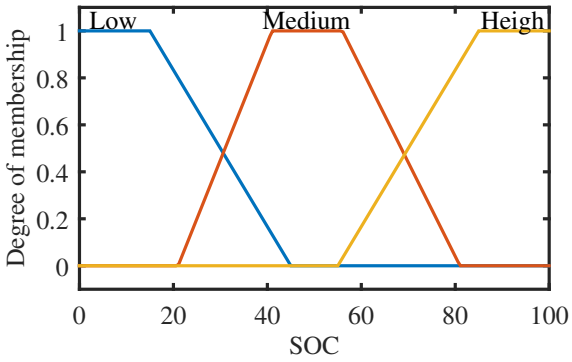

(a) ,SOC_{SC}

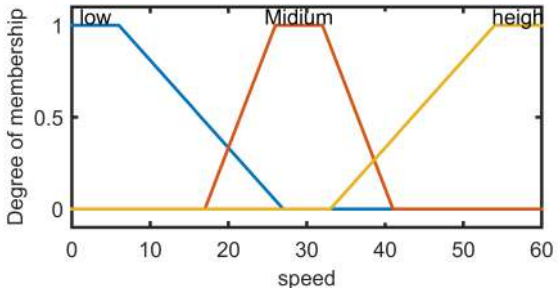

(b) speed

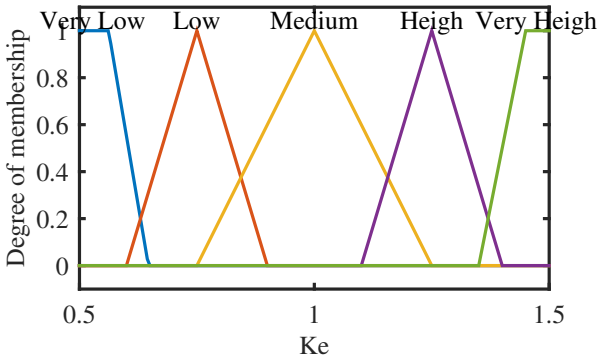

(c) scale factor K_ε

Figure 4.7: Inputs and output membership functions of:4.7a SOC_{SC} , 4.7b speed,4.7c scale factor K_ε

As shown in Table 4.4, the nine rules provided for the PMS in the architecture proposed here contain all the best operating parameters for the FC, the supercapacitor in various load scenarios.

4.5 Non-linear Backstepping Controller Theory

Backstepping is a systematic, recursive approach for synthesizing nonlinear control laws with Lyapunov functions, which stabilize every phase throughout the step-by-step synthesis. A virtual control is produced

Table 4.4: Fuzzy Logic Rule

		SOC		
K_ε		L	M	H
speed	L	VH	H	M
	M	H	M	L
	H	M	L	VL

at each stage of the process to ensure the system's convergence to its steady state. This approach makes it possible to establish control laws that take into account system disturbances or unknowns. Backstepping control depends on the principle of making closed-loop systems equal to first-order subsystems in a stable Lyapunov cascade, providing them resilience and asymptotic global stability [109]. The following nonlinear system can be considered:

$$\begin{cases} \dot{x}_1 = f_1(x_1) + g_0(x_1)x_2 \\ \dot{x}_2 = f_2(x_1,x_2) + g_1(x_1,x_2)x_3 \\ \vdots \\ \dot{x}_n = f_2(x_1,..x_n) + g_{n-1}(x_1,..x_n)u \end{cases} \tag{4.14}$$

Step I:

The first virtual law To begin with, the initial system has the following equation, (4.14), where x_2 will be treated as an intermediate virtual command.The first desirable reference of the subsystem x_1 is defined as following the reference y_{ref}, as follows:

$$(x_1)_d \triangleq y_{ref} = \alpha_0 \tag{4.15}$$

where $(x_1)_d$ represents the expected state. The subsystem's first error variable is specified as follows:

$$e_1 = x_1 - \alpha_0 \tag{4.16}$$

and

$$\dot{e}_1 = f_1(x_1) + g_0(x_1)x_2 - \dot{\alpha}_0 \tag{4.17}$$

For this particular subsystem, the initial step involves the creation of the Lyapunov V_1 function in a

quadratic form.

$$V_1 = \frac{1}{2} e_1^2 \tag{4.18}$$

Its derivative is given by:

$$\begin{cases} \dot{V}_1 = e_1 \dot{e}_1 \\ \dot{V}_1 = e_1 \left[f_1(x_1) + g_0(x_1) x_2 - \dot{\alpha}_0 \right] \end{cases} \tag{4.19}$$

In order to ensure the stability of the subsystem according to Lyapunov, $\dot{V}_1$ must be negative. For this we choose in the form:

$$\dot{V}_1 = -k_1 e_1^2 \leq 0 \tag{4.20}$$

where $k_1 > 0$ represents a conception condition. By substituting (4.20) in (4.19), gives :

$$\dot{V}_1 = e_1 \left[f_1(x_1) + g_0(x_1) x_2 - \dot{\alpha}_0 \right] = -k_1 e_1^2 \tag{4.21}$$

This gives the virtual law x_2.

$$x_2 = \frac{1}{g_0(x_1)} \left[-k_1 e_1 + \dot{\alpha}_0 - f_1(x_1) \right] \tag{4.22}$$

Hence the asymptotic stability of the origin. The latter will be the desired new reference x2ref of the following system.

Step II:

The second virtual law We consider the first two equations of the system defined in (4.14). where the new desired reference α_1 will be the command x_{ref} such as:

$$x_{2ref} \stackrel{\Delta}{=} \alpha_1 \tag{4.23}$$

The new error variable is defined as :

$$e_2 = x_2 - \alpha_1 \tag{4.24}$$

this implies that the Lyapunov function is designed to guarantee the stability of the following subsystem:

$$\dot{x}_2 = f_2(x_1, x_2) + g_1(x_1, x_2) x_3 \tag{4.25}$$

These functions necessarily depend on the previous states of the subsystem defined by:

$$\dot{x}_1 = f_1(x_1) + g_0(x_1)x_2$$

For the subsystem (4.25), Lyapunov implements another function.

$$\begin{cases} V_2 = V_1 + \frac{1}{2}e_2^2 \\ V_2 = \frac{1}{2}\left[e_1^2 + e_2^2\right] \end{cases} \tag{4.26}$$

The second argument therefore is derived from :

$$\begin{cases} \dot{V}_2 = e_1\dot{e}_1 + e_2\dot{e}_2 \\ \dot{V}_2 = e_1\dot{e}_1 + e_2\left[f_2(x_1,x_2) + g_1(x_1,x_2)x_3 - \dot{\alpha}_1\right] \end{cases} \tag{4.27}$$

For the subsystem to be stable, according to Lyapunov $\dot{V}_2$ should be negative. To this end, the form of $\dot{V}_2$ is chosen:

$$\dot{V}_2 = -k_1e_1^2 - k_2e_2^2 \leq 0 \tag{4.28}$$

where $k_2 > 0$ represents a conception condition. By substituting (4.25) into (4.27), this gives :

$$\dot{V}_2 = -k_1e_1^2 + e_2\left[f_2(x_1,x_2) + g_1(x_1,x_2)x_3 - \dot{\alpha}_1\right] \tag{4.29}$$

Therefore, the virtual law x_3 is produced.

$$x_3 = \frac{1}{g_1(x_1,x_2)}\left[-k_2e_2 + \dot{\alpha}_1 - f_2(x_1,x_2)\right] \tag{4.30}$$

with

$$\begin{aligned} \dot{\alpha}_1 = \frac{\partial\alpha_1}{\partial x_1} = &\frac{g_0(x_1)\left[-k_1\dot{e}_1 + \ddot{\alpha}_0 - \dot{f}_1(x_1)\right]}{g_0^2(x_1)} \\ &\underline{-\left[-k_1e_1 + \dot{\alpha}_0 - f_1(x_1)\right]\dot{g}_0(x_1)} \\ &\underline{\qquad g_0^2[x_1)} \end{aligned} \tag{4.31}$$

The system latter will utilize x_{3ref} as the required new reference.

We put $x_{3ref} \overset{\Delta}{=} \alpha_2$ and continue until the last expression of the subsystem (4.14) where we reach the actual control law calculation. In fact, the value of $x_{3ref} \overset{\Delta}{=} \alpha_2$ and continuing to the last expression of the

subsystem (4.14) in which the calculation of the current control law is achieved.

Step n

The principle of last order is applied to the whole system as represented by equation (4.14). Similarly, for this particular step, the subsequent reference to be respected will be as follows:

$$(x_n)_d \stackrel{\Delta}{=} \alpha_{n-1} \tag{4.32}$$

error expression:

$$e_n = x_n - \alpha_{n-1} \tag{4.33}$$

the time derivative :

$$\begin{cases} \dot{e}_n = \dot{x}_n - \dot{\alpha}_{n-1} \\ \dot{e}_n = f_n(x_1, \cdots x_n) + g_{n-1}(x_1, \cdots x_n)\, u + \dot{\alpha}_{n-1} \end{cases} \tag{4.34}$$

with the function of expended lyapunov.

$$\begin{cases} V_n = V_1 + \cdots + \frac{1}{2} e_n^2 \\ V_n = \frac{1}{2}\left[e_1^2 + \cdots + e_n^2\right] \end{cases} \tag{4.35}$$

The derivative becomes:

$$\begin{cases} \dot{V}_n = e_1 \dot{e}_1 + \cdots + e_n \dot{e}_n \\ \dot{V}_n = -k_1 e_1^2 + \cdots + e_n\left[f_n(x_1, \cdots x_n) + g_{n-1}(x_1, \cdots x_n)\, u + \dot{\alpha}_{n-1}\right] \end{cases} \tag{4.36}$$

In effect, at this final stage, the fundamental control law u that achieves the design objectives of the overall system has been deduced, unlike the xi laws, which are virtual laws. A good choice of the control law must satisfy :

$$f_n(x_1, \cdots x_n) + g_{n-1}(x_1, \cdots x_n)\, u + \dot{\alpha}_{n-1} = -k_n e_n^2 \tag{4.37}$$

where $k_n > 0$ represents a control condition. Consequently, this system will be governed by the following control law:

$$u = \frac{1}{g_{n-1}(x_1, \cdots x_n)} + \left[-k_n e_n + \dot{\alpha}_{n-1} - f_n(x_1, \cdots x_n)\right] \tag{4.38}$$

This ensures that the derivative of the Lyapunov function is negative:

$$\dot{V}_n = -k_1 e_1^2 - \cdots - k_n e_n^2 \leq 0 \tag{4.39}$$

4.6 Form of a backstepping supertwisting sliding mode controller

The concept of backstepping is based on the concept of recursive control law synthesis. Some state vector items are treated as "virtual commands" and intermediary control rules are built according to [213].

4.6.1 PEMFC converter control loop

Error signals must be generated in order to match the power source currents to the target values. The following is the FC's current error:

$$\Gamma_1 = x_1 - i_{fcref} \tag{4.40}$$

using fuzzy logic supervision, i_{fcref} is produced.The behavior of the equation (4.40) can be better understood. By using the time derivative as described in the following:

$$\dot{\Gamma_1} = \dot{x_1} - \dot{i_{fcref}} \tag{4.41}$$

The actual behavior of the error can be calculated as follows:

$$\dot{\Gamma_1} = -(1-u_1)\frac{x_3}{L_1} - \frac{R_1}{L_1}x_1 + \frac{v_{fc}}{L_1} - \dot{i_{fcref}} \tag{4.42}$$

The Lyapunov function serves this purpose in the following form:

$$V_1 = \frac{1}{2}\Gamma_1^2 \tag{4.43}$$

The derivative with regard to time of $\dot{V}_1$ is as follows:

$$\dot{V}_1 = \Gamma_1 \dot{\Gamma_1} \tag{4.44}$$

The $\dot{\Gamma_1}$ value is used to deduce :

$$\dot{V}_1 = \Gamma_1 \left(-(1-u_1)\frac{x_3}{L_1} - \frac{R_1}{L_1}x_1 + \frac{v_{fc}}{L_1} - \dot{i_{fcref}} \right) \tag{4.45}$$

in addition, for $\dot{V}_1$ to remain defined and negative, it must satisfy the conditions described, which can be expressed as follows:

$$\dot{V}_1 < 0 \Rightarrow \dot{V}_1 = -K\dot{\Gamma_1^2} \tag{4.46}$$

Therefore, from (4.45) and (4.46), the following can be obtained:

$$-K\dot{\Gamma_1^2} = \Gamma_1 \left(-(1-u_1)\frac{x_3}{L_1} - \frac{R_1}{L_1}x_1 + \frac{v_{fc}}{L_1} - \dot{i_{fcref}} \right) \tag{4.47}$$

where K is a parameter that has a positive constant value. Using $\frac{x_3}{L_1}$ as a virtual command and expressing it with λ, as the following shows:

$$\lambda = \frac{K\Gamma_1 - \frac{R_1}{L_1}x_1 + \frac{v_{fc}}{L_1} - \dot{i_{fcref}}}{(1-u_1)} \tag{4.48}$$

for the system to be effectively stable, $\frac{x_3}{L_1} = \lambda$ must be true at all times. As a result,Γ_2 is defined as follows:

$$\Gamma_2 = \frac{x_3}{L_1} - \lambda \tag{4.49}$$

By applying the value of the virtual control $\frac{x_3}{L_1}$ to (4.42), achieves:

$$\dot{\Gamma} = -(1-u_1)(\Gamma_2 + \lambda) - \frac{R_1}{L_1}x_1 + \frac{v_{fc}}{L_1} - \dot{i_{fcref}} \tag{4.50}$$

Replacing the value of λ from (4.48) in (4.50),this gives:

$$\dot{\Gamma_1} = -K_1\Gamma_1 - (1-u_1)\Gamma_2 \tag{4.51}$$

Indeed, (4.46) is expressed as follows:

$$\dot{V}_1 = -K_1\Gamma_1^2 - (1-u_1)\Gamma_2\Gamma_1 \tag{4.52}$$

The time derivative of the $\dot{\Gamma_2}$ values, according to (4.49), is as follows:

$$\dot{\Gamma_2} = \frac{\dot{x_3}}{L_1} - \dot{\lambda} \tag{4.53}$$

The time derivative of lambda from (4.48) gives:

$$\dot{\lambda} = \frac{\varepsilon}{(1-u_1)} - \frac{\dot{u_1}\lambda}{(1-u_1)} \tag{4.54}$$

in other terms, consider the value of ε as follows:

$$\varepsilon = K_1\dot{\Gamma_1} - \frac{R_1}{L_1}\dot{x_1} + \frac{v_{fc}}{L_1} - \ddot{i}_{fcref} \tag{4.55}$$

by substituting the values of $\dot{x_3}$ and λ from (3.56) and (4.55) into (4.53) it gives:

$$\begin{aligned}\dot{\Gamma_2} = \frac{1}{L_1}\left[(1-u_1)\frac{x_1}{c_0} + u_{23}\frac{x_2}{c_0} - \frac{\dot{i}_0}{c_0}\right] \\ - \frac{\varepsilon}{(1-u_1)} - \frac{\dot{u_1}\lambda}{(1-u_1)}\end{aligned} \tag{4.56}$$

Then, define the new combined Lyapunov function form:

$$V = V_1 + \frac{1}{2}\Gamma_2^2 \tag{4.57}$$

from (4.57), the derivative with respect to time becomes

$$\dot{V} = \Gamma_1\dot{\Gamma_1} + \Gamma_2\dot{\Gamma_2} \tag{4.58}$$

when the value of the $\dot{V_1}$ of (4.52) is updated, the following is obtained:

$$\dot{V} = -K_1\Gamma_1^2 - \Gamma_2\left[(1-u_1)\Gamma_1 - \dot{\Gamma_2}\right] \tag{4.59}$$

to define $\dot{V}$ in terms of negativity, it must be

$$K_2\Gamma_2^2 = \Gamma_2\left[(1-u_1)\Gamma_1 - \dot{\Gamma_2}\right] \tag{4.60}$$

where K_2 is the design parameter of the control, and K_2 is always greater than 0. Therefore, (4.59) has the form :

$$\dot{V} = -K_1\Gamma_1^2 - K_1\Gamma_2^2 \tag{4.61}$$

changing from (4.56) into (4.60) the control law is calculated as:

$$\dot{u_1} = \frac{(1-u_1)}{\lambda} K_2 \Gamma_2 (1-u_1) \Gamma_1 + \\ + \frac{1}{L} \left((1-u_1) \frac{x_1}{c_0} + u_{23} \frac{x_2}{c_0} - \frac{i_0}{c_0} \right) - \frac{\varepsilon}{(1-u_1)} \tag{4.62}$$

A sliding surface is now presented to enhance robustness in backstepping.

$$S = a_1 \Gamma_1 + a_2 \Gamma_2 \tag{4.63}$$

The super-twist with backstepping control is created by extending a commutation phase to the surface-based drive law $\dot{u_1}$.

The second-order sliding mode control super-twisting algorithm (SOSMC-STA) provides robust control action u_{st} that drives and maintains system trajectories on the S surface in finite time, as shown in:

$$\begin{cases} u_{st} = -\gamma \cdot |s|^{\frac{1}{2}} \cdot sgn(s) + w \\ \dot{w} = -\alpha \cdot sgn(s) \end{cases} \tag{4.64}$$

the terms α and γ which must be provided as chosen next, refer to configurable indicators.

$$\begin{cases} \alpha = \sqrt{2\beta(t)} \\ \gamma = \frac{\beta(t)}{2} \end{cases} \tag{4.65}$$

with

$$\dot{\beta}(t) = \begin{cases} \delta \sqrt{|s|} & |s| \leq \tilde{\rho} \\ 0 & \text{Otherwise} \end{cases} \tag{4.66}$$

Using the $\dot{u_1}$ form (4.62) and the u_{st} form (4.64), the resultant driving signal u_1 may be computed as follows:

$$u_1 = \int \dot{u_1} dt + u_{st} \tag{4.67}$$

Figure 4.8 is a schematic layout of the BS STSMC structure.

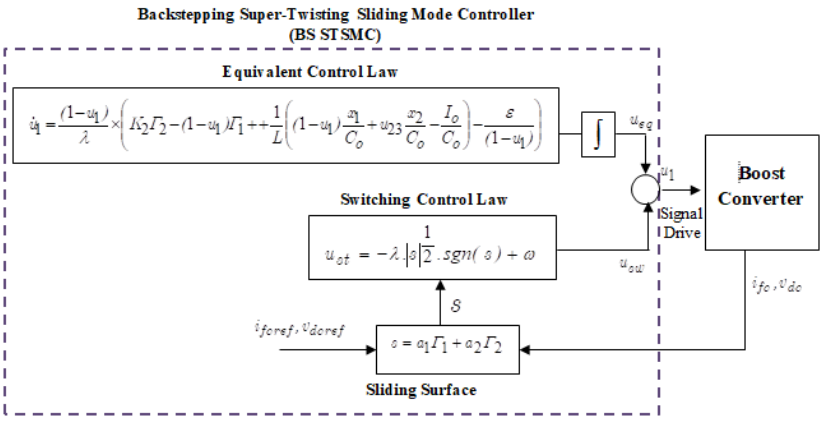

Figure 4.8: schema of Boost converter controlled by Backstepping supertwisting sliding mode controller(BS STSMC)

4.6.2 Supercapacitor Converter Control loop

To construct the control law for the additional energy sources, u_{23} must first be evaluated in order to maintain x_2 at its set point i_{scref}. The following error expression illustrates the situation of the supercapacitors:

$$\Gamma_3 = x_2 - i_{scref} \tag{4.68}$$

by using the value of ui_1 in equation (3.56) and the time derivative of Γ_3 from (4.68), the following result is obtained:

$$\dot{\Gamma_3} = -u_{23}\frac{x_3}{L_2} - \frac{R_2}{L_2}x_2 + \frac{v_{sc}}{L_2} - \dot{i_{scref}} \tag{4.69}$$

the following Lyapunov candidate is selected as having the subsequent important function of the obvious error:

$$V_2 = \frac{1}{2}\Gamma_3^2 \tag{4.70}$$

the time derivative of V_2 will get:

$$\dot{V_2} = \Gamma_3\dot{\Gamma_3} \tag{4.71}$$

the final negative value, $\dot{V_2}$ will be established using the following:

$$\dot{\Gamma_3} = -K_3\Gamma_3 \tag{4.72}$$

consequently, (4.69) and (4.72) produce:

$$-u_{23}\frac{x_3}{L_2} - \frac{R_2}{L_2}x_2 + \frac{v_{sc}}{L_2} - \dot{i_{scref}} = -K_3\Gamma_3 \tag{4.73}$$

subsequently, (4.72) has the following form:

$$\dot{V}_2 = -K_3\Gamma_3 \tag{4.74}$$

The control signal u_{23} is obtained by means of the calculation (4.73), which is given:

$$u_{23} = \frac{1}{x_3}\left[L_2K_3\Gamma_3 - R_2x_2 + v_{sc} - L_2\dot{i_{scref}}\right] \tag{4.75}$$

The system becomes stable if $\dot{V}$ is at all times negatively defined for all $t \to 0$. Also, sliding variables S will converge to zero as $t \to \infty$.

The cumulative mathematical procedure, which is a more accurate explanation, is the following:

$$\dot{V} = -K_3\Gamma_1^2 - K_2\Gamma_2^2 - K_3\Gamma_3^2 \leqslant 0 \tag{4.76}$$

4.7 Simulation Results and Discussion

The findings of this work are presented in this section. Two different scenarios were simulated using the MATLAB/Simulink software. The first scenario utilized a speed profile known as the New European Driving Cycle (NEDC), which is extensively used in Europe. This speed profile can be seen in Figure 4.9a. The corresponding torque reference profile derived from the speed profile is displayed in Figure 4.9b. The second scenario employed a speed profile called the exact urban driving cycle, which is depicted in Figure 4.14a. The torque reference profile derived from this speed profile is shown in Figure 4.14b.

4.7.1 Scenario 1: Frequency based Energy Management

In this scenario, we implement energy management based frequency splitting as the initial control layer, followed by BS STSMC as the secondary layer.

Figure 4.9a depicts the New European Driving Cycle (NEDC), which is widely utilized in Europe.The NEDC comprises various driving patterns, including four consecutive segments of the Urbain Drive Cycle (UDC) that replicate typical urban driving conditions (from 0 to 800 seconds), characterized by frequent stops and starts. This is then succeeded by an Extra Urbain Drive Cycle (EUDC) segment (from 800 to 1200 seconds) that simulates suburban driving conditions with higher and sustained speeds.

The Figure 4.10a demonstrates that the BS STSMC-based frequency distribution technique efficiently manages fluctuations in power demand. Additionally, Figure 4.10b illustrates that the control system effectively maintains a stable DC bus voltage, thereby highlighting the successful voltage regulation loop.

The voltage and current of the fuel cell during frequency-based energy management with a BS STSMC controller over the NEDC are shown in Figure 4.11a and 4.11b, respectively. These measurements are influenced by fluctuating power loads. This study considers the "double layer charge" behavior of the fuel cell, where a value of $3\mu F$ was used for the simulation.

In Figure 4.13a, it can be observed that the supercapacitor voltage v_{sc} is maintained close to the optimal value of $v_{\text{sc}} = 38V$. Figure 4.13b illustrates the supercapacitor current i_{sc}, showing that it closely tracks its set point $i_{\text{sc, ref}}$ under the frequency-based energy management strategy.

Figure 4.13c presents the state of charge (SOC) of the supercapacitor, SOC_{sc}, which starts at an initial value of 80%. The fully charged and discharged values are $SOC_{\text{sc}} = 80.02\%$ and $SOC_{\text{sc}} = 80\%$, respectively. This indicates that the proposed frequency-based energy management approach, utilizing a BS STSMC controller over the NEDC, effectively monitors and maintains the state of charge at optimal levels.

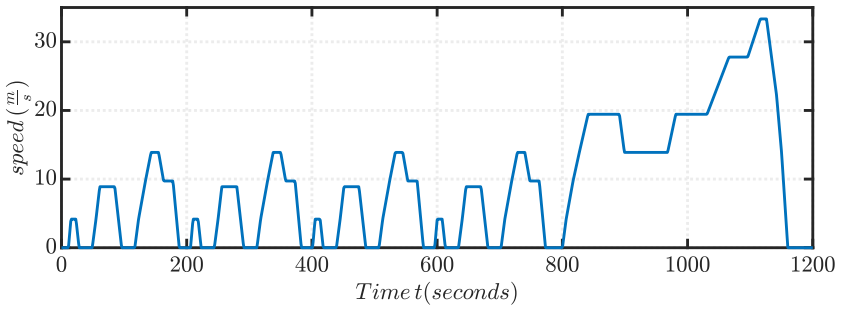

(a) Speed

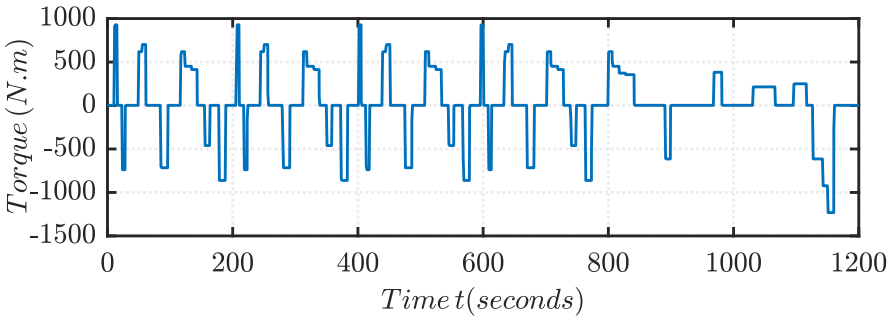

(b) Torque

Figure 4.9: Torque applied to motor and Speed of FCHEV over the NEDC driving cycle

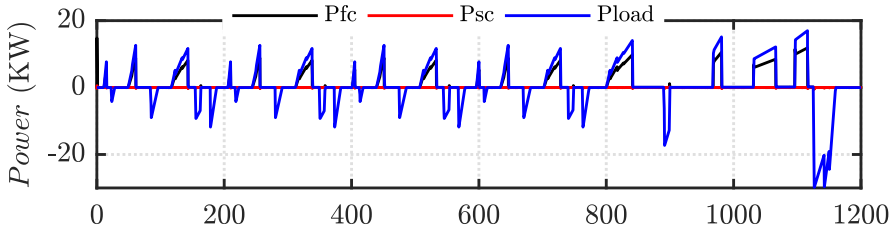

(a) Power distribution results

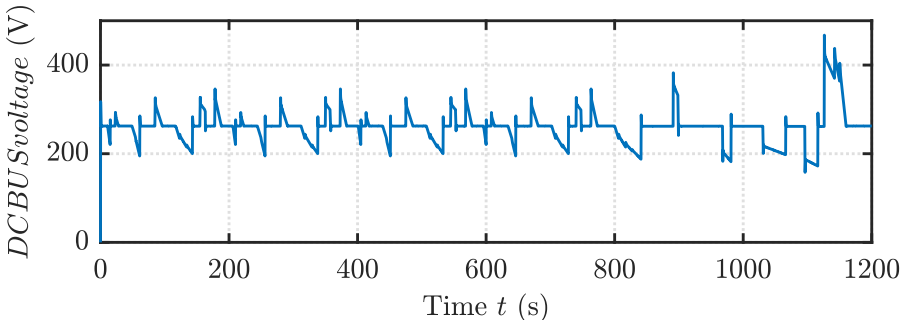

(b) DC BUS voltage

Figure 4.10: Results of frequency-based energy management with BS STSMC controller over the NEDC

4.7.2 Scenario 2:Comparative with Fuzzy logic and Detrministic Rules based Energy management

Table 4.5 explains the management regimes selected by an EMS based on deterministic distribution criteria [18]. The operational stages are regulated by torque (T), power load, operating speed, and SOC and include "Run", "Fuel Cell", "Supercapacitor Power", "Hybrid Drive Power", "Deceleration", and "Park".

As illustrated in Figure 4.14a, the comparison analysis is carried out utilizing the hybrid energy system in the EUDC, defined test driving cycle and speed-time lines, and their traction torque in Figure 4.14b.

A rule-based approach is defined by a PI-deterministic rule-based EMS. The hybrid electric system includes a supercapacitor with a SOC 80% precondition to replicate the energy distribution in the EUDC driving cycle.Figures 4.15a and 4.15b show the energy management outcomes according to the two EMS in consecutive order. Variations in driving behavior are visible after evaluating the energy distribution outcomes of both techniques.

The application of deterministic PI rules in the control of a hybrid power system can manage energy without having to react to massive transient power fluctuations. Yet, deterministic rules must be flexible

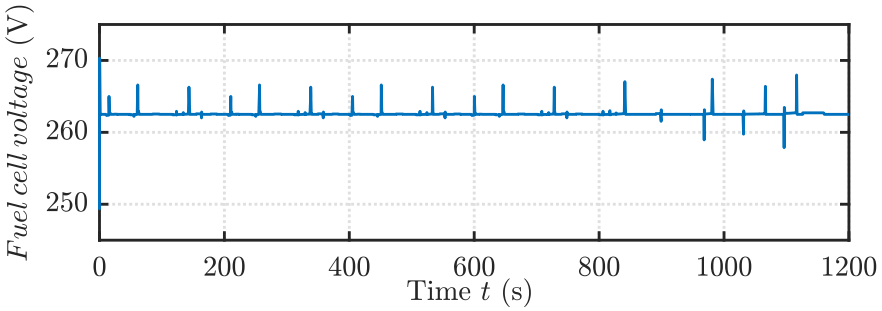

(a) Fuel cell voltage

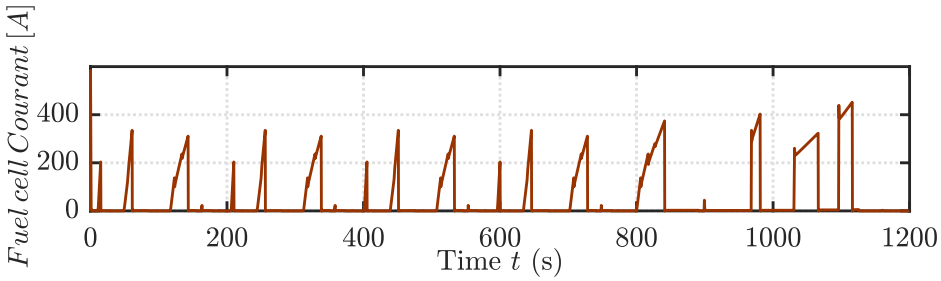

(b) Fuel cell current

Figure 4.11: Fuel cell voltage and current results of frequency-based energy management with the BS STSTM controller on the NEDC

and optimized in pursuit of successful performance. At high load conditions, the fuel cell's power capacity may be limited, and the SCs must share a considerable amount of energy. This limitation is addressed by combining BS STSMC as well as fuzzy logic, which ensure that the fuel cell can produce maximum power while being protected by a limited rate of power change. Importantly, the power profile of the fuel cell generated using the proposed fuzzy logic approach has greater follow-up characteristics to the load power, and its power supply ability can be fully proved as the primary power source.

In Figure 4.16a, the power curve of the PI deterministic fuel cell exhibits rapid changes when the operating mode shifts, which are caused by the transient response of the fuel cell. However, in Figure 4.16b, the PI deterministic rule-based EMS demonstrates slow dynamics in the discharge of the supercapacitor (SC). In contrast, the BS STSMC and fuzzy logic EMS smooth the fuel cell's power profile by taking into consideration the PEMFC dynamic, which may order to protect the fuel cell from the trouble of starvation and is appropriate for the fuel cell's real operating characteristics, as can be seen in the PEMFC voltage in figure 4.18.

Furthermore, in the SOC graphs 4.17a, there is a significant difference between the SOC governed by BS STSMC, fuzzy logic-based EMS, and PI deterministic rules-based EMS. When SOC is governed

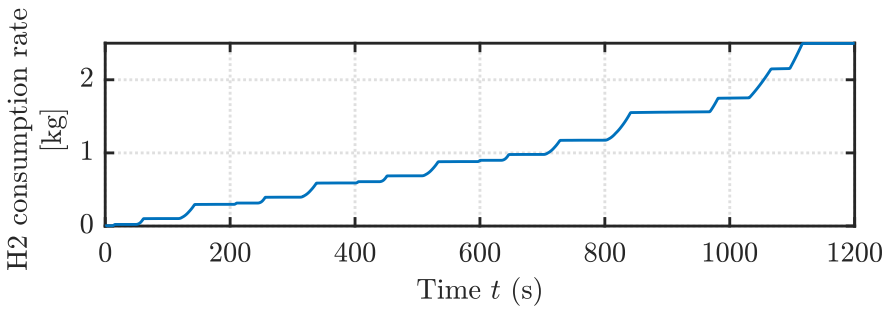

Figure 4.12: Fuel cell stack hydrogen consumption for the case Frequency based energy management with BS STSMC controller over the NEDC.

Table 4.5: Management regimes chosen by an EMS on the basis of deterministic distribution criteria [18]

Management regimes	Torque	Power load	Operating speed	SOC	SC power	Power balance
Run	>0	$<P_L$	$<V_T$	$>SOC_L$	+	$P_{Load}=P_{sc}$
Fuel cell	$<T$	$P_L<P<P_H$	$>V_T$	$>SOC_M$	0	$P_{Load}=P_{fc}$
SC power	$<T$	$P_L<P<P_H$	$>V_T$	$<SOC_M$	$-$	$P_{Load}=P_{fc}-P_{sc}$
Hybrid drive	$>T$	$>P_H$	$>V_T$	$>SOC_L$	+	$P_{Load}=P_{fc}+P_{sc}$
Deceleration	<0	$<$	$>$	$>SOC_H$	$-$	$P_{Load}=P_{sc}$
Park	$=0$	$=0$	$=0$	/	0	/

by BS STSMC and fuzzy logic-based EMS is governed by EUDC, the percentage changes from 80% to 78.71%. On the other hand, when SOC is governed by PI deterministic rule-based EMS,the range changes from 80% to 76%. From the obtained results, it can be seen that energy management based on fuzzy logic with BS STSMC led to a good reduction of the hydrogen consumption as shown in figure 4.17b while respecting the limits imposed by the sources, a good control of the SOC, and the stability of the FC during its operation.

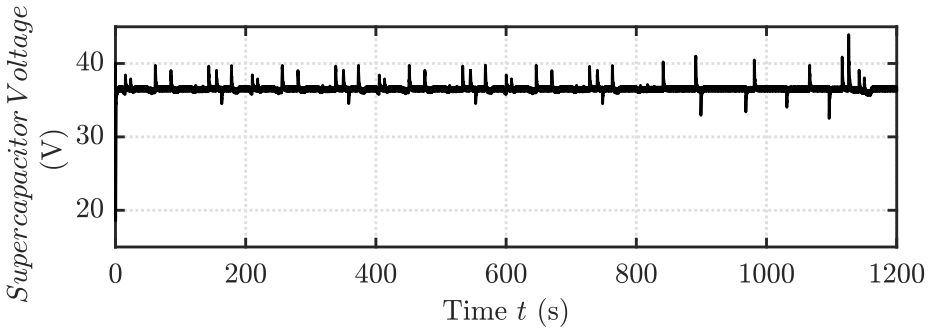

(a) Supercapacitor voltage

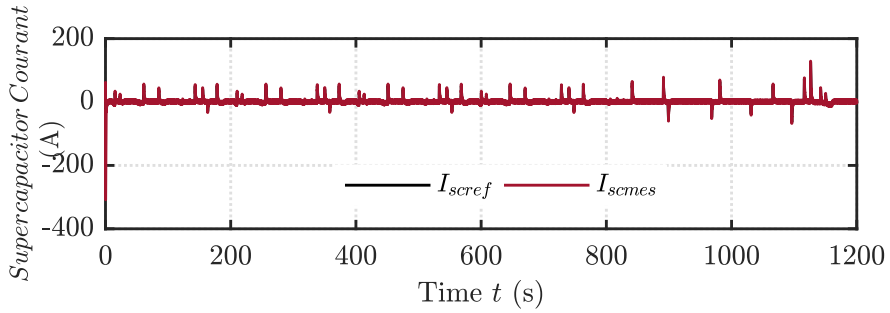

(b) Supercapacitor current

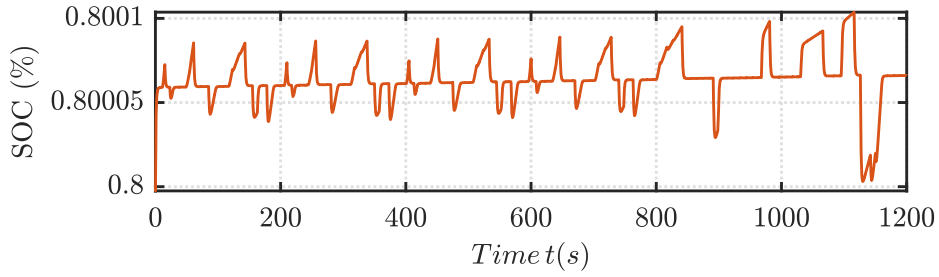

(c) State of charge of supercapacitor

Figure 4.13: supercapacitor Results under frequency-based energy management with BS STSMC controller over the NEDC

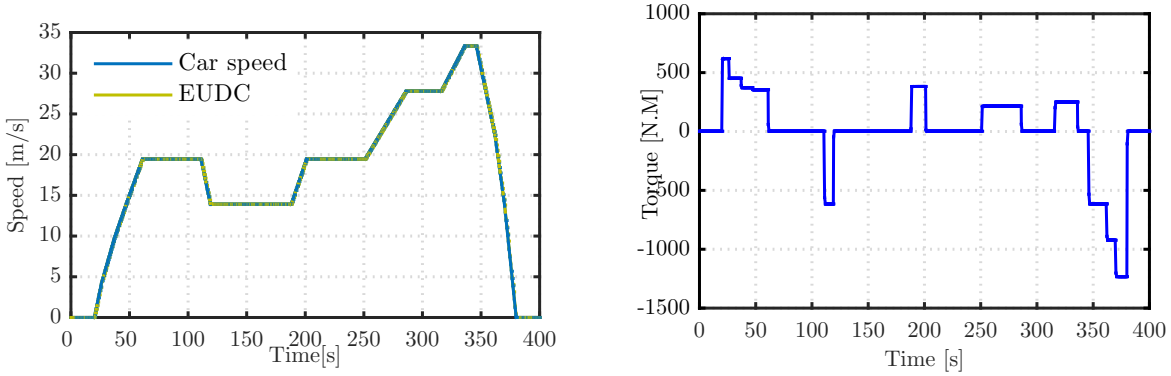

(a) Speed (b) Torque

Figure 4.14: Driving cycle: 4.14a Car speed under EUDC 4.14b Traction Torque under EUDC

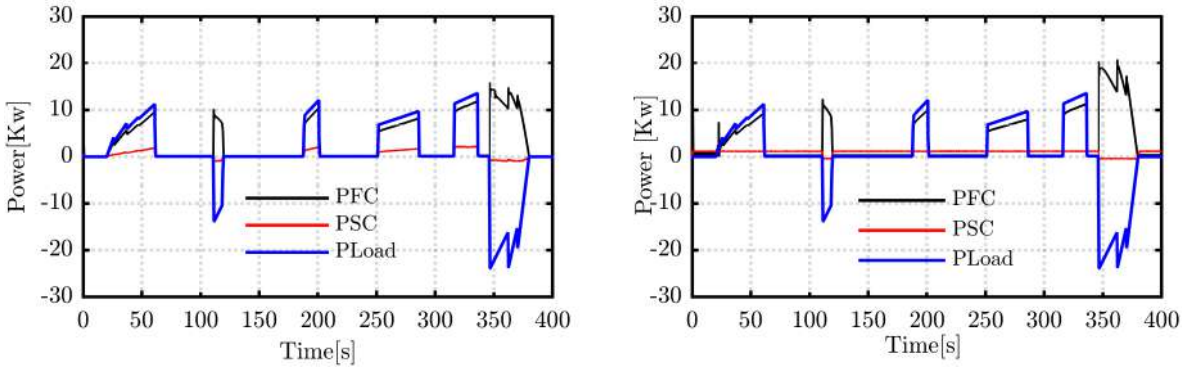

(a) BS STSMC (b) PI Deterministic rule

Figure 4.15: Energy distribution results:4.15a BS STSMC fuzzy logic based EMS for EUDC. 4.15b PI - Deterministic rule based EMS for EUDC.

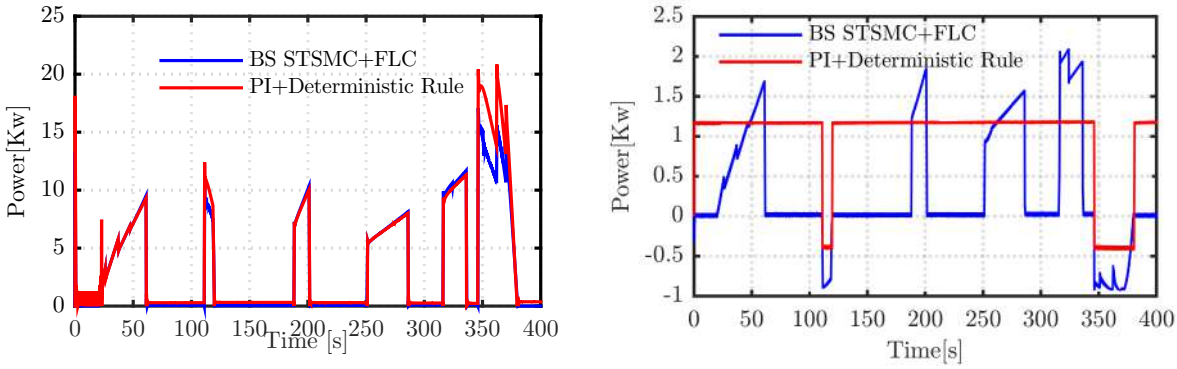

(a) Fuel cell power (b) SC power

Figure 4.16: Supercapacitor and PEMFC Comparisons results: 4.16a PEMFC power . 4.16b Supercapacitor power

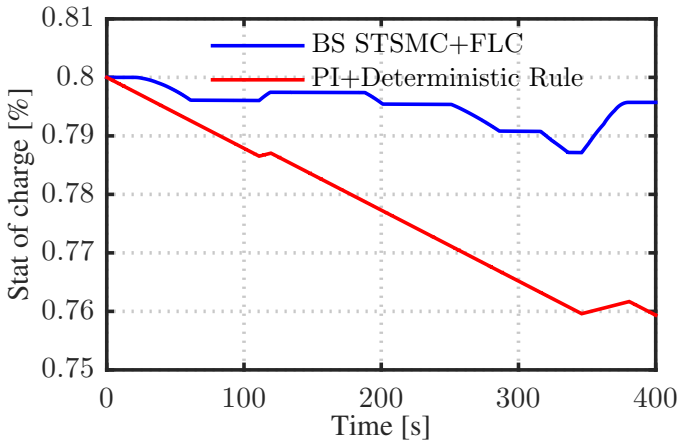

(a) SOC_{SC}

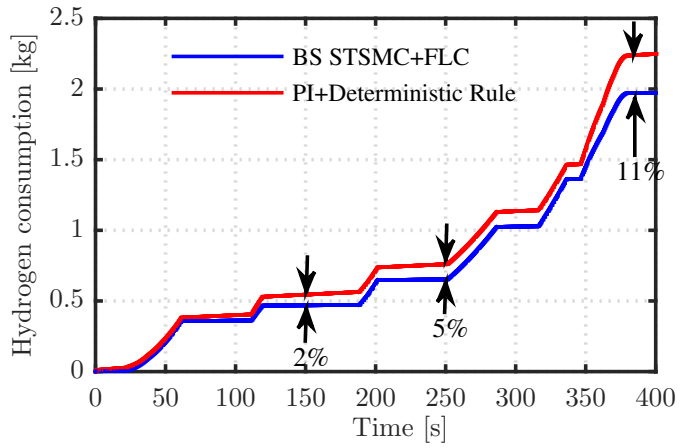

(b) H_2 consumption

Figure 4.17: Supercapacitor and PEMFC result: 4.17a Supercapacitor SOC with an initial value of 80%. 4.17b PEMFC Hydrogen consumption H2.

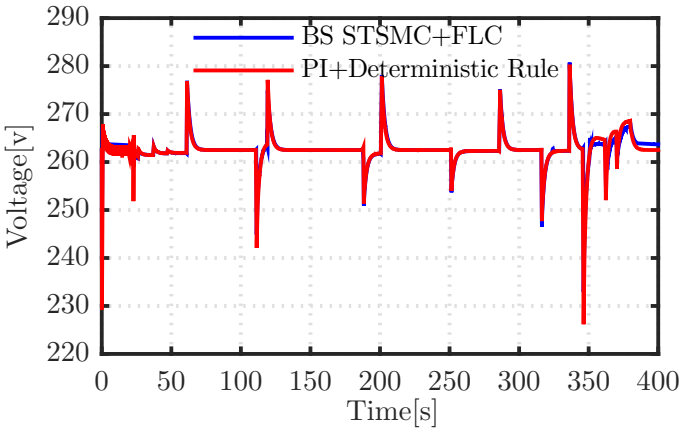

Figure 4.18: PEMFC Comparisons results: PEMFC voltage under the effect of membrane capacitance

4.8 Conclusion

This chapter focused on studying a unidirectional converter connected to a PEM fuel cell. It was evident that incorporating a storage element and bidirectional DC-DC converter is essential as a backup system for efficient energy storage and retrieval. To ensure strong control against external fluctuations and temporal variations in system parameters, the use of a back-stepping controller was justified. This choice offers a high level of robustness and allows for effective adaptation to dynamic conditions. By implementing these control strategies, the overall performance and reliability of the system can be significantly improved.

Additionally, we investigated an energy management approach based on fuzzy logic, utilizing a back-stepping controller, and compared it with a deterministic rule that uses a PI controller. We also explored a second scenario that applied energy management based on the Frequency split technique. Finally, simulation results and discussions were presented to validate the effectiveness of these approaches.

GENERAL CONCLUSION

A summary

The subject of this thesis is within the scope of design and control aspects of hybrid electric vehicles (HEVs). Due to their unique and challenging characteristics, such as frequent stops and intermittent acceleration/braking, urban driving scenarios are of particular interest. The design process of the proposed FCHEVs involves the following procedures:

- Select and model the FCHEV power/energy sources appropriately.
- Integrate the identified sources into a suitable topological design.
- Propose an efficient energy processing stage.
- Finally, size the propulsion elements based on the required road response and the dimensions of the chosen vehicle.

In this context, a hybrid combination structure is being studied. This structure is equipped with a fuel cell that is interfaced with the DC bus via a boost converter. Furthermore, the need to use energy storage systems hybridized with the PEMFC to provide an optimally operating system is demonstrated. The storage devices are connected to the DC bus via bi-directional DC/DC converters. These converters regulate the DC bus voltage and manage the transfer of power to the load.

In the first phase of this research, the primary difficulties linked to the FCHEV's energy management system and the modeling of power converters and their control are addressed. The EMS is a critical component in the further improvement of the FCHEV's drive train. The FCHEV must satisfy the requirements for both driving cycles and acceleration by operating the powertrain system more efficiently. Moreover, the EMS proposes an energy split based on the reference power of the fuel cells and supercapacitors identified by the fuzzy controller.

The proposed controller supports effective performance in terms of fuel consumption reduction, power supply reliability, and keeping the supercapacitors's state of charge (SOC) within an acceptable working range. Furthermore, fuel cell and supercapacitor converters use backstepping supertwisting techniques to drive the real currents of the fuel cell and supercapacitor to meet their provided reference values.

To emphasize this study, an EMS with PI - deterministic algorithms is built to be comparable to the proposed EMS in the extra-urban driving cycle (EUDC). In addition, the stability of the controlled system is ensured at all times. Moreover, the SOC of the supercapacitor remained within the required range.As a result, the conducted comparative tests have decisively established the effectiveness and viability of the proposed techniques.

Future directions

- Investigation of the topology of interleaved DC-DC converters for FCEVs interfaced to supercapacitors and PEMFCs.
- Developing an intelligent energy management control system for fuel cells, batteries, and supercapacitors in hybrid electric vehicles.
- Investigation into the integration of fuel cells and supercapacitors in hybrid electric vehicles, with the development of an efficient model predictive controller.

5 Appendix A Parameters

The power sources and DC-DC converter parameters used for the HESS are listed in the tables below.

Table 5.1: Power sources specifications

PEMFuel cell parameters	Value
Nominal voltage	$270V$
Nominal current	$100A$
maximum power	$30Kw$
Supercapacitor parameters	**Value**
Rated voltage	$48V$
Rated capacity	$33F$
Number of series capacitors	5
Number of parallel capacitors	1
Capacitance of individual cells	$165F$

Table 5.2: Component values of the DC-DC converters

Parameters	Value
Inductors L_1 L_2 L_3	$2mH$
Inductor resistors R_1 R_2 R_3	0.2Ω
Output capacitance C_0	$2mF$
Switching frequency	$10KHz$

REFERENCES

[1] T. Selmi, A. Khadhraoui, and A. Cherif, "Fuel cell–based electric vehicles technologies and challenges," *Environmental Science and Pollution Research*, vol. 29, no. 52, pp. 78 121–78 131, 2022.

[2] P. K. Pathak, A. K. Yadav, S. Padmanaban, P. Alvi, and I. Kamwa, "Fuel cell-based topologies and multi-input dc–dc power converters for hybrid electric vehicles: A comprehensive review," *IET Generation, Transmission & Distribution*, vol. 16, no. 11, pp. 2111–2139, 2022.

[3] J. Bernard, M. Hofer, U. Hannesen, A. Toth, A. Tsukada, F. N. Büchi, and P. Dietrich, "Fuel cell/-battery passive hybrid power source for electric powertrains," *Journal of Power Sources*, vol. 196, no. 14, pp. 5867–5872, 2011.

[4] M. Iqbal, "Design and control of hybrid electric vehicle for efficient urban use," Theses, Université Bourgogne Franche-Comté, Sep. 2022. [Online]. Available: https://theses.hal.science/tel-03826955

[5] A. Pramuanjaroenkij and S. Kakaç, "The fuel cell electric vehicles: The highlight review," *International Journal of Hydrogen Energy*, vol. 48, no. 25, pp. 9401–9425, mar 2023.

[6] G. Oluleye, M. Gandiglio, M. Santarelli, and A. Hawkes, "Pathways to commercialisation of biogas fuelled solid oxide fuel cells in european wastewater treatment plants," *Applied Energy*, vol. 282, p. 116127, 2021.

[7] GCC. (2021) Boeing's Insitu advances its fuel cell technology; LH2 fueling green car congress. Accessed: 2023-07-23. [Online]. Available: https://www.greencarcongress.com/2021/03/20210322-insitu.html

[8] P. Breeze, "Chapter 5 - the phosphoric acid fuel cell," in *Fuel Cells*, P. Breeze, Ed. Academic Press, 2017, pp. 45–51.

[9] M. K. Debe, "Electrocatalyst approaches and challenges for automotive fuel cells," *Nature*, vol. 486, no. 7401, pp. 43–51, jun 2012.

[10] J. Han, J. Feng, P. Chen, Y. Liu, and X. Peng, "A review of key components of hydrogen recirculation subsystem for fuel cell vehicles," *Energy Conversion and Management: X*, p. 100265, 2022.

[11] K.-Y. Shen, S. Park, and Y.-B. Kim, "Hydrogen utilization enhancement of proton exchange membrane fuel cell with anode recirculation system through a purge strategy," *International journal of hydrogen energy*, vol. 45, no. 33, pp. 16 773–16 786, 2020.

[12] S. Cheng, C. Fang, L. Xu, J. Li, and M. Ouyang, "Model-based temperature regulation of a pem fuel cell system on a city bus," *International Journal of Hydrogen Energy*, vol. 40, no. 39, pp. 13 566–13 575, 2015.

[13] Transportation applications | ztt supercapacitor. [Online]. Available: https://www.zttsupercap.com/applications/transportation/

[14] M. M. Whiston, M. M. Bilec, and L. A. Schaefer, "Influence of the charge double layer on solid oxide fuel cell stack behavior," *Journal of Power Sources*, vol. 293, pp. 767–777, 2015.

[15] Y. Wang, B. Seo, B. Wang, N. Zamel, K. Jiao, and X. C. Adroher, "Fundamentals, materials, and machine learning of polymer electrolyte membrane fuel cell technology," *Energy and AI*, vol. 1, p. 100014, 2020.

[16] G. Gautham Prasad, N. Shetty, S. Thakur, Rakshitha, and K. Bommegowda, "Supercapacitor technology and its applications: a review," in *IOP Conference Series: Materials Science and Engineering*, vol. 561, no. 1. IOP Publishing, 2019, p. 012105.

[17] Emission test cycles. DieselNet. Accessed on April 18, 2024. [Online]. Available: https://dieselnet.com/standards/cycles/index.php#eu

[18] Q. Ning, D. Xuan, and Y. Kim, "Modeling and control strategy development for fuel cell hybrid vehicles," *International Journal of Automotive Technology*, vol. 11, no. 2, pp. 229–238, 2010.

[19] V. Smil, *Energy and Civilization: A History*. The MIT Press, 05 2017. [Online]. Available: https://doi.org/10.7551/mitpress/9780262035774.001.0001

[20] CSS. (2021) Center for Sustainable Systems University of Michigan u.s. energy system factsheet. pub. no. css03-11. Accessed: 2023-03-19. [Online]. Available: https://css.umich.edu/publications/factsheets/energy/us-energy-system-factsheet

[21] S. Mukhopadhyay, "Solar energy and gasification of msw: two promising green energy options," in *Green Energy Systems*. Elsevier, 2023, pp. 93–125.

[22] H. Ritchie, P. Rosado, and M. Roser. (2024, Jan.) Emissions by sector: where do greenhouse gases come from? Our World in Data. [Online]. Available: https://ourworldindata.org/emissions-by-sector

[23] C. Osorio and K. Nanduri, "Urban transportation emissions mitigation: Coupling high-resolution vehicular emissions and traffic models for traffic signal optimization," *Transportation Research Part B: Methodological*, vol. 81, pp. 520–538, 2015.

[24] P. G. Kumar, P. Lekhana, M. Tejaswi, and S. Chandrakala, "Effects of vehicular emissions on the urban environment-a state of the art," *Materials Today: Proceedings*, vol. 45, pp. 6314–6320, 2021.

[25] S. Unal and H. Biyik, "Driving performance enhancement using fuel cell in e-scooters," *International Journal of Hydrogen Energy*, 2024.

[26] A. Olabi, M. A. Abdelkareem, T. Wilberforce, A. Alkhalidi, T. Salameh, A. G. Abo-Khalil, M. M. Hassan, and E. T. Sayed, "Battery electric vehicles: Progress, power electronic converters, strength (s), weakness (w), opportunity (o), and threats (t)," *International Journal of Thermofluids*, vol. 16, p. 100212, 2022.

[27] IEA. (2021) The future of hydrogen. Accessed: 2023-03-19. [Online]. Available: https://www.iea.org/reports/the-future-of-hydrogen

[28] M. M. Mohideen, Y. Liu, and S. Ramakrishna, "Recent progress of carbon dots and carbon nanotubes applied in oxygen reduction reaction of fuel cell for transportation," *Applied Energy*, vol. 257, p. 114027, 2020.

[29] M. M. Mohideen, B. Subramanian, J. Sun, J. Ge, H. Guo, A. V. Radhamani, S. Ramakrishna, and Y. Liu, "Techno-economic analysis of different shades of renewable and non-renewable energy-based hydrogen for fuel cell electric vehicles," *Renewable and Sustainable Energy Reviews*, vol. 174, p. 113153, 2023.

[30] E. Ogungbemi, T. Wilberforce, O. Ijaodola, J. Thompson, and A. Olabi, "Selection of proton exchange membrane fuel cell for transportation," *International Journal of Hydrogen Energy*, vol. 46, no. 59, pp. 30 625–30 640, 2021.

[31] J. Hu, Y. Wang, L. Zou, and Z. Wang, "Adaptive rule control strategy for composite energy storage fuel cell vehicle based on vehicle operating state recognition," *Renewable Energy*, vol. 204, pp. 166–175, mar 2023.

[32] B. Tanç, H. T. Arat, E. Baltacıoğlu, and K. Aydın, "Overview of the next quarter century vision of hydrogen fuel cell electric vehicles," *International Journal of Hydrogen Energy*, vol. 44, no. 20, pp. 10 120–10 128, 2019.

[33] S. Mansour and M. Raeesi, "Performance assessment of fuel cell and electric vehicles taking into account the fuel cell degradation, battery lifetime, and heating, ventilation, and air conditioning system," *International Journal of Hydrogen Energy*, 2023.

[34] L. Fan, Z. Tu, and S. H. Chan, "Recent development of hydrogen and fuel cell technologies: A review," *Energy Reports*, vol. 7, pp. 8421–8446, 2021.

[35] R. Saadi, M. Hammoudi, O. Kraa, M. Ayad, and M. Bahri, "A robust control of a 4-leg floating interleaved boost converter for fuel cell electric vehicle application," *Mathematics and Computers in Simulation*, vol. 167, pp. 32–47, 2020.

[36] H. S. Das, C. W. Tan, and A. Yatim, "Fuel cell hybrid electric vehicles: A review on power conditioning units and topologies," *Renewable and Sustainable Energy Reviews*, vol. 76, pp. 268–291, 2017.

[37] K. V. Singh, H. O. Bansal, and D. Singh, "A comprehensive review on hybrid electric vehicles: architectures and components," *Journal of Modern Transportation*, vol. 27, pp. 77–107, 2019.

[38] L. Xu, J. Li, J. Hua, X. Li, and M. Ouyang, "Adaptive supervisory control strategy of a fuel cell/battery-powered city bus," *Journal of Power Sources*, vol. 194, no. 1, pp. 360–368, 2009.

[39] F. Z. Peng, M. Shen, and K. Holland, "Application of z-source inverter for traction drive of fuel cell—battery hybrid electric vehicles," *IEEE Transactions on Power Electronics*, vol. 22, no. 3, pp. 1054–1061, 2007.

[40] X. Hu, C. Zou, X. Tang, T. Liu, and L. Hu, "Cost-optimal energy management of hybrid electric vehicles using fuel cell/battery health-aware predictive control," *ieee transactions on power electronics*, vol. 35, no. 1, pp. 382–392, 2019.

[41] X. Li, Y. Wang, D. Yang, and Z. Chen, "Adaptive energy management strategy for fuel cell/battery hybrid vehicles using pontryagin's minimal principle," *Journal of Power Sources*, vol. 440, p. 227105, 2019.

[42] C. Deutsch, A. Chiche, S. Bhat, C. Lagergren, G. Lindbergh, and J. Kuttenkeuler, "Evaluation of energy management strategies for fuel cell/battery-powered underwater vehicles against field trial data," *Energy Conversion and Management: X*, vol. 14, p. 100193, 2022.

[43] Z. U. Bayrak, U. Kaya, and E. Oksuztepe, "Investigation of pemfc performance for cruising hybrid powered fixed-wing electric uav in different temperatures," *International Journal of Hydrogen Energy*, vol. 45, no. 11, pp. 7036–7045, 2020.

[44] Q. Xun, S. Lundberg, and Y. Liu, "Design and experimental verification of a fuel cell/supercapacitor passive configuration for a light vehicle," *Journal of Energy Storage*, vol. 33, p. 102110, 2021.

[45] K. Gérardin, S. Raël, C. Bonnet, D. Arora, and F. Lapicque, "Direct coupling of pem fuel cell to supercapacitors for higher durability and better energy management," *Fuel Cells*, vol. 18, no. 3, pp. 315–325, 2018.

[46] Q. Xun, *Control and Optimization of Fuel cell Based Powertrain for Automotive Applications*. Chalmers Tekniska Hogskola (Sweden), 2022.

[47] H. Fathabadi, "Novel fuel cell/battery/supercapacitor hybrid power source for fuel cell hybrid electric vehicles," *Energy*, vol. 143, pp. 467–477, 2018.

[48] Z. Huang, C. Zhang, T. Zeng, C. Lv, and S. H. Chan, "Modeling and energy management of a photovoltaic-fuel cell-battery hybrid electric vehicle," *Energy Storage*, vol. 1, no. 3, p. e61, 2019.

[49] M. Ezzat and I. Dincer, "Development, analysis and assessment of fuel cell and photovoltaic powered vehicles," *International Journal of Hydrogen Energy*, vol. 43, no. 2, pp. 968–978, 2018.

[50] S. Verma, S. Mishra, A. Gaur, S. Chowdhury, S. Mohapatra, G. Dwivedi, and P. Verma, "A comprehensive review on energy storage in hybrid electric vehicle," *Journal of Traffic and Transportation Engineering (English Edition)*, vol. 8, no. 5, pp. 621–637, 2021.

[51] M. Ezzat and I. Dincer, "Development, analysis and assessment of a fuel cell and solar photovoltaic system powered vehicle," *Energy conversion and management*, vol. 129, pp. 284–292, 2016.

[52] C.-N. Huang and Y.-S. Chen, "Design of magnetic flywheel control for performance improvement of fuel cells used in vehicles," *Energy*, vol. 118, pp. 840–852, 2017.

[53] E.-L. Molina-Ibáñez, E. Rosales-Asensio, C. Perez-Molina, F. M. Pérez, and A. Colmenar-Santos, "Analysis on the electric vehicle with a hybrid storage system and the use of superconducting magnetic energy storage (smes)," *Energy Reports*, vol. 7, pp. 854–873, 2021.

[54] Z. A. Arfeen, M. P. Abdullah, R. Hassan, B. M. Othman, A. Siddique, A. U. Rehman, and U. U. Sheikh, "Energy storage usages: Engineering reactions, economic-technological values for electric vehicles—a technological outlook," *International Transactions on Electrical Energy Systems*, vol. 30, no. 9, p. e12422, 2020.

[55] B. B. Adetokun, O. Oghorada, and S. J. Abubakar, "Superconducting magnetic energy storage systems: Prospects and challenges for renewable energy applications," *Journal of Energy Storage*, vol. 55, p. 105663, 2022.

[56] O. Folorunso, P. O. Olukanmi, and T. Shongwe, "Progress towards sustainable energy storage: A concise review," *Engineering Reports*, vol. n/a, no. n/a, p. e12731. [Online]. Available: https://onlinelibrary.wiley.com/doi/abs/10.1002/eng2.12731

[57] T. Zimmermann, P. Keil, M. Hofmann, M. F. Horsche, S. Pichlmaier, and A. Jossen, "Review of system topologies for hybrid electrical energy storage systems," *Journal of Energy Storage*, vol. 8, pp. 78–90, 2016.

[58] M. Robayo, M. Mueller, S. Sharkh, and M. Abusara, "Assessment of supercapacitor performance in a hybrid energy storage system with an ems based on the discrete wavelet transform," *Journal of Energy Storage*, vol. 57, p. 106200, 2023.

[59] S. M. Lukic, J. Cao, R. C. Bansal, F. Rodriguez, and A. Emadi, "Energy storage systems for automotive applications," *IEEE Transactions on industrial electronics*, vol. 55, no. 6, pp. 2258–2267, 2008.

[60] Q. Zhang and G. Li, "Experimental study on a semi-active battery-supercapacitor hybrid energy storage system for electric vehicle application," *IEEE Transactions on Power Electronics*, vol. 35, no. 1, pp. 1014–1021, 2019.

[61] L. Kouchachvili, W. Yaïci, and E. Entchev, "Hybrid battery/supercapacitor energy storage system for the electric vehicles," *Journal of Power Sources*, vol. 374, pp. 237–248, 2018.

[62] K. Elakkiya, K. SatheeshKumar, S. Rathinamala, and K. Pradheep, "Energy management system based hybrid energy storage system using supercapacitor for ev," in *2023 9th International Conference on Advanced Computing and Communication Systems (ICACCS)*, vol. 1. IEEE, 2023, pp. 2359–2364.

[63] Y. Wang, L. Wang, M. Li, and Z. Chen, "A review of key issues for control and management in battery and ultra-capacitor hybrid energy storage systems," *ETransportation*, vol. 4, p. 100064, 2020.

[64] S. Hajiaghasi, A. Salemnia, and M. Hamzeh, "Hybrid energy storage system for microgrids applications: A review," *Journal of Energy Storage*, vol. 21, pp. 543–570, 2019.

[65] M. J. Lencwe, S. P. D. Chowdhury, and T. O. Olwal, "Hybrid energy storage system topology approaches for use in transport vehicles: A review," *Energy Science & Engineering*, vol. 10, no. 4, pp. 1449–1477, 2022.

[66] F. Naseri, C. Barbu, and T. Sarikurt, "Optimal sizing of hybrid high-energy/high-power battery energy storage systems to improve battery cycle life and charging power in electric vehicle applications," *Journal of Energy Storage*, vol. 55, p. 105768, 2022.

[67] T. S. Babu, K. R. Vasudevan, V. K. Ramachandaramurthy, S. B. Sani, S. Chemud, and R. M. Lajim, "A comprehensive review of hybrid energy storage systems: Converter topologies, control strategies and future prospects," *IEEE Access*, vol. 8, pp. 148 702–148 721, 2020.

[68] U. Manandhar, N. R. Tummuru, S. K. Kollimalla, A. Ukil, G. H. Beng, and K. Chaudhari, "Validation of faster joint control strategy for battery-and supercapacitor-based energy storage system," *IEEE Transactions on Industrial Electronics*, vol. 65, no. 4, pp. 3286–3295, 2017.

[69] Z. Song, Y. Pan, H. Chen, and T. Zhang, "Effects of temperature on the performance of fuel cell hybrid electric vehicles: A review," *Applied Energy*, vol. 302, p. 117572, 2021.

[70] H. F. Gharibeh, A. S. Yazdankhah, and M. R. Azizian, "Energy management of fuel cell electric vehicles based on working condition identification of energy storage systems, vehicle driving performance, and dynamic power factor," *Journal of Energy Storage*, vol. 31, p. 101760, 2020.

[71] Y.-T. Zhang, C. G. Claudel, M.-B. Hu, Y.-H. Yu, and C.-L. Shi, "Develop of a fuel consumption model for hybrid vehicles," *Energy Conversion and Management*, vol. 207, p. 112546, 2020.

[72] A. S. Mohammed, S. M. Atnaw, A. O. Salau, and J. N. Eneh, "Review of optimal sizing and power management strategies for fuel cell/battery/super capacitor hybrid electric vehicles," *Energy Reports*, vol. 9, pp. 2213–2228, 2023.

[73] Q. Li, H. Yang, Y. Han, M. Li, and W. Chen, "A state machine strategy based on droop control for an energy management system of pemfc-battery-supercapacitor hybrid tramway," *International Journal of Hydrogen Energy*, vol. 41, no. 36, pp. 16 148–16 159, 2016.

[74] Z. Mokrani, D. Rekioua, N. Mebarki, T. Rekioua, and S. Bacha, "Proposed energy management strategy in electric vehicle for recovering power excess produced by fuel cells," *International Journal of Hydrogen Energy*, vol. 42, no. 30, pp. 19 556–19 575, 2017.

[75] A. Badji, D. O. Abdeslam, D. Chabane, and N. Benamrouche, "Real-time implementation of improved power frequency approach based energy management of fuel cell electric vehicle considering storage limitations," *Energy*, vol. 249, p. 123743, jun 2022.

[76] E. Naderi, K. Bibek, M. Ansari, and A. Asrari, "Experimental validation of a hybrid storage framework to cope with fluctuating power of hybrid renewable energy-based systems," *IEEE Transactions on Energy Conversion*, vol. 36, no. 3, pp. 1991–2001, 2021.

[77] E. Naderi and A. Asrari, "Experimental validation of grid-tied and standalone inverters on a lab-scale wind-pv microgrid," in *2021 IEEE International Power and Renewable Energy Conference (IPRECON)*. IEEE, 2021, pp. 1–6.

[78] E. Çelik, "Performance analysis of SSA optimized fuzzy 1pd-PI controller on AGC of renewable energy assisted thermal and hydro-thermal power systems," *Journal of Ambient Intelligence and Humanized Computing*, vol. 13, no. 8, pp. 4103–4122, feb 2022.

[79] E. CELİK and N. ÖZTÜRK, "Attenuating saturated-regulator operation effect of brushless DC motors through genetic-based fuzzy logic estimator," *TURKISH JOURNAL OF ELECTRICAL ENGINEERING COMPUTER SCIENCES*, vol. 26, no. 6, pp. 3208–3224, nov 2018.

[80] E. Celik and N. Öztürk, "Commutation current ripple minimization of brushless DC motor drive based on programmed phase current references," *Electrical Engineering*, vol. 103, no. 6, pp. 2661–2674, mar 2021.

[81] H. Jia, J. Tang, Y. Yu, Y. Sun, B. Yin, and C. Zhang, "Energy management strategy of fuel cell/battery hybrid vehicle based on series fuzzy control," *International Journal of Automotive Technology*, vol. 22, pp. 1545–1556, 2021.

[82] K. V. Singh, H. O. Bansal, and D. Singh, "Feed-forward modeling and real-time implementation of an intelligent fuzzy logic-based energy management strategy in a series–parallel hybrid electric vehicle to improve fuel economy," *Electrical Engineering*, vol. 102, no. 2, pp. 967–987, jan 2020.

[83] T. Zhu, R. G. Wills, R. Lot, H. Ruan, and Z. Jiang, "Adaptive energy management of a battery-supercapacitor energy storage system for electric vehicles based on flexible perception and neural network fitting," *Applied Energy*, vol. 292, p. 116932, 2021.

[84] M. Sellali, A. Betka, S. Drid, A. Djerdir, L. Allaoui, and M. Tiar, "Novel control implementation for electric vehicles based on fuzzy-back stepping approach," *Energy*, vol. 178, pp. 644–655, 2019.

[85] K. Davis and J. G. Hayes, "Fuel cell vehicle energy management strategy based on the cost of ownership," *IET Electrical Systems in Transportation*, vol. 9, no. 4, pp. 226–236, 2019. [Online]. Available: https://ietresearch.onlinelibrary.wiley.com/doi/abs/10.1049/iet-est.2019.0021

[86] R. Xiong, H. Chen, C. Wang, and F. Sun, "Towards a smarter hybrid energy storage system based on battery and ultracapacitor-a critical review on topology and energy management," *Journal of cleaner production*, vol. 202, pp. 1228–1240, 2018.

[87] J. Snoussi, S. B. Elghali, M. Benbouzid, and M. F. Mimouni, "Optimal sizing of energy storage systems using frequency-separation-based energy management for fuel cell hybrid electric vehicles," *IEEE Transactions on Vehicular Technology*, vol. 67, no. 10, pp. 9337–9346, 2018.

[88] Q. Li, W. Chen, Y. Li, S. Liu, and J. Huang, "Energy management strategy for fuel cell/battery/ultracapacitor hybrid vehicle based on fuzzy logic," *International Journal of Electrical Power and Energy Systems*, vol. 43, no. 1, pp. 514–525, 2012. [Online]. Available: https://www.sciencedirect.com/science/article/pii/S0142061512002888

[89] A. Same, A. Stipe, D. Grossman, and J. W. Park, "A study on optimization of hybrid drive train using advanced vehicle simulator (advisor)," *Journal of Power Sources*, vol. 195, no. 19, pp. 6954–6963, 2010.

[90] X. Zhao, L. Wang, Y. Zhou, B. Pan, R. Wang, L. Wang, and X. Yan, "Energy management strategies for fuel cell hybrid electric vehicles: Classification, comparison, and outlook," *Energy Conversion and Management*, vol. 270, p. 116179, 2022.

[91] A. Badji, D. O. Abdeslam, D. Chabane, and N. Benamrouche, "Real-time implementation of improved power frequency approach based energy management of fuel cell electric vehicle considering storage limitations," *Energy*, vol. 249, p. 123743, 2022.

[92] M. Iqbal, H. S. Ramadan, and M. Becherif, "Health-aware frequency separation method for online energy management of fuel cell hybrid vehicle considering efficient urban utilization," *International Journal of Hydrogen Energy*, vol. 46, no. 29, pp. 16 030–16 047, 2021.

[93] H.-A. Trinh, H. V. A. Truong, T. C. Do, M. H. Nguyen, K. K. Ahn *et al.*, "Optimization-based energy management strategies for hybrid construction machinery: A review," *Energy Reports*, vol. 8, pp. 6035–6057, 2022.

[94] Y. Zhou, "Predictive energy management for fuel cell hybrid electric vehicle," Theses, Université Bourgogne Franche-Comté, Nov. 2020. [Online]. Available: https://theses.hal.science/tel-03080574

[95] R. S. Sankarkumar and R. Natarajan, "Energy management techniques and topologies suitable for hybrid energy storage system powered electric vehicles: An overview," *International Transactions on Electrical Energy Systems*, vol. 31, no. 4, p. e12819, 2021. [Online]. Available: https://onlinelibrary.wiley.com/doi/abs/10.1002/2050-7038.12819

[96] J. Moreno, M. Ortuzar, and J. Dixon, "Energy-management system for a hybrid electric vehicle, using ultracapacitors and neural networks," *IEEE Transactions on Industrial Electronics*, vol. 53, no. 2, pp. 614–623, 2006.

[97] J. Shen and A. Khaligh, "A supervisory energy management control strategy in a battery/ultracapacitor hybrid energy storage system," *IEEE Transactions on Transportation Electrification*, vol. 1, no. 3, pp. 223–231, 2015.

[98] A. Mehraban, T. Ghanbari, and E. Farjah, "Ai-based control of storage capacity in high power density energy storage systems, used in electric vehicles," *IEEE Transactions on Transportation Electrification*, pp. 1–1, 2023.

[99] G. Li, R. Gomez, K. Nakamura, and B. He, "Human-centered reinforcement learning: A survey," *IEEE Transactions on Human-Machine Systems*, vol. 49, no. 4, pp. 337–349, 2019.

[100] S. Whiteson *et al.*, *Adaptive representations for reinforcement learning*. Springer, 2010, vol. 291.

[101] M. R. Habib, K. Ahmed, A. Y. Suhan, A. Vadher, M. R. Arefin, M. S. Tanvir, S. H. Rizvee, and M. A. R. Swapno, "Recent progress in energy management system for fuel cell hybrid electric vehicle," in *Proceedings of Fourth International Conference on Inventive Material Science Applications*, V. Bindhu, J. M. R. S. Tavares, and Ş. Ţălu, Eds. Singapore: Springer Singapore, 2022, pp. 737–750.

[102] Z. Song, J. Hou, H. Hofmann, J. Li, and M. Ouyang, "Sliding-mode and lyapunov function-based control for battery/supercapacitor hybrid energy storage system used in electric vehicles," *Energy*, vol. 122, pp. 601–612, 2017.

[103] K. Ye and P. Li, "A new adaptive pso-pid control strategy of hybrid energy storage system for electric vehicles," *Advances in Mechanical Engineering*, vol. 12, no. 9, p. 1687814020958574, 2020.

[104] X. Zhang, Z. Lu, X. Yuan, Y. Wang, and X. Shen, "L2-gain adaptive robust control for hybrid energy storage system in electric vehicles," *IEEE Transactions on Power Electronics*, vol. 36, no. 6, pp. 7319–7332, 2020.

[105] C. Napole, M. Derbeli, and O. Barambones, "A global integral terminal sliding mode control based on a novel reaching law for a proton exchange membrane fuel cell system," *Applied Energy*, vol. 301, p. 117473, 2021.

[106] J. Rodriguez and P. Cortes, *Predictive control of power converters and electrical drives*. John Wiley & Sons, 2012.

[107] H. Sartipizadeh, F. Harirchi, M. Babakmehr, and P. Dehghanian, "Robust model predictive control of dc-dc floating interleaved boost converter with multiple uncertainties," *IEEE Transactions on Energy Conversion*, vol. 36, no. 2, pp. 1403–1412, 2021.

[108] C. Ekaputri and A. Syaichu-Rohman, "Model predictive control (mpc) design and implementation using algorithm-3 on board spartan 6 fpga sp605 evaluation kit," in *2013 3rd International Conference on Instrumentation Control and Automation (ICA)*, 2013, pp. 115–120.

[109] S. Vaidyanathan and A. T. Azar, *Backstepping control of nonlinear dynamical systems*. Academic Press, 2020.

[110] A. Swikir and V. Utkin, "Chattering analysis of conventional and super twisting sliding mode control algorithm," in *2016 14th international workshop on variable structure systems (VSS)*. IEEE, 2016, pp. 98–102.

[111] X. Hao, I. Salhi, S. Laghrouche, Y. Ait-Amirat, and A. Djerdir, "Robust control of four-phase interleaved boost converter by considering the performance of pem fuel cell current," *International Journal of Hydrogen Energy*, vol. 46, no. 78, pp. 38 827–38 840, 2021.

[112] I. Staffell, D. Scamman, A. V. Abad, P. Balcombe, P. E. Dodds, P. Ekins, N. Shah, and K. R. Ward, "The role of hydrogen and fuel cells in the global energy system," *Energy & Environmental Science*, vol. 12, no. 2, pp. 463–491, 2019.

[113] A. G. Olabi, T. Wilberforce, and M. A. Abdelkareem, "Fuel cell application in the automotive industry and future perspective," *Energy*, vol. 214, p. 118955, 2021.

[114] P. Grimes, "Historical pathways for fuel cells. the new electric century," in *Fifteenth Annual Battery Conference on Applications and Advances (Cat. No. 00TH8490)*. IEEE, 2000, pp. 41–45.

[115] J. M. Andújar and F. Segura, "Fuel cells: History and updating. a walk along two centuries," *Renewable and sustainable energy reviews*, vol. 13, no. 9, pp. 2309–2322, 2009.

[116] S. Institution. (2004) . Accessed: 2023-07-16. [Online]. Available: https://americanhistory.si.edu/fuelcells/phos/pafcmain.htm#hist

[117] P. Thounthong, "Conception d'une source hybride utilisant une pile à combustible et des supercondensateurs," Ph.D. dissertation, Institut National Polytechnique de Lorraine-INPL, 2005.

[118] O. Z. Sharaf and M. F. Orhan, "An overview of fuel cell technology: Fundamentals and applications," *Renewable and sustainable energy reviews*, vol. 32, pp. 810–853, 2014.

[119] M. Gandiglio, A. Lanzini, and M. Santarelli, "Large stationary solid oxide fuel cell (sofc) power plants," *Modeling, Design, Construction, and Operation of Power Generators with Solid Oxide Fuel Cells: From Single Cell to Complete Power System*, pp. 233–261, 2018.

[120] Y. Luo, Y. Wu, B. Li, T. Mo, Y. Li, S.-P. Feng, J. Qu, and P. K. Chu, "Development and application of fuel cells in the automobile industry," *Journal of Energy Storage*, vol. 42, p. 103124, 2021.

[121] M. Aminudin, S. Kamarudin, B. Lim, E. Majilan, M. Masdar, and N. Shaari, "An overview: Current progress on hydrogen fuel cell vehicles," *International Journal of Hydrogen Energy*, vol. 48, no. 11, pp. 4371–4388, 2023.

[122] T. Wilberforce, A. Alaswad, A. Palumbo, M. Dassisti, and A.-G. Olabi, "Advances in stationary and portable fuel cell applications," *International journal of hydrogen energy*, vol. 41, no. 37, pp. 16 509–16 522, 2016.

[123] Q. Liu, F. Lan, J. Chen, C. Zeng, and J. Wang, "A review of proton exchange membrane fuel cell water management: Membrane electrode assembly," *Journal of Power Sources*, vol. 517, p. 230723, 2022.

[124] O. B. Inal and C. Deniz, "Assessment of fuel cell types for ships: Based on multi-criteria decision analysis," *Journal of Cleaner Production*, vol. 265, p. 121734, 2020.

[125] T. B. Ferriday and P. H. Middleton, "Alkaline fuel cell technology-a review," *International journal of hydrogen energy*, vol. 46, no. 35, pp. 18 489–18 510, 2021.

[126] A. T. Hamada, M. F. Orhan, and A. M. Kannan, "Alkaline fuel cells: Status and prospects," *Energy Reports*, vol. 9, pp. 6396–6418, 2023.

[127] Y. Lu, Y. Cai, L. Souamy, X. Song, L. Zhang, and J. Wang, "Solid oxide fuel cell technology for sustainable development in china: An over-view," *international journal of hydrogen energy*, vol. 43, no. 28, pp. 12 870–12 891, 2018.

[128] S. Kazula, S. de Graaf, and L. Enghardt, "Review of fuel cell technologies and evaluation of their potential and challenges for electrified propulsion systems in commercial aviation," *Journal of the Global Power and Propulsion Society*, vol. 7, pp. 43–57, 2023.

[129] S. Dwivedi, "Solid oxide fuel cell: Materials for anode, cathode and electrolyte," *International Journal of Hydrogen Energy*, vol. 45, no. 44, pp. 23 988–24 013, 2020.

[130] L. M. Hadelu, A. Noorpoor, F. A. Boyaghchi, and S. Mirjalili, "A new molten carbonate fuel cell hybrid power generation system using two-stage sodium thermo-electrochemical converter/two-stage thermoelectric generator: Performance analysis and multi-objective grasshopper optimization," *Journal of Power Sources*, vol. 547, p. 232006, 2022.

[131] M. Mehrpooya, M. Raeesi, F. Pourfayaz, and M. Delpisheh, "Investigation of a hybrid solar thermochemical water-splitting hydrogen production cycle and coal-fueled molten carbonate fuel cell power plant," *Sustainable Energy Technologies and Assessments*, vol. 47, p. 101458, 2021.

[132] M. Tawalbeh, A. Al-Othman, and M. E. H. Assad, "Graphene oxide—nafion composite membrane for effective methanol crossover reduction in passive direct methanol fuel cells," in *2018 5th international conference on renewable energy: generation and applications (ICREGA)*. IEEE, 2018, pp. 192–196.

[133] Y. Wang, D. F. R. Diaz, K. S. Chen, Z. Wang, and X. C. Adroher, "Materials, technological status, and fundamentals of pem fuel cells–a review," *Materials today*, vol. 32, pp. 178–203, 2020.

[134] K. Xiong, W. Wu, S. Wang, and L. Zhang, "Modeling, design, materials and fabrication of bipolar plates for proton exchange membrane fuel cell: A review," *Applied Energy*, vol. 301, p. 117443, 2021.

[135] E. Majlan, D. Rohendi, W. Daud, T. Husaini, and M. Haque, "Electrode for proton exchange membrane fuel cells: A review," *Renewable and Sustainable Energy Reviews*, vol. 89, pp. 117–134, 2018.

[136] H. Guo, L. Chen, S. A. Ismail, L. Jiang, S. Guo, J. Gu, X. Zhang, Y. Li, Y. Zhu, Z. Zhang *et al.*, "Gas diffusion layer for proton exchange membrane fuel cells: A review," *Materials*, vol. 15, no. 24, p. 8800, 2022.

[137] W. Wu and F. Jiang, "Microstructure reconstruction and characterization of pemfc electrodes," *International journal of hydrogen energy*, vol. 39, no. 28, pp. 15 894–15 906, 2014.

[138] L. Xia, S. Tao, M. Ni, Y. Wang, C. Wu, Q. Xu, Y. Dai, and C. Cheng, "Reconstruction and optimization of catalyst layer of high temperature proton exchange membrane fuel cell," *International Journal of Hydrogen Energy*, vol. 47, no. 84, pp. 35 778–35 789, 2022.

[139] Z. Zhan, H. Song, X. Yang, P. Jiang, R. Chen, H. B. Harandi, H. Zhang, and M. Pan, "Microstructure reconstruction and multiphysics dynamic distribution simulation of the catalyst layer in pemfc," *Membranes*, vol. 12, no. 10, p. 1001, 2022.

[140] C. Zhao, S. Yuan, X. Cheng, Z. Zheng, J. Liu, J. Yin, S. Shen, X. Yan, and J. Zhang, "The effect of catalyst layer design on catalyst utilization in pemfc studied via stochastic reconstruction method," *Energy and AI*, vol. 13, p. 100245, 2023.

[141] N. H. Jawad, A. A. Yahya, A. R. Al-Shathr, H. G. Salih, K. T. Rashid, S. Al-Saadi, A. A. AbdulRazak, I. K. Salih, A. Zrelli, and Q. F. Alsalhy, "Fuel cell types, properties of membrane, and operating conditions: A review," *Sustainability*, vol. 14, no. 21, 2022. [Online]. Available: https://www.mdpi.com/2071-1050/14/21/14653

[142] D. Wu, C. Peng, C. Yin, and H. Tang, "Review of system integration and control of proton exchange membrane fuel cells," *Electrochemical Energy Reviews*, vol. 3, pp. 466–505, 2020.

[143] P. Ren, P. Pei, Y. Li, Z. Wu, D. Chen, and S. Huang, "Degradation mechanisms of proton exchange membrane fuel cell under typical automotive operating conditions," *Progress in Energy and Combustion Science*, vol. 80, p. 100859, 2020.

[144] S. M. Andersen, R. Dhiman, M. J. Larsen, and E. Skou, "Importance of electrode hot-pressing conditions for the catalyst performance of proton exchange membrane fuel cells," *Applied Catalysis B: Environmental*, vol. 172, pp. 82–90, 2015.

[145] Y. Song, C. Zhang, C.-Y. Ling, M. Han, R.-Y. Yong, D. Sun, and J. Chen, "Review on current research of materials, fabrication and application for bipolar plate in proton exchange membrane fuel cell," *International Journal of Hydrogen Energy*, vol. 45, no. 54, pp. 29 832–29 847, 2020.

[146] A. Baroutaji, A. Arjunan, M. Ramadan, J. Robinson, A. Alaswad, M. A. Abdelkareem, and A.-G. Olabi, "Advancements and prospects of thermal management and waste heat recovery of pemfc," *International Journal of Thermofluids*, vol. 9, p. 100064, 2021.

[147] F. Gonzatti, M. Miotto, and F. Farret, "Proposal for automation and control of a pem fuel cell stack," *Journal of Control, Automation and Electrical Systems*, vol. 28, pp. 493–501, 2017.

[148] Z. Belkhiri, M. Zeroual, H. B. Moussa, and B. Zitouni, "Effect of temperature and water content on the performance of pem fuel cell," *Journal of Renewable Energies*, vol. 14, no. 1, pp. 121–130, 2011.

[149] T. Lochner, R. M. Kluge, J. Fichtner, H. A. El-Sayed, B. Garlyyev, and A. S. Bandarenka, "Temperature effects in polymer electrolyte membrane fuel cells," *ChemElectroChem*, vol. 7, no. 17, pp. 3545–3568, 2020.

[150] C. Werner, F. Gores, L. Busemeyer, J. Kallo, S. Heitmann, and M. Griebenow, "Characteristics of pemfc operation in ambient-and low-pressure environment considering the fuel cell humidification," *CEAS Aeronautical Journal*, vol. 6, pp. 229–243, 2015.

[151] Y. Qin, Q. Du, M. Fan, Y. Chang, and Y. Yin, "Study on the operating pressure effect on the performance of a proton exchange membrane fuel cell power system," *Energy Conversion and Management*, vol. 142, pp. 357–365, 2017.

[152] Y. Zhao, Y. Liu, G. Liu, Q. Yang, L. Li, and Z. Gao, "Air and hydrogen supply systems and equipment for pem fuel cells: a review," *International Journal of Green Energy*, vol. 19, no. 4, pp. 331–348, 2022.

[153] Q. Wu, H. Li, W. Yuan, Z. Luo, F. Wang, H. Sun, X. Zhao, and H. Fu, "Performance evaluation of an air-breathing high-temperature proton exchange membrane fuel cell," *Applied energy*, vol. 160, pp. 146–152, 2015.

[154] C.-Q. Su, J.-F. Sun, G.-D. Meng, X. Liu, and Y.-P. Wang, "Thermal management control strategy of liquid-cooled fuel cell vehicle," *Energy Reports*, vol. 8, pp. 141–153, 2022.

[155] M. H. Bargal, M. A. Abdelkareem, Q. Tao, J. Li, J. Shi, and Y. Wang, "Liquid cooling techniques in proton exchange membrane fuel cell stacks: A detailed survey," *Alexandria Engineering Journal*, vol. 59, no. 2, pp. 635–655, 2020.

[156] I. Zakaria, W. Mohamed, W. Azmi, A. Mamat, R. Mamat, and W. Daud, "Thermo-electrical performance of pem fuel cell using al2o3 nanofluids," *International Journal of Heat and Mass Transfer*, vol. 119, pp. 460–471, 2018.

[157] H. N. Vu, X. L. Nguyen, and S. Yu, "A lumped-mass model of membrane humidifier for pemfc," *Energies*, vol. 15, no. 6, 2022. [Online]. Available: https://www.mdpi.com/1996-1073/15/6/2113

[158] S. Hamel, "Importance de l'humidification de l'anode pour une pile à combustible miniature fonctionnant en convection naturelle," Ph.D. dissertation, 2011. [Online]. Available: http://savoirs.usherbrooke.ca/handle/11143/1639

[159] K. Subin and P. Jithesh, "Experimental study on self-humidified operation in pem fuel cells," *Sustainable Energy Technologies and Assessments*, vol. 27, pp. 17–22, 2018.

[160] L. Xingsheng, L. Yong, D. Chunhui, W. Jun, and Z. Zhenxing, "Experimental study on performance of anode humidification system of large power fuel cell stack," *IOP Conference Series: Materials Science and Engineering*, vol. 895, no. 1, p. 012005, jul 2020. [Online]. Available: https://dx.doi.org/10.1088/1757-899X/895/1/012005

[161] Y. Dandeville, "Analyse thermique et électrochimique de supercondensateurs carbone-mno2 en milieu aqueux," Ph.D. dissertation, Université de Nantes, 2012.

[162] N. Rizoug, "Modélisation électrique et énergétique des supercondensateurs et méthodes de caractérisation: Application au cyclage d'un module de supercondensateurs basse tension en grande puissance," Ph.D. dissertation, Université des Sciences et Technologie de Lille-Lille I, 2006.

[163] J. M. Rodríguez-Rego, J. P. Carrasco-Amador, L. Mendoza-Cerezo, A. C. Marcos-Romero, and A. Macías-García, "Guide for the development and evaluation of supercapacitors with the proposal of a novel design to improve their performance," *Journal of Energy Storage*, vol. 68, p. 107816, 2023.

[164] A. G. Pandolfo and A. F. Hollenkamp, "Carbon properties and their role in supercapacitors," *Journal of power sources*, vol. 157, no. 1, pp. 11–27, 2006.

[165] S. Samantaray, D. Mohanty, I.-M. Hung, M. Moniruzzaman, and S. K. Satpathy, "Unleashing recent electrolyte materials for next-generation supercapacitor applications: a comprehensive review," *Journal of Energy Storage*, vol. 72, p. 108352, 2023.

[166] N. Vukajlović, D. Milićević, B. Dumnić, and B. Popadić, "Comparative analysis of the supercapacitor influence on lithium battery cycle life in electric vehicle energy storage," *Journal of Energy Storage*, vol. 31, p. 101603, 2020.

[167] F. N. U. Khan, M. G. Rasul, A. Sayem, and N. Mandal, "Maximizing energy density of lithium-ion batteries for electric vehicles: A critical review," *Energy Reports*, vol. 9, pp. 11–21, 2023.

[168] N. Belyakov, "Chapter seventeen - solar energy," in *Sustainable Power Generation*, N. Belyakov, Ed. Academic Press, 2019, pp. 417–438. [Online]. Available: https://www.sciencedirect.com/science/article/pii/B9780128170120000311

[169] F. Diaz-González, C. Chillón-Antón, M. Llonch-Masachs, S. Galceran-Arellano, J. Rull-Duran, J. Bergas-Jané, and E. Bullich-Massagué, "A hybrid energy storage solution based on supercapacitors and batteries for the grid integration of utility scale photovoltaic plants," *Journal of Energy Storage*, vol. 51, p. 104446, 2022.

[170] Nick. (2023, Apr.) Supercapacitor applications - e-mobility engineering. E-Mobility Engineering. [Online]. Available: https://www.emobility-engineering.com/supercapacitor-applications/

[171] P. Harrop. (2014, Jul.) Supercapacitors for electric vehicles are gaining traction. IDTechEx. [Online]. Available: https://www.idtechex.com/tw/research-article/supercapacitors-for-electric-vehicles-are-gaining-traction/6708

[172] K. Kakouche, T. Rekioua, S. Mezani, A. Oubelaid, D. Rekioua, V. Blazek, L. Prokop, S. Misak, M. Bajaj, and S. S. Ghoneim, "Model predictive direct torque control and fuzzy logic energy management for multi power source electric vehicles," *Sensors*, vol. 22, no. 15, p. 5669, 2022.

[173] H. Pourkheirollah, J. Keskinen, M. Mäntysalo, and D. Lupo, "Simplified exponential equivalent circuit models for prediction of printed supercapacitor's discharge behavior-simulations and experiments," *Journal of Power Sources*, vol. 567, p. 232932, 2023.

[174] D. Xu, L. Zhang, B. Wang, and G. Ma, "Modeling of supercapacitor behavior with an improved two-branch equivalent circuit," *IEEE Access*, vol. 7, pp. 26 379–26 390, 2019.

[175] H. EDUCATIONAL. (2023) Fuel cells: A unique historyA historical overview of fuel cell technological development from 1800 to the present day. Accessed: 2023-08-02. [Online]. Available: https://www.horizoneducational.com/fuel-cells-a-unique-history/t1483

[176] P. H. A. Nóbrega, "A review of physics-based low-temperature proton-exchange membrane fuel cell models for system-level water and thermal management studies," *Journal of Power Sources*, vol. 558, p. 232585, 2023.

[177] J. Zhao, X. Li, C. Shum, and J. McPhee, "A review of physics-based and data-driven models for real-time control of polymer electrolyte membrane fuel cells," *Energy and AI*, vol. 6, p. 100114, 2021.

[178] S. Wright, "Comparison of the theoretical performance potential of fuel cells and heat engines," *Renewable Energy*, vol. 29, no. 2, pp. 179–195, 2004.

[179] S. Ahmad, T. Nawaz, A. Ali, M. F. Orhan, A. Samreen, and A. M. Kannan, "An overview of proton exchange membranes for fuel cells: Materials and manufacturing," *International Journal of Hydrogen Energy*, vol. 47, no. 44, pp. 19 086–19 131, may 2022.

[180] S. Knights, "Pem fuel cell principles and introduction to contamination issues," *Proton Exchange Membrane Fuel Cells: Contamination and Mitigation Strategies*, p. 1, 2010.

[181] Y. Cai, "Open circuit voltage of polymer electrolyte membrane fuel cells," Ph.D. dissertation, Ph. D. thesis, RWTH Aachen University, 2019.

[182] D. Zalka and L. Péter, "On the evolution and application of the concept of electrochemical polarization," *Journal of Solid State Electrochemistry*, vol. 24, no. 11-12, pp. 2595–2602, 2020.

[183] T. Shinagawa, A. T. Garcia-Esparza, and K. Takanabe, "Insight on tafel slopes from a microkinetic analysis of aqueous electrocatalysis for energy conversion," *Scientific reports*, vol. 5, no. 1, p. 13801, 2015.

[184] S. A. Ansari, M. Khalid, K. Kamal, T. Abdul Hussain Ratlamwala, G. Hussain, and M. Alkahtani, "Modeling and simulation of a proton exchange membrane fuel cell alongside a waste heat recovery system based on the organic rankine cycle in matlab/simulink environment," *Sustainability*, vol. 13, no. 3, p. 1218, 2021.

[185] I. Rossetti, "Modelling of fuel cells and related energy conversion systems," *ChemEngineering*, vol. 6, no. 3, p. 32, 2022.

[186] Y. Cao, Y. Li, G. Zhang, K. Jermsittiparsert, and M. Nasseri, "An efficient terminal voltage control for pemfc based on an improved version of whale optimization algorithm. energy reports 6: 530-542," 2020.

[187] S. Srinivasan, *Fuel cells: from fundamentals to applications*. Springer Science & Business media, 2006.

[188] S. Mitsushima, B. Gollas, and V. Hacker, "Chapter 1 - introduction," in *Fuel Cells and Hydrogen*, V. Hacker and S. Mitsushima, Eds. Elsevier, 2018, pp. 1–13. [Online]. Available: https://www.sciencedirect.com/science/article/pii/B9780128114599000013

[189] A. L. Dicks and D. A. Rand, *Fuel Cell Systems Explained :Introducing Fuel Cells*. John Wiley & Sons, Ltd, 2018.

[190] A. Abd El Monem, A. M. Azmy, and S. Mahmoud, "Effect of process parameters on the dynamic behavior of polymer electrolyte membrane fuel cells for electric vehicle applications," *Ain Shams Engineering Journal*, vol. 5, no. 1, pp. 75–84, 2014.

[191] J. T. Pukrushpan, *Modeling and control of fuel cell systems and fuel processors*. University of Michigan, 2003.

[192] M. H. Nehrir and C. Wang, *Modeling and control of fuel cells: distributed generation applications*. John Wiley & Sons, 2009, vol. 41.

[193] F. Naseri, S. Karimi, E. Farjah, and E. Schaltz, "Supercapacitor management system: A comprehensive review of modeling, estimation, balancing, and protection techniques," *Renewable and Sustainable Energy Reviews*, p. 111913, 2021.

[194] N. Devillers, S. Jemei, M.-C. Péra, D. Bienaimé, and F. Gustin, "Review of characterization methods for supercapacitor modelling," *Journal of Power Sources*, vol. 246, pp. 596–608, 2014.

[195] H.-A. Trinh, H. V. A. Truong, M. D. Pham, T. C. Do, H.-H. Lee, and K. K. Ahn, "Comprehensive control strategy and verification for pem fuel cell/battery/supercapacitor hybrid power source," *International Journal of Precision Engineering and Manufacturing-Green Technology*, vol. 10, no. 2, pp. 421–436, 2023.

[196] J. Wang, B. Wang, L. Zhang, J. Wang, N. Shchurov, and B. Malozyomov, "Review of bidirectional dc-dc converter topologies for hybrid energy storage system of new energy vehicles," *Green Energy and Intelligent Transportation*, p. 100010, 2022.

[197] J. Wu, J. Wang, C. Gan, Q. Sun, and W. Kong, "Efficiency optimization of pmsm drives using field-circuit coupled fem for ev/hev applications," *IEEE Access*, vol. 6, pp. 15 192–15 201, 2018.

[198] K. Hartani, A. Merah, and A. Draou, "Stability enhancement of four-in-wheel motor-driven electric vehicles using an electric differential system," *Journal of Power Electronics*, vol. 15, no. 5, pp. 1244–1255, 2015.

[199] K. Hartani, Y. Miloud, and A. Miloudi, "Improved direct torque control of permanent magnet synchronous electrical vehicle motor with proportional-integral resistance estimator," *Journal of Electrical Engineering and Technology*, vol. 5, no. 3, pp. 451–461, 2010.

[200] P. Nyberg, E. Frisk, and L. Nielsen, "Driving cycle equivalence and transformation," *IEEE Transactions on Vehicular Technology*, vol. 66, no. 3, pp. 1963–1974, 2016.

[201] R. Ma, E. Breaz, and F. Gao, "Power demand for fuel cell system in hybrid vehicles," in *Fuel Cells for Transportation*. Elsevier, 2023, pp. 279–303.

[202] L. Berzi, M. Delogu, and M. Pierini, "Development of driving cycles for electric vehicles in the context of the city of florence," *Transportation Research Part D: Transport and Environment*, vol. 47, pp. 299–322, 2016.

[203] A. Hamlat, M. Sekkour, M. Mankour, and M. Khalfaoui, "An improved energy management system for fuel cell/ ultra-capacitor electric vehicle based fuzzy logic control," in *Artificial Intelligence and Heuristics for Smart Energy Efficiency in Smart Cities*, M. Hatti, Ed. Cham: Springer International Publishing, 2022, pp. 183–189.

[204] N. V. Martyushev, B. V. Malozyomov, S. N. Sorokova, E. A. Efremenkov, and M. Qi, "Mathematical modeling the performance of an electric vehicle considering various driving cycles," *Mathematics*, vol. 11, no. 11, p. 2586, 2023.

[205] A. K. Sharma, "Contribution à la synthèse d'observateur à gain variable pour les systèmes non linéaires: Application à l'estimation de la résistance au roulement," Ph.D. dissertation, Ecole centrale de Nantes, 2020.

[206] A. Ravey, "Design and control strategy of powertrain in hybrid electric vehicles," Theses, Université de Technologie de Belfort-Montbeliard, Dec. 2012. [Online]. Available: https://theses.hal.science/tel-00863541

[207] M. Kamran, "Chapter 10 - electric vehicles and smart grids," in *Fundamentals of Smart Grid Systems*, M. Kamran, Ed. Academic Press, 2023, pp. 431–460. [Online]. Available: https://www.sciencedirect.com/science/article/pii/B9780323995603000028

[208] "Rolling resistance and fuel efficiency," https://www.y-yokohama.com/global/product/tire/learn/care_safety/rolling_resistance/, accessed: August 28, 2023.

[209] L. Guo, Z. Li, and R. Outbib, "Reinforcement learning based energy management for fuel cell hybrid electric vehicles," in *IECON 2021–47th Annual Conference of the IEEE Industrial Electronics Society*. IEEE, 2021, pp. 1–6.

[210] S. Alrasheed, *Newton's Laws*. Springer International Publishing, 2019, pp. 37–51. [Online]. Available: https://doi.org/10.1007/978-3-030-15195-9_3

[211] A. hamlat, M. Sekour, M. mankour, M. yahiaoui, M. khalfaoui, and B. brahmi, "Advanced power management and control using fuzzy backstepping super-twisting controls designed for fuel cell supercapacitors hybrid power systems for traction applications," *Journal of Control, Automation and Electrical Systems*, vol. 34, no. 5, pp. 996–1012, 2023.

[212] X. Luo, J. V. Barreras, C. L. Chambon, B. Wu, and E. Batzelis, "Hybridizing lead–acid batteries with supercapacitors: A methodology," *Energies*, vol. 14, no. 2, 2021. [Online]. Available: https://www.mdpi.com/1996-1073/14/2/507

[213] X. Hao, I. Salhi, S. Laghrouche, Y. Ait-Amirat, and A. Djerdir, "Backstepping supertwisting control of four-phase interleaved boost converter for PEM fuel cell," *IEEE Transactions on Power Electronics*, vol. 37, no. 7, pp. 7858–7870, jul 2022.